University of Bergen

Master's Thesis

Climate forcing of summer carbon drawdown in the subpolar North Atlantic

Author:
Magni Svanevik

Supervisor:
Are Olsen
Siv Kari Lauvset

Master of Science in Meteorology and Oceanography
Specialization: Chemical Oceanography

August 2015

UNIVERSITY OF BERGEN

UNIVERSITY OF BERGEN

Abstract

Faculty of Mathematics and Natural Sciences
Geophysical Institute

Master of Science

Climate forcing of summer carbon drawdown in the subpolar North Atlantic

by Magni Svanevik

This thesis present a 9-year long time series of surface seawater fCO_2 data obtained aboard the MV *Nuka Arctica*. The *Nuka Arctica* provide full seasonal fCO_2 measurements which give a good picture of the fCO_2 variability between Denmark and Greenland. The ultimate aim is to identify climate forcing of summertime fCO_2 variations as observed from the *Nuka* data. The observed variations in interannual summertime fCO_2 result from both physical and biological processes. To separate these effects, fCO_2 was normalised to a constant temperature and to a reference year. This leaves fCO_2 variations caused only by biology and mixing, the main drivers behind summertime fCO_2. The oceanic drivers, represented by chlorophyll-a and MLD data, were used to detect and determine the strength of the biological activity (the primary production). Environmental parameters were applied to identify climate forcing of the oceanic drivers and ultimately the fCO_2. Temperature were found to have the strongest effect on May MLD, which determined the timing of the primary production and fCO_2 drawdown. In the summer months a combination of wind and temperature governed the MLD and stratification, which ultimately determined the strength of the fCO_2 drawdown.

Acknowledgements

I would like to express gratitude to my supervisor Are Olsen. It has been educational and fun thanks to your good ideas and guidance through this year.
Thanks to my co-supervisor Siv Kari Lauvset for your good advice and proof reading.
I also want to thank Friederike Frob for the help with the Argo data and Matlab scripting.
Thanks to Laurent Bertino at NERSC for providing me with the TOPAZ data.
Finally, a big thanks to Eirik Steine Frivåg for the last minute proof reading.

Contents

List of Figures

List of Tables

Chapter 1

Introduction

One of the major environmental concerns today is the accumulation of CO_2 in the atmosphere, the Mauna Loa observatory has recently recorded atmospheric CO_2 over 400 ppm. CO_2 is one of the most important greenhouse gases, its increased concentration affect the radiative balance of the atmosphere and is the major driving force behind the ongoing climate change. The global carbon cycle moderate the atmospheric CO_2 rise and associated climate change by the uptake of CO_2 of land and ocean. Studies have shown that over half the anthropogenic CO_2 emitted due to burning of fossil fuel, land use change and cement production has been taken up by the terrestrial and the ocean reservoirs (Le Quéré et al. (2009), Tjiputra et al. (2014)). The increased atmospheric CO_2 alter the climate, and hence the physical properties of the ocean, and the biogeochemical processes which ultimately determine the ocean uptake (Tjiputra et al., 2012). How climate change affect the carbon cycle and to witch degree uptake of CO_2 will be sustained in the future is, however, uncertain (Olsen et al., 2008). It is therefore crucial to understand the CO_2 variability in todays climate in order to predict the future feedback of increased atmospheric CO_2. The oceanic carbon uptake is largely inhomogeneous in time and space, and is affected by environmental and biological driving factors on different time scales. It is therefore important to assess the regional and temporal variability of the sea-air flux in order to understand the global carbon cycle and the possible future feedback processes. As part of the project of surveying the global ocean the Voluntary Observing Ships (VOS) contribute to annual, full seasonal carbon measurements collected by autonomous instruments aboard the VOS ships (Watson et al., 2009). This thesis will use a 9 year long time series (2005-2013) of pCO_2 data collected aboard the MV *Nuka Arctica*, the northernmost VOS line, crossing the North Atlantic from Denmark to Greenland. The focus will be on the summertime pCO_2, which is mainly determined by biological activity.

The thesis is organized as follows: Chapter 2 introduces pCO_2 and a description of its driving mechanisms and thesis motivation and aims. Instrument and calculations, a presentation of the data and a description of the study area are presented in chapter 3. Chapter 4 starts out with a presentation of the pCO_2 data collected aboard the MV *Nuka Arctica*. Then follows an assessment of the interannual pCO_2 variations and its dependence on oceanic drivers (chlorophyll-*a* and mixed layer depth). In chapter 5 the pCO_2 variations identified in chapter 4 will be linked to climate forcing by assessing how environmental parameters govern its oceanic drivers.

Chapter 2

Theoretical background

This chapter will start out with a short description of the processes involved in the sea-air carbon flux, where the difference between the atmospheric and the oceanic $p\mathrm{CO}_2$ is the thermodynamic driving factor. Thereafter, the various parameters that control the oceanic $p\mathrm{CO}_2$, and the $p\mathrm{CO}_2$ sensitivity to changes in these parameters, will be presented. The last section describe the thesis motivation and aims.

2.1 Sea-air flux of CO_2

The sea-air flux of CO_2, F, is governed by:

$$F = k \cdot S(pCO_2^{oc} - pCO_2^{atm}) \tag{2.1}$$

where k is the gas transfer velocity, S is the CO_2 solubility and $p\mathrm{CO}_2^{oc}$ and $p\mathrm{CO}_2^{atm}$ are the sea surface and atmospheric partial pressure of CO_2. The solubility is a function of salinity and temperature, where temperature has the strongest effect. The gas transfer velocity is governed by the turbulence at the sea-air interface, normally expressed as a function of wind speed. Oversaturation of CO_2 in the ocean causes a net flux of CO_2 from the ocean to the atmosphere (positive F), and undersaturation causes a net flux of CO_2 from the atmosphere to the ocean (negative F). The global annual net uptake flux of CO_2, including the anthropogenic CO_2, by the surface waters has been estimated to be 2.0 $\pm$ 1.0 petagrams carbon (Pg C yr^{-1}) in 2000 by using the (wind speed)^2 dependence of the CO_2 gas transfer velocity of Wanninkhof (1992). This estimate is based on approximately 3.0 million measurements of surface-water $p\mathrm{CO}_2$ (Takahashi et al., 2009). The wind speed dependence has not yet been properly quantified, and

about half of the ± 1.0 Pg C yr^{-1} uncertainty in net uptake flux estimate is attributed to the uncertainty in the gas transfer velocity (Takahashi et al., 2009).

2.2 pCO_2 and its governing factors

The partial pressure of CO_2, pCO_2, is determined through Henry's law

$$pCO_2 = \frac{[C]_{co_2}}{K_0} \tag{2.2}$$

where $[C]_{CO_2}$ is the concentration of CO_2 (μmol kg^{-1}) in water, K_0 is the solubility (mol kg^{-1} atm^{-1}) and pCO_2 is the sea surface partial pressure of carbon dioxide (μatm) (Emerson and Hedges, 2008). pCO_2 is the partial pressure CO_2 would have in the atmosphere if in equilibrium with the ocean. Partial pressure is the favourable quantity to use in regard to the surface ocean CO_2, because of its thermodynamic dependency and the physical processes involved in the sea surface gas exchange (Zeebe and Wolf-Gladrow, 2001).

The surface ocean pCO_2 is determined by the sea surface temperature (SST), the sea surface salinity (SSS), dissolved inorganic carbon (DIC) and Alkalinity (Alk). DIC is the total concentration of dissolved inorganic carbon and Alk is a measure of the excess of bases (proton acceptors) over acids (proton donors) (Sarmiento and Gruber, 2006). DIC is defined as:

$$DIC = [CO_2] + [HCO_3^-] + [CO_3^{2-}] \tag{2.3}$$

where CO_2 is the sum of aqueous CO_2, $CO_2(aq)$, and carbonic acid, H_2CO_3 (Zeebe and Wolf-Gladrow, 2001):

$$CO_2 = CO_2(aq) + H_2CO_3$$

At the pH of seawater, Alk is defined as:

$$Alk = [HCO_3^-] + 2[CO_3^{2-}] + [OH^-] - [H^+] + [B(OH)_4^-] + minor\ bases. \tag{2.4}$$

Equation 2.5 express the relative contribution of these two parameters to the pCO_2 (Sarmiento and Gruber, 2006). K_0, K_1 and K_2 are equilibrium constants, and give the thermodynamic temperature and salinity dependence of pCO_2. This equation shows that pCO_2 decreases when DIC decreases, but it increases when Alk decreases, and that what controls the surface ocean pCO_2 is the ratio of the equilibrium constants, $K_2/(K_0 \cdot K_1)$, DIC and Alk (Sarmiento and Gruber, 2006).

$$pCO_2 = \frac{K_2}{K_0 \cdot K_1} \frac{(2 \cdot DIC - Alk)^2}{Alk - DIC} \tag{2.5}$$

To determine what controls the pCO_2, it is necessary to understand what controls DIC, Alk and the equilibrium constants in the surface ocean, and the relative contribution of each parameter to the pCO_2. The following sections will be dedicated to each of these parameters and how they govern the pCO_2.

2.2.1 Temperature and salinity

Temperature and salinity determines pCO_2 through the solubility constant, K_0, and the dissociation constants, K_1 and K_2, all functions of temperature and salinity. The collective term for these three constants is equilibrium constants because thermodynamic equilibrium is assumed when they are applied.

Equilibrium constants

When CO_2(g) dissolves in seawater, it first forms aqueous CO_2 (CO_2(aq)), which then forms H_2CO_3 when it reacts with water. H_2CO_3 then dissociates to form bicarbonate, HCO_3^-, and carbonate, CO_3^{2-}. The reactions can be summarized as follows (Zeebe and Wolf-Gladrow, 2001):

$$CO_2(g) \overset{K_0}{\Longleftrightarrow} CO_2(aq) + H_2O \Longleftrightarrow H_2CO_3 \overset{K_1}{\Longleftrightarrow} HCO_3^- + H^+ \overset{K_2}{\Longleftrightarrow} CO_3^{2-} + H^+ \tag{2.6}$$

CO_2(aq) and H_2CO_3 are usually combined and expressed as $H_2CO_3^*$ or CO_2, the latter will be used here. These reactions occur very fast, and for all practical purposes thermodynamic equilibrium is assumed between the different carbon species. The equilibrium relationship between the species is given by:

$$K_0 = \frac{[CO_2]}{pCO_2} \tag{2.7}$$

$$K_1 = \frac{[H^+][HCO_3^-]}{[CO_2]} \tag{2.8}$$

$$K_2 = \frac{[H^+][CO_3^{2-}]}{[HCO_3^-]} \tag{2.9}$$

where K_0 is the solubility constant and K_1 and K_2 are the dissociation constants (Sarmiento and Gruber, 2006). For detailed equations of how to calculate the equilibrium constants, see Sarmiento and Gruber (2006), chapter 8, table 8.2.2. Equation 2.7 is a rewriting of Henry's law, 2.2, which will be discussed in the next paragraph.

Solubility

Henry's law state that at thermodynamic equilibrium, the partial pressure of a gas above a liquid is directly proportional to the concentration of the gas dissolved in the liquid (Sarmiento and Gruber, 2006). This is related through the solubility constant, K_0 (sometimes referred to as Henry's constant, K_h). Henry's law, with respect to CO_2, is expressed in equation 2.2. K_0 is a function of temperature and is relatively insensitive to salinity. Solubility increases with decreasing temperature for most gasses (Sarmiento and Gruber, 2006). To determine pCO_2 from the concentration, we rearrange equation 2.2 and get $pCO_2 = K_0^{-1} \cdot [C]_{CO_2}$. If a water parcel is cooled, the solubility of the gasses in that parcel will increase, K_0^{-1} will decrease (moles pr. kg atm increases) and pCO_2 will decrease. This shows that the partial pressure of CO_2 increases with increasing temperature.

The net effect of temperature and salinity on pCO_2

Keeping DIC and Alk constant, Takahashi et al. (1993) deduced relationships that summarize the net effect of changing temperature and salinity on pCO_2,

$$(\frac{\partial pCO_2}{\partial T})/pCO_2 = 0.0423^\circ C^{-1} \tag{2.10}$$

and

$$(\frac{\partial pCO_2}{\partial S})(\frac{S}{pCO_2}) = 0.93 \tag{2.11}$$

These equations show that with an initial pCO_2 of 300 μatm, temperature of 20°C and a salinity of 35, a warming of one degree increases pCO_2 by approximately 13 μatm, and a salinity increase of one increases the pCO_2 by 9 μatm. In our study area

the seasonal variation in temperature is typical 6°C, much larger than the seasonal variation in salinity (which rarely exceeds 1). This shows that on a seasonal time scale the temperature driven changes in pCO_2 are much larger than the salinity driven changes. This is why temperature is regarded as the dominant physical driver of pCO_2 (Sarmiento and Gruber, 2006).

2.2.2 Dissolved inorganic carbon

DIC affects pCO_2 through its effect on the carbon concentration, $[C]_{CO_2}$. DIC itself is affected by dilution, ocean circulation, primary production and air-sea gas exchange. Dilution and primary production also affect alkalinity, and the effect of these processes on Alk will be described in this subsection.

Dilution and mixing

Precipitation is the main source of freshwater and reason for dilution of seawater in the North Atlantic. Freshwater contains very little DIC and Alk, and dilution by precipitation reduces DIC and Alk. However, the DIC:Alk ratio is kept constant, so the net effect on pCO_2 is small (Sarmiento and Gruber, 2006). Ocean circulation changes DIC by mixing and advection. Mixing is the dominant driver in the North Atlantic due to low winter temperatures and strong storms that induce deep winter mixing which brings up DIC rich water from the deep. Alk is also brought to the surface, but the relative change in Alk is smaller than for DIC, and the net effect of mixing is to increase the surface pCO_2.

Primary Production

Primary production is the net uptake of CO_2 by phytoplankton in the surface layer, and this occurs mostly though photosynthesis. During photosynthesis, phytoplankton use inorganic carbon and energy from light to produce organic matter, which decreases the amount of DIC and nutrients in the surface waters. The reaction is:

$$106CO_2 + 16HNO_3^- + HPO_4^{2-} + 78H_2O + 18H^+ \Longleftrightarrow C_{106}H_{175}O_{42}N_{16}P + 150O_2. \quad (2.12)$$

Photosynthesis decreases the pCO_2 in the surface ocean due to its utilization of DIC. Net community production is the primary production minus the respiration carried out by both autotrophs (phytoplankton) and heterotrophs (zooplankton). Respiration is the reverse process of photosynthesis since it converts oxygen and organic matter back to

CO_2 and nutrients (Sarmiento and Gruber, 2006). This process increases DIC in the deep ocean, which is brought up to the surface during winter mixing, eventually increasing the surface pCO_2, as mentioned earlier. Since the production of organic matter during photosynthesis decreases the concentration of free protons, H^+, the alkalinity increases as a result of primary production (Sarmiento and Gruber, 2006). Decreased surface DIC and increased surface Alk due to primary production result in a pCO_2 decrease.

Air-sea gas exchange

Air-sea gas exchange affect DIC but not Alk. Equations 2.3 and 2.4 show that the exchange of CO_2 between the air-sea interface only affect DIC since the charge balance is not affected (Zeebe and Wolf-Gladrow, 2001). Air-sea gas exchange for CO_2 is slower than for other gasses, for example oxygen, where all the O_2 molecules dissolves in seawater and contribute to the partial pressure change. The air-sea equilibrium timescale of oxygen is approximately 12 days, while that for CO_2 is approximately 240 days (Zeebe and Wolf-Gladrow, 2001). The reason for the slow CO_2 equilibrium is the chemical reactions that CO_2 is involved in when entering or leaving the surface ocean. Of the total carbon inventory in the ocean (DIC), only roughly 0.5% exists as CO_2, the rest is in the form of carbonate, CO_3^{2-}, and bicarbonate HCO_3^-, which do not transfer between the air and sea. CO_3^{2-} is the strongest base of the inorganic carbon system, and 19 of 20 CO_2 molecules that enters the ocean react with carbonate to form bicarbonate, hence only 1 of 20 CO_2 molecules acts to increase the pCO_2. This is known as the buffer effect, as the reaction buffer the changes in CO_2 concentration, and slow down the equilibration. If CO_2 behaved like oxygen its equilibrium time would be similar, but since only 1 of 20 CO_2 molecules contribute to increased or decreased pCO_2, it takes 20 times longer, resulting in an equilibration time of approximately 240 days (Sarmiento and Gruber (2006), Zeebe and Wolf-Gladrow (2001)).

The net effect of DIC on pCO_2

The sensitivity of pCO_2 to changes in DIC is quantified through the buffer capacity, or Revelle factor. The magnitude of the changes is dependent on the relative difference in concentration between DIC and Alk. Based on equation 2.5, Sarmiento and Gruber (2006) arrive at an equation for the Revelle factor:

$$\lambda_{DIC} \approx \frac{3 \cdot Alk \cdot DIC - 2 \cdot DIC^2}{(2 \cdot DIC - Alk)(Alk - DIC)} \tag{2.13}$$

Inserting typical values for the surface ocean gives a Revelle factor, λ_{DIC}, of about 10. This means that a relative increase in DIC of 1 gives a relative increase in pCO_2 of

10 (Sarmiento and Gruber, 2006). Increasing λ_{DIC} equals a reduced buffer capacity, which means that the Revelle factor is the inverse of the buffer factor (Zeebe and Wolf-Gladrow, 2001). Since there is about 200 times more DIC than CO_2 in the ocean (as CO_2 is $\sim 0.5\%$ of the total inorganic carbon inventory), this indicate that if CO_2 did not undergo any chemical reactions when entering the ocean, the oceanic carbon uptake would be 20 times less than it is (Emerson and Hedges, 2008).

2.2.3 Alkalinity

Alkalinity is defined as the excess of bases (proton acceptors) over acids (proton donors), see equation 2.4. Alkalinity determines $p\mathrm{CO}_2$ through its effect on the buffer capacity of sea water. CO_2^{2-} rich waters (high Alk) have a large buffer capacity, and buffers the CO_2 that enters the water by transferring CO_2 to HCO_3^-. Water with low CO_3^{2-} concentration (low Alk) has a smaller buffer capacity, and the CO_2 that enters the ocean will not be as well buffered. The net reaction is expressed as:

$$CO_2 + CO_3^{2-} + H_2O \Leftrightarrow 2HCO_3^-$$

In surface seawater $\sim 10\%$ of the total alkalinity exists as CO_3^{2-} and $\sim 90\%$ exists as HCO_3^-, and due to its limited supply in seawater CO_3^{2-} is the limiting species in the buffer system (Sarmiento and Gruber, 2006). Alkalinity is controlled by dilution and primary production (see section 2.2.2) and calcium carbonate formation and dissolution (the carbonate pump).

Carbonate pump

Formation and dissolution of calcium carbonate, CaCO_3, in the form of calcite or aragonite is the main process that affect the alkalinity. It is expressed as:

$$\mathrm{Ca}^{2+} + 2\mathrm{HCO}_3^- \rightarrow \mathrm{CaCO}_3 + \mathrm{CO}_2 + \mathrm{H}_2\mathrm{O}.$$

Precipitation or dissolution of CaCO_3 affect Alk twice as much as DIC. Precipitation of 1 mol of CaCO_3 decreases Alk by 2 mol and DIC by 1 mol, and net effect of precipitation of CaCO_3 is a $p\mathrm{CO}_2$ increase.

The net effect of Alk on $p\mathrm{CO}_2$

The sensitivity of $p\mathrm{CO}_2$ to changes in Alk is called the alkalinity factor. Its magnitude is dependent on the relative difference in concentration between DIC and Alk. Based

on equation 2.5, with some modifications, Sarmiento and Gruber (2006) arrive at an equation for the Alkalinity factor, λ_{Alk}:

$$\lambda_{Alk} \approx \frac{Alk^2}{(2 \cdot DIC - Alk)(Alk - DIC)} \tag{2.14}$$

Inserting typical values for the surface ocean gives λ_{Alk} = -9.4, which means that a relative increase in Alk of 1 result in a relative decrease of pCO_2 by 9.4 (Sarmiento and Gruber, 2006).

2.2.4 Summertime pCO_2 in the subpolar North Atlantic

Section 2.2 started with a representation of the relative contribution of each of the governing factors on the pCO_2, given by equation 2.5. To emphasize which is the governing factor controlling the summertime pCO_2, a short summary will be given. Temperature and salinity affect pCO_2 through their influence on the equilibrium constants, K_0, K_1 and K_2. The contribution of salinity to the solubility constant is negligible, and temperature is regarded as the dominant physical driver of pCO_2. The high latitude waters are undersaturated with respect to atmospheric CO_2 during summer, and summertime air-sea gas exchange results in a DIC increase. However, the effect of summer gas exchange on pCO_2 has found to be relatively small (Olsen et al., 2008). Dilution has a minor effect on pCO_2 since it changes DIC and Alk in a constant ratio. Mixing affect DIC mostly during winter when DIC rich water is brought to the surface, leading to increased pCO_2. Primary production at high latitudes is limited to the summer months when the water column is stratified, trapping phytoplankton and nutrients in the well lit surface layer, and decreases DIC and hence pCO_2. The main process affecting the surface alkalinity is calcium carbonate formation. Surface ocean alkalinity decreases when $CaCO_3$ is precipitated, which lead to an increase in pCO_2.

At high latitudes, observations show a decrease in pCO_2 from winter to summer. This suggest that the effect of increased temperature on pCO_2 in the summer is counteracted by the reduction in pCO_2 induced by changes in DIC and/or Alk. To counteract the temperature effect, DIC would have to decrease and/or Alk to increase. In the North Atlantic, seasonal variations in Alk are small, and the decrease in winter to summer pCO_2 is mostly caused by a summer reduction in DIC caused by primary production (Sarmiento and Gruber (2006), Olsen et al. (2008)).

2.3 $x\mathrm{CO}_2$, $p\mathrm{CO}_2$ and $f\mathrm{CO}_2$

For atmospheric CO_2 the most common quantity to use is mole fraction, $x\mathrm{CO}_2$ (μmol mol^{-1}). The mole fraction does not change with pressure like $p\mathrm{CO}_2$, so it is fairly uniform at different altitudes, and it does not depend on the water vapour pressure. $x\mathrm{CO}_2$ and $p\mathrm{CO}_2$ has the same values only in dry air and at standard pressure (1 atm). $p\mathrm{CO}_2$, is calculated from $x\mathrm{CO}_2$, which is analytically determined. They are related through the equation

$$pCO_2 = p^{tot} \cdot xCO_2 \tag{2.15}$$

where p^{tot} is the total amount of pressure exerted by the gases in the sample. This is a simplified equation, and a more thorough description of the conversion will be given in chapter 3. When using the partial pressure to quantify oceanic CO_2, one assumes that CO_2 is an ideal gas, which it is not. Correcting for this gives the sea surface CO_2 fugacity, $f\mathrm{CO}_2$. The calculation is shown in equation 3.2 in chapter 3. The $p\mathrm{CO}_2$ and $f\mathrm{CO}_2$ are often used interchangeably, and they are *almost* the same number. The fugacity coefficient, the ratio of CO_2 fugacity and partial pressure, over the temperature range $0°\mathrm{C} \geq \mathrm{T}_c \leq 30°\mathrm{C}$ at 1 atm, is between ~ 0.996 and ~ 0.997. This means that with a $p\mathrm{CO}_2$ of 360 μatm the difference is about 1 μatm (Zeebe and Wolf-Gladrow (2001), Weiss (1974)). The CO_2 from *Nuka Arctica* and used here are reported in fugacity.

2.4 Thesis motivation and aims

Biological production is a strong driver of $f\mathrm{CO}_2$ variations, and this causes a distinct seasonal cycle, particularly at high latitudes. The aim of this thesis is to investigate the relationship between the magnitude of the primary production and the $f\mathrm{CO}_2$ drawdown in the subpolar North Atlantic using a 9-year long time series of data from MV *Nuka Arctica*. Primary production is controlled mainly by the mixed layer depth (MLD), and to infer the magnitude of primary production, chlorophyll-*a* data are used. Therefore I evaluate relationships between $f\mathrm{CO}_2$, chl-*a* and MLD with the ultimate aim to determine interannual variations in summertime $f\mathrm{CO}_2$ drawdown based on the oceanic drivers (chl-*a* and MLD) and to identify climate forcing.

Chapter 3

Methods and data

3.1 Instrument and fCO_2 measurements

The MV *Nuka Arctica* fCO_2 data set was downloaded from the Surface Ocean CO_2 Atlas (SOCAT) database. The SOCAT database is a uniform format, quality controlled, regularly updated global data set of marine surface CO_2 data (Pfeil et al. (2012), Bakker et al. (2014)). The fCO_2 system aboard Nuka Arctica has operated since 2005, and provides data on variations in fCO_2 in the subpolar North Atlantic. The ship track extends from Denmark to Greenland at approximately 60°N (see figure 3.1). The fCO_2 data was supplemented by an equal number of associated data, such as SST, xCO_2, air temperature and depth. fCO_2 data from 2012 and 2013 are not yet made publicly available in the SOCAT database. These data were provided by Omar Abdirahman, along with depth data from the ETOPO1 global relief model which were merged with the fCO_2 data.

Instrument

The underway instrument used aboard *Nuka Arctica* was described in detail by Pierrot et al. (2009) and Olsen et al. (2008). The instrument works by rapidly equilibrating seawater and air. The equilibration is conducted in a main equilibrator, where seawater enters the system at a rate of 1.5-2 l min^{-1}. A spiral nozzle creates a spray of seawater into the headspace of the equilibrator. The total volume of the equilibrator is 1.5 l, and a constant stream of seawater into the equilibrator gives a volume of water that is much larger than the volume of the air. The equilibrated gas in the equilibrator headspace first circulates to a condenser, were the gas is dried, and then enters the analyser. The analyser used to measure the CO_2 concentration in the gas stream is a non-dispersive infrared analyzer (NDIR) build by LICOR, and the model used at the *Nuka Arctica* is

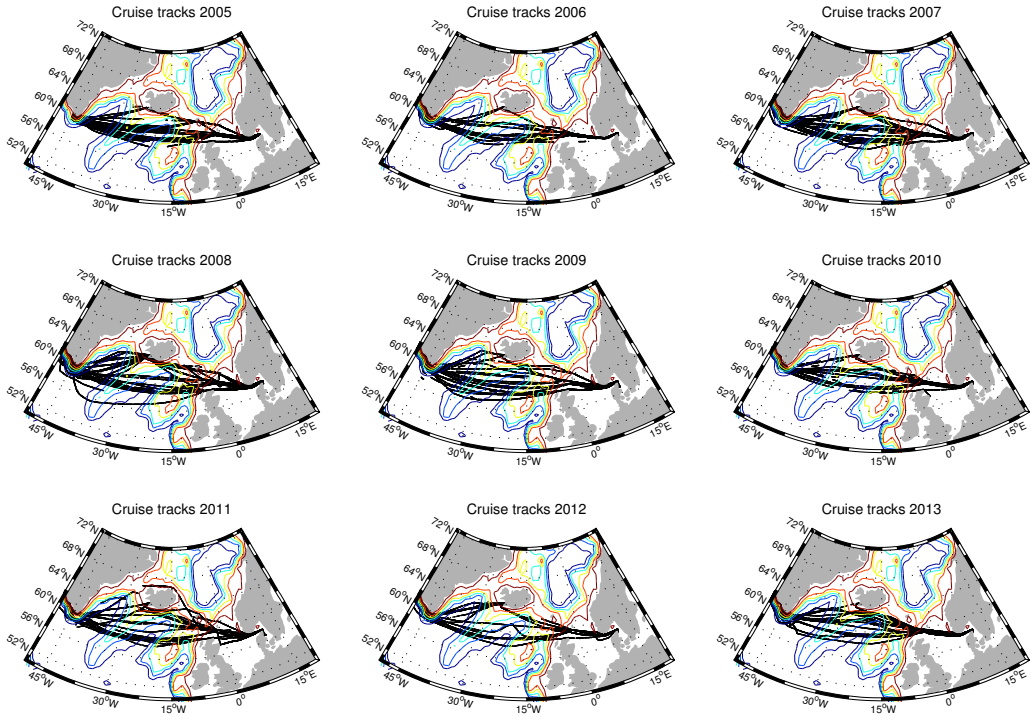

FIGURE 3.1: MV *Nuka Arctica* fCO_2 sampling positions from 2005 to 2013.

LI-6262. The headspace samples are analysed every 2.5 min, and a calibration of the instrument is conducted every 5 hour with three standard gases. These standard gases should have concentrations covering the range of the concentration in the relevant area, and at the *Nuka Arctica* these reference gasses range from 200 ppm to 430 ppm (Pierrot et al. (2009), Olsen et al. (2008)). The reported dry mole fraction of CO_2, xCO_2^{dry}, from the NDIR was standardised using a linear fit between measured concentrations and the offsets from the calibrated values of the gas standards. This gives a xCO_2 value that is corrected for any instrument drift (Pierrot et al., 2009).

These fCO_2 systems have been installed on several VOS ships over the years, and Pierrot et al. (2009) compared the system aboard MV *Nuka Arctica* with a similar system placed aboard MV *Skogafoss*. MV *Skogafoss* transits between Iceland and Boston, MA, and the comparison was made at their cross-over region, at about 60°N and 29.4-31°W. The data collected in February 2005 from these two vessels show an agreement of better than 2 μatm, which is within the specified accuracy of the instruments.

fCO_2 calculations

The fCO_2 data in SOCAT were computed from the analysed xCO_2^{dry} and pCO_2 using the equations recommended by Dickson et al. (2007). The measurements were made for dry gas, but the humidity in the equilibrator is assumed to be 100%. Therefore, a correction for the water vapor pressure was carried out following:

$$pCO_2 = xCO_2^{dry}(p^{eq} - pH_2O) \tag{3.1}$$

where $p\mathrm{H_2O}$ is the water vapor pressure (Weiss and Price, 1980), and $x\mathrm{CO_2}$ is the dry mole fraction measured in the analyzer. Then the $f\mathrm{CO_2}$ was calculated from the $p\mathrm{CO_2}$ at 100% humidity as

$$fCO_2 = pCO_2 \cdot e^{p^{eq}\frac{\beta+d\delta}{RT_{eq}}} \tag{3.2}$$

where p^{eq} is the pressure of equilibration, T_{eq} is the temperature of equilibration, R is the gas constant, and β and δ is the virial coefficients for $\mathrm{CO_2}$ (Weiss, 1974). $p\mathrm{CO_2}$ is highly dependent on temperature, so a correction for the difference between *in situ* and equilibrator temperatures needs to be made. This was done following Takahashi et al. (1993), which corrected for the approximately 0.5° temperature difference (Olsen et al., 2008).

3.2 Chlorophyll-*a* data

The sea surface chl-*a* data used here were obtained from the ocean color group at Goddard Space Flight Center at `http://oceandata.sci.gsfc.nasa.gov/MODISA/Mapped/8Day/9km/chlor`. The data used were the MODISA Level-3 mapped eight day data, at a resolution of 9 km at the equator. This compares to 1/12° in both longitude and latitude, and at 60°N this corresponds to a distance of 9.2 km in latitude and 4.6 km in longitude. The available data cover roughly the time period from 20 February to 20 October. Chl-*a* can not be measured in cloudy weather and darkness, which is why no measurements are available from the winter months at high latitudes. The chl-*a* data were treated two ways. They were collocated in time and space with the $f\mathrm{CO_2}$ data obtained from *Nuka Arctica*. And also monthly mean concentrations were estimated directly from the eight days, 9 km resolution, satellite data to determine monthly averages in selected regions.

3.3 Mixed layer depth data

The mixed layer depth data used were the 12.5 km monthly mean data obtained from the Arctic Ocean Physics Reanalysis (1991-2013) of the TOPAZ4 model. This is the latest version of TOPAZ, a coupled ocean-sea ice data assimilation (DA) system for

the North Atlantic Ocean and Arctic (Sakov et al., 2012). The data were obtained in NetCDF format from http://thredds.met.no/thredds/catalog/myocean/arc-mfc/ran-arc-myoceanv2/arctic/myocean-class1/catalog.html via the THREDDS data server (TDS). The Arctic components of MyOcean are a shared responsibility between The Norwegian Meteorological Institute (MET) together with the Institute of Marine Research (IMR) and Nansen Environmental and Remote Sensing Center (NERSC). The MLD data were also treated in two ways. They were collocated in time and space with the fCO_2 data obtained from *Nuka Arctica*, and also the monthly mean, 12.5 km resolution, mixed layer depths were used directly to give monthly averages in selected regions.

3.4 Sea surface temperature and air temperature data

The sea surface temperature data used were the NOAA Optimum Interpolation (OI) Sea Surface Temperature (SST) V2, provided by the NOAA/OAR/ESRL PSD, Boulder, Colorado, USA, at their Web site. These sea surface temperature data are bias corrected satellite data (Reynolds et al., 2002). They provide monthly mean SST data on a 1° x 1° global grid from 1981 to 2014 at http://www.esrl.noaa.gov/psd/data/gridded/data.noaa.oisst.v2.html. The air temperature data used were the NCEP Reanalysis Derived data provided by the NOAA/OAR/ESRL PSD, Boulder, Colorado, USA, at their Web site (Kalnay et al., 1996). They provide 2 meter monthly mean air temperatures on a T62 Gaussian grid from 1948 to 2014 at http://www.esrl.noaa.gov/psd/data/gridded/data.ncep.reanalysis.derived.surfaceflux.html.

3.5 Wind data

The wind data used were 10 meter, 4 times daily u-wind and v-wind components on a T62 Gaussian grid from the NCEP Reanalysis data provided by the NOAA/OAR/ESRL PSD, Boulder, Colorado, USA, at their Web site (Kalnay et al., 1996). The wind components were obtained from http://www.esrl.noaa.gov/psd/data/gridded/data.ncep.reanalysis.surfaceflux.html. The wind speed, w, was calculated from the u-wind and v-wind components using the equation:

$$w = \sqrt{u^2 + v^2} \tag{3.3}$$

3.6 Atmospheric fCO_2

Atmospheric fCO_2, fCO_2^{atm}, needed to be estimated in order to calculate ΔfCO_2 (fCO_2^{oc} - fCO_2^{atm}). The SOCAT data base provide xCO_2 (μmol mol^{-1}) data from the Global View marine boundary layer CO_2 data interpolated from http://www.esrl.noaa.gov/gmd/ccgg/globalview/co2/co2_description.html#gv_mtx. To calculate fCO_2^{atm} from xCO_2, equations 3.1 and 3.2 were used, but p^{eq} was replaced by sea level pressure (SLP), and T_{eq} by the sea surface temperature (Olsen et al., 2008). The SOCAT data needed to be supplemented with sea level pressure data from 2012 and 2013. 4 times daily surface pressure on a T62 Gaussian grid were obtained from the NCEP Reanalysis data provided by the NOAA/OAR/ESRL PSD, Boulder, Colorado, USA, at their Web site (Kalnay et al., 1996). This was merged with the SLP data obtained from the SOCAT database.

Monthly mean atmospheric xCO_2^{dry} data from 2005 to 2013 were obtained from the the NOAA ESRL Carbon Cycle Cooperative Global Air Sampling Network at http://www.esrl.noaa.gov/gmd/dv/data/index.php?site=mhd&parameter_name=Carbon%2BDioxide (Dlugokencky et al., 2015). Atmospheric xCO_2^{dry} were used to normalise the *Nuka* fCO_2 data to a reference year, removing the underlying fCO_2 trend due to uptake of anthropogenic CO_2 (see section 3.9).

3.7 Argo data

Argo data were downloaded from the USGODAE server. Argo is a global array containing more than 3000 free-floating profiling floats, which covers the upper 2000 m of the global ocean with temperature and salinity measurements. The Argo float temperature and salinity profiles were used to calculate density profiles.

3.8 Hydrographic settings

Bathymetry and sea surface salinities taken along a crossing on 2-6 April 2005 are shown in figure 3.3, and figure 3.2 present the main features of the surface circulation in the subpolar North Atlantic (NA). Figure 3.2 shows that the water masses in the subpolar North Atlantic (NA) are mainly derivatives of the North Atlantic Current (NAC). In the subpolar NA the NAC takes two paths, it either branches off to form the northward Irminger Current, which flows along the Reykjanes Ridge and circulates in the Irminger Sea. The second path is north-eastward, it passes the Iceland Basin, flows between

Britain and Iceland and ends up in the Norwegian, Greenland and North Sea and the Arctic Ocean (Brown et al., 2001). The main outflow of water from the Arctic Sea is the East Greenland Current through the Denmark Strait. This current carries cold and fresh water from the polar seas, and it converges with the southward Irminger Current. Some of this water flows to the west of Greenland to become part of the Labrador Sea Water and travels southward in the Labrador Current or it flows back into the Irminger Sea. The circulation system causes the water in the western part of the subpolar NA, which is directly influenced by the NAC, to be warm and saline, and the eastern part which is mostly dominated by the Arctic water mass outflow to be cold and fresher (see figure 3.3).

Since different water masses and processes dominate in the region covered by *Nuka*, the sampling area is divided into three regions: The Irminger Sea (IrB), the Iceland basin (IcB), and the North Sea (NS). The Irminger Sea is defined zonally between the 2750-m isobath along the Greenland coast and the top of the Reykjanes Ridge around 30°W, and meridionally between 56.5° N and the 2750-m isobath at about 63.5° N (see figure 3.4). This definition is relatively conservative compared to other studies (Henson et al. (2006), Holliday et al. (2006)), but it was chosen to minimize the influence of data from the East Greenland Current and the shelf around Iceland (i.e excluding data from port calls), which has different hydrographic conditions. The Iceland Basin is defined zonally between the top of the Reykjanes Ridge 30°W and the 1000 m isobath along the Rockall plateau, and meridionally between 56.5° N and the 1000-m isobath at about 63° N (see figure 3.4). The North Sea is defined as the area east of 10°W, and will only be discussed in section 4.1. It is excluded from the discussion of the interannual variations due to the complexity of the variations. Olsen et al. (2008) found little relationship between fCO_2 and MLD and chl-a in their study of this region from 2005. The interannual fCO_2 variations in the NS should be investigated in a study more dedicated to this area.

3.9 Data analyses

In addition to the fCO_2 data, fCO_2 which is normalised to a reference year and to a fixed temperature, will be presented. The year and temperature normalised fCO_2 will be denoted fCO_2^{ytn}. fCO_2 represent variations caused by temperature, biology, mixing and the underlying fCO_2 trend. When normalising, the contribution of the measurable parameters affecting fCO_2 is excluded (SST and fCO_2 trend), and left are the fCO_2 variations caused only by biology and mixing. Hence, fCO_2^{ytn} represent the variation caused only by biology and mixing, which are the main drivers behind the summertime fCO_2. In chapter 4 where the results are presented, both the non-normalized fCO_2

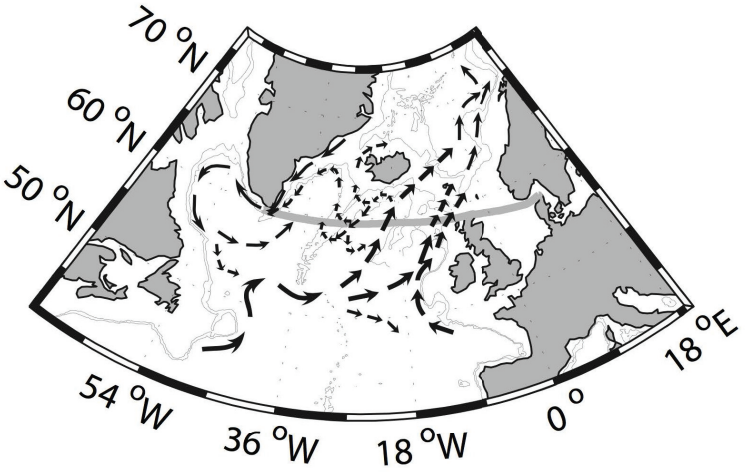

FIGURE 3.2: Main features of the surface circulation scheme in the subpolar North Atlantic. The grey line show ship tracks from 2-6 April 2005. Figure obtained from Olsen et al. (2008).

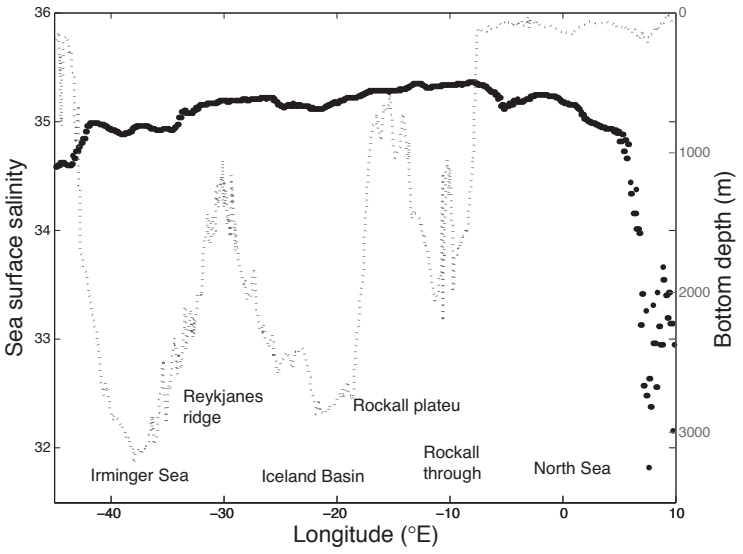

FIGURE 3.3: Bathymetry (grey) and sea surface salinity (black) along a crossing 2-6 April 2005. Salinity estimates were obtained from the TOPAZ4 model.

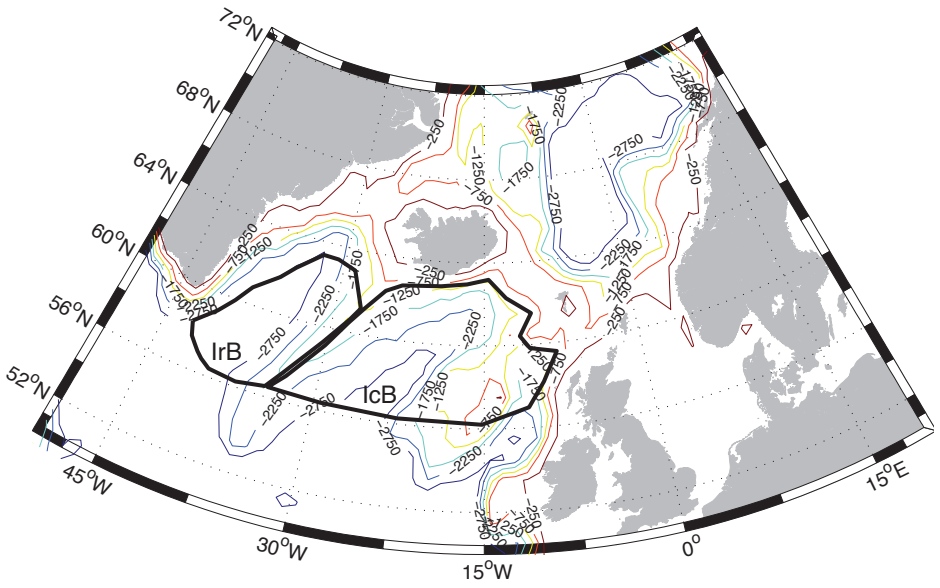

FIGURE 3.4: The regional definitions of the Irminger Sea and the Iceland Basin.

and the normalized fCO_2^{ytn} values are represented. This is to emphasize the effect temperature and biology have on the summertime fCO_2. In chapter 5 only fCO_2^{ytn} will be discussed.

Normalising to a year

The fCO_2 has changed over the study period due to invasion of anthropogenic CO_2 from the atmosphere. In order to remove this underlying fCO_2 trend, a correction is made, adjusting the monthly mean fCO_2 to a common year following Takahashi et al. (2009). 2009 is the median year of the observations, and chosen as the reference year.

$$fCO_2^{yn} = \overline{fCO_{2oc}^{mm,yyyy}} + (\overline{fCO_{2atm}^{2009}} - \overline{fCO_{2atm}^{yyyy}}) \tag{3.4}$$

This means that the monthly mean fCO_2 prior to 2009 will increase, the monthly mean fCO_2 after 2009 will be reduced, and the monthly mean 2009 values will remain unchanged.

Normalising to temperature

fCO_2 is affected by SST (the thermodynamic effect), and SSS, DIC and Alk (the carbon chemistry). Interannual fCO_2 variations can be caused by all of these processes. To

partially separate these effects, monthly mean fCO_2 is normalised to a constant temperature each month following Takahashi et al. (2002), where T_{mean} is the mean monthly temperature. This temperature normalisation was performed on the fCO_2 adjusted to a common year, fCO_2^{yn}.

$$(fCO_2 \quad at \quad T_{mean}) = (fCO_2)_{obs} * exp[0.0423(T_{mean} - T_{obs})], \tag{3.5}$$

Regression analyses

Linear regression is preformed between fCO_2^{ytn} and chl-a and fCO_2^{ytn} and mixed layer depths. Linear regression uses the ordinary least squares method, which gives the least difference between the observed (fCO_2^{ytn}) and the regressed value (chl-a and MLD). The regression is performed in order to see when and how dependent fCO_2^{ytn} is to changes in chl-a and MLD. The coefficient of determination, r^2, is the measure of the goodness of fit of the regression curves, i.e how well the variables vary together (Thomson and Emery, 2014). For assessing significant relationships a significance level of 90% was chosen. This was chosen since other processes also affect the fCO_2, and a near 100% agreement between the parameters can not be expected. P-values > 0.1 are therefore not considered statistically significant.

Chapter 4

Results

4.1 Presentation of the data in time and space

In this section, Hovmöller plots are used to present the data collected aboard the MV *Nuka Arctica*. Hovmöller diagrams visualize the spatial and temporal changes in the area of interest, in this case along the cruise tracks of *Nuka Arctica* (see figure 3.1). Figures 4.1-4.9 show Hovmöller diagrams of (**a**) the bathymetry and ship tracks, (**b**) sea surface temperature (SST), (**c**) surface seawater CO_2 fugacity (fCO_2), (**d**) ΔfCO_2 (fCO_2^{oc} - fCO_2^{atm}), (**e**) chlorophyll-a concentration (chl-a) and (**f**) the mixed layer depth (MLD). All observations are included in the figures, including observations from shallow areas, such as the Iceland shelf and the Greenland shelf. The reoccurring shallow depths at 25-30°W in figures 4.1-4.9 are due to port calls to Reykjavik, and abnormal high chl-a concentrations and low fCO_2 coincide with these port calls. Values from these shallow areas are therefore excluded from the analysis of the interannual variations (section 4.2), where the focus will be on the Iceland Basin and the Irminger Sea only. Areas that lack data are left blank. Satellite chlorophyll-a data is only available from March to October due to light limitation in winter. Other gaps in the chl-a data are due to cloud cover. Numbers of measurements from each year are provided in table 4.1. The fall supersaturation occurring at 5°W in September 2007, November 2010, from August-November 2011 and in October 2012 is unrealistic high, and due to ship tracks close to Aberdeen, Scotland. These data are excluded from further analysis and will not be mentioned again.

Section 4.1.1 will start out with a thorough review of the seasonal cycle in 2005. For 2006 to 2013, the seasonal cycle will be analysed and compared to previous years. This way major differences in the seasonal cycle between the years will be highlighted, and years with unusually characteristics will be identified.

The area covered by *Nuka Arctica* is divided into three regions, the North Sea, the Iceland Basin and the Irminger Sea. The North Sea is defined here as the area east of 10°W, with bottom depths < 500 m. The Iceland Basin is defined between 15°W and 30°W, with bottom depths between 1500 m and 2500 m. The Irminger Sea is defined between 30°W and 40°W, and is the deepest of the three, with bottom depths > 2000 m. The East Greenland Current (EGC), east of 40°W, is not included in the analysis.

	2005	2006	2007	2008	2009	2010	2011	2012	2013
January	3488	0	7328	7054	5364	5042	0	2989	1849
February	2669	0	5295	6099	6444	5733	3297	5808	7760
March	3040	0	1366	4485	7617	1810	1784	4539	2878
April	4547	0	7766	0	1595	2179	3327	4486	3365
May	4853	2794	5982	4787	7368	8411	2006	484	791
June	5262	4463	5280	6100	545	2669	1140	0	3069
July	4286	6469	7324	7587	5992	0	2712	2	1333
August	5612	4263	4427	2567	8029	0	2613	491	3150
September	2932	5495	3871	4042	2682	0	4620	915	4890
October	5240	5347	5485	6407	0	0	4783	979	3038
November	3325	604	7356	6235	0	994	5489	5895	4737
Desember	757	6169	1294	3210	5031	1680	5122	4338	3508
Total	46011	35604	62774	58573	50667	28518	36893	30926	40368

TABLE 4.1: Number of measurements from *Nuka* each month and year from 2005-2013. Months with less than 1000 measurements are marked red.

4.1.1 2005 *Nuka* data

The 2005 *Nuka* data, figure 4.1, have a good spatial and temporal resolution. A total of 46011 measurements were obtained in 2005 (see table 4.1). The cruises were evenly distributed throughout the year, and the data clearly show the seasonal cycle along the ship tracks.

Winter (January-March)

Figure 4.1 (**b**) shows that the lowest sea surface temperature occurred from January to March. The North Sea and the Irminger Sea were the coldest regions, with temperatures down to 2°C and 4°C, respectively. The Iceland Basin had the highest winter temperatures, between 5 and 9°C. In the IcB and the IrB, the MLD was deep, the fCO_2 was high and the chl-*a* concentration was low, which is consistent with winter values in subpolar regions (Takahashi et al., 1993). While the SST in the IcB was clearly higher than in the IrB, the fCO_2 were approximately the same. This is a remarkable feature, and could be explained by deeper mixing in the IrB.

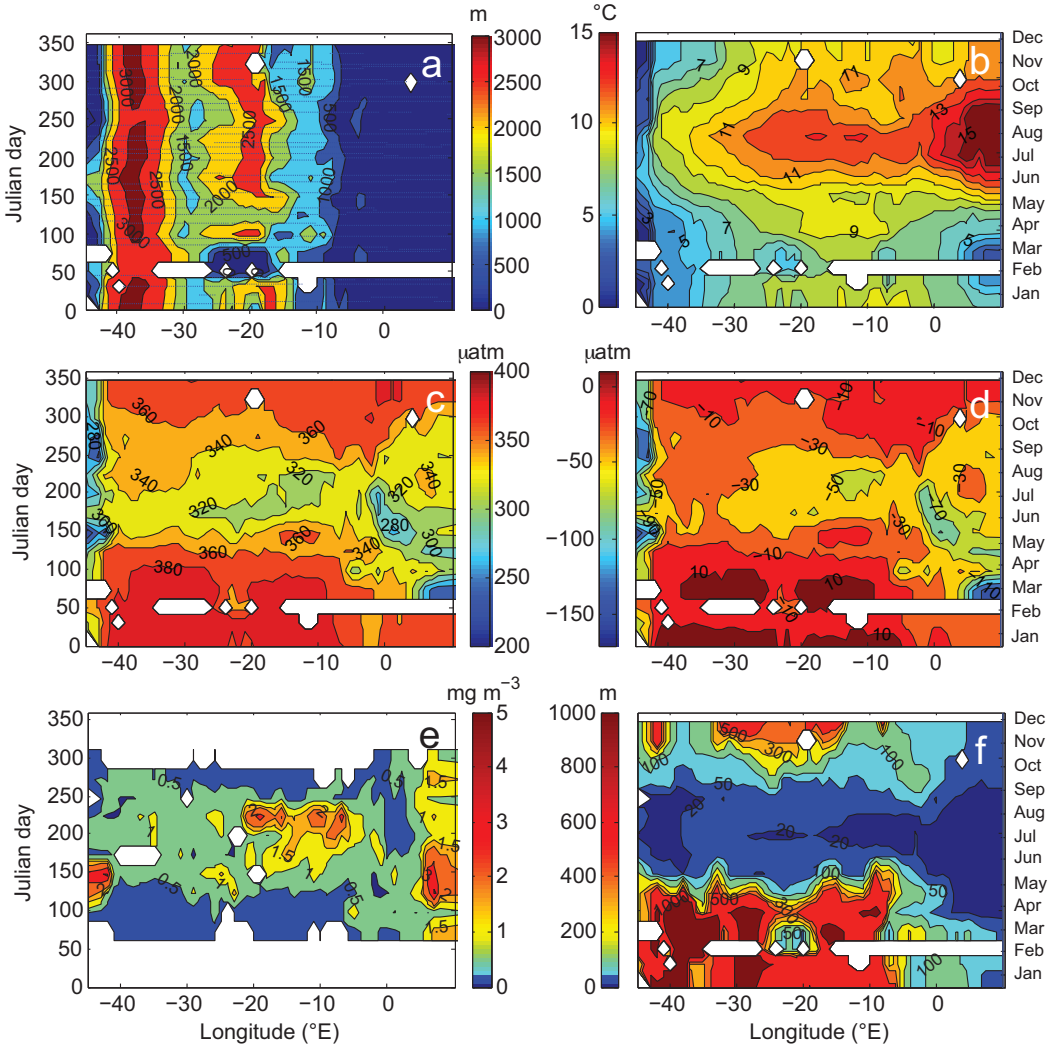

FIGURE 4.1: Hovmöller diagrams of (**a**) *Nuka* bathymetry ship tracks (blue lines), (**b**) SST, (**c**) fCO_2, (**d**) ΔfCO_2, (**e**) chl-*a*, and (**f**) MLD along the ship tracks of *Nuka* in 2005.

A study done by Metzl et al. (2010) reveal a positive trend in DIC and a negative trend in alkalinity, increasing fCO_2, in the North Atlantic Subpolar Gyre (NASPG) from 2001 to 2008. In the winter of 2007/2008 deep convection/strong vertical mixing in the Irminger Sea was presented as a possible explanation for the high DIC and low alkalinity (relative to DIC) (Vage et al., 2009). The vertical mixing is weaker in the IcB and deep convection is rarely initiated. This is evident in figure 4.1 (**f**), where the winter MLD in the IcB rarely exceeds 500 m, whereas the winter MLD in the IrB is around 1000 m or deeper. In addition, IrB is affected by Arctic water masses flowing across the Denmark Strait, causing the temperature in the Basin to be much lower than the IcB, which is mostly affected by warm water masses from the NAC. This could explain the observed features. The higher DIC in the IrB gives higher fCO_2, but with sea surface

temperatures several degrees lower than the IcB, the thermodynamic effect reduce fCO_2 and cause the wintertime fCO_2 in the IrB and IcB to be approximately the same.

To test this I normalise the wintertime fCO_2, 390 μatm, in the two basins to a constant temperature of 7.5°C using equation 3.5. This result in fCO_2 values in the IrB of ∼430 μatm, and fCO_2 values in the IcB of ∼ 370 μatm. This simple experiment shows that if the temperature in the two basins was the same the difference in fCO_2 would be as much as 60 μatm.

Spring and summer (April to September)

In May the SST started to increase across the entire area. During summer the warmest waters occurred in the NS, with gradually colder waters towards the west, because of the inflowing Atlantic water with the North Atlantic current. The summer warming stratifies the water column, shoaling the MLD. Figure 4.1 (**f**) shows that MLDs < 50 m was reached during May and June in both the IcB and IrB. In the North Sea, the MLD was never deeper than 500 m, and normally between 20 and 100 m throughout all season. In the summer the MLD in the NS shoal to depths < 20 m. Due to the stratification, phytoplankton becomes trapped in a well-illuminated and nutrient rich environment where conditions for photosynthesis is ideal, and the spring bloom is initiated (Sverdrup, 1953). This results in an increased chl-*a* concentration and a biological drawdown of fCO_2 in all regions. If there was no biological activity and fCO_2 was only dependent on temperature, the summer fCO_2 would be much higher. Following the formula from Takahashi et al. (1993) (equation 4.1) I calculate the potential increase in fCO_2 solely due to the winter to summer SST increase. This is to illustrate the magnitude of the effect of the biological activity.

$$(\partial pCO_2/\partial T)/pCO_2 = 0.0423^{\circ}C^{-1} \tag{4.1}$$

With a winter fCO_2 of 390 μatm, and a winter to summer SST increase of 5°C, the increase in fCO_2 would be 82 μatm, resulting in a summer fCO_2 of 472 μatm. This is 142 μatm higher than the observed mean summer value of approximately 330 μatm, as evident in figure 4.1 (**c**). In September the water started to cool, which eventually caused the stratification to collapse, the MLD to deepen, and the fCO_2 and chl-*a* concentrations were restored to winter values, around 390 μatm and < 0.5 mg m^{-3} respectively.

Figure 4.1 (**c**) reveal that the lowest summertime fCO_2 occurred in the NS, with values down to 280 μatm. The lowest fCO_2, at around 5-10°E, coincided with a chl-*a* peak that occurred from April to July, with concentrations up to 3 mg m^{-3} (see figure 4.1 (**e**)). The chl-*a* concentrations in the eastern NS was overall high throughout the duration of the

satellite observations, around 0.5-1.5 mg m^{-3} from March to October. The summertime fCO_2 values in the IcB were higher than in the NS, with values around 320-340 μatm. A chl-*a* peak occurred in the IcB from July to September, with concentrations up to 2 mg m^{-3}. In the IrB the situation was different with no occurrences of a strong chl-*a* peak, and relatively high fCO_2, between 320 and 360 μatm, during summer. The MLD was shallow all year in the eastern NS, with depths < 100 m, and did not undergo a large seasonal change like in the other basin. High chl-*a* concentrations in eastern NS in March indicates that primary production had already started. This suggests that the mixed layer depth is always shallower than Sverdrup's critical depth, and light is the limiting factor. Therefore, the spring bloom starts as soon as the light availability is sufficient, around March, which is the reason for the earlier onset of the spring bloom compared to the IcB and IrB, where formation of a shallow mixed layer depth is required. Sverdrup (1953) defined the critical depth as the depth where the phytoplankton growth is the same as losses due to respiration. The mixed layer depth need to be shallower than this critical depth in order to have a net growth in phytoplankton biomass.

The ΔfCO_2, presented in figure 4.1 (**d**), reveals that the IcB and IrB were supersaturated by 10 μatm in the winter. Wintertime supersaturation is linked to convective processes/vertical mixing which change the chemistry of the seawater by increasing DIC and decreasing Alk (relative to DIC) (Metzl et al., 2010). The winter supersaturation will be mentioned in the following presentation of the *Nuka* data (section 4.1.2-4.1.9), but wintertime pCO_2 trends will be the focus of others studies and will not be given much emphasize in this thesis. From April to August all basins were undersaturated. The largest undersaturation, down to -110 μatm, occurred in the NS in February and March. This strong undersaturation was most likely caused by relatively cold waters together with primary production.

4.1.2 2006 *Nuka* data

Hovmöller diagrams of the 2006 *Nuka* data are shown in figure 4.2. Unfortunately no data were available from January to April because *Nuka Arctica* was on an assignment in the Baltic Seas during these months. A total of 35604 measurements were obtained in 2006 (see table 4.1). The shallow bottom depth in November between 20 and 25°W, evident in figure 4.2 (**a**), indicate that the ship had a port call in Reykjavik.

The SST started to increase in June, and like in 2005, the warmest water occurred in the NS with colder water towards the east (see figure 4.2 (**b**)). Depending on longitude, the SST did not start to decrease until October-November, up to two months later than

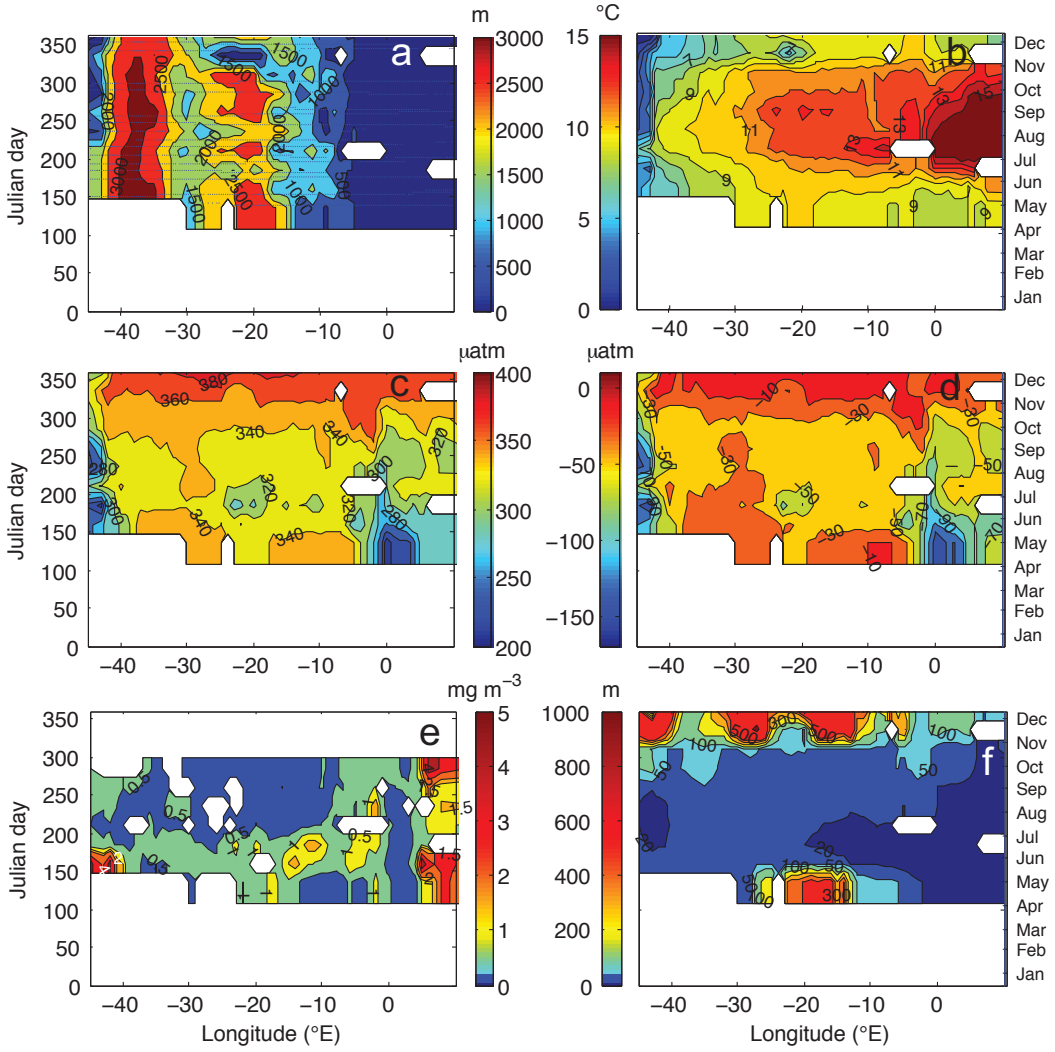

FIGURE 4.2: Hovmöller diagrams of (**a**) *Nuka* bathymetry ship tracks (blue lines), (**b**) SST, (**c**) fCO_2, (**d**) ΔfCO_2, (**e**) chl-*a*, and (**f**) MLD along the ship tracks of *Nuka* in 2006.

in 2005. This was also reflected in the MLD: its errosion was delayed by two months compared to 2005.

Figure 4.2 (**e**) reveal that the chl-*a* peaked twice in the NS, compared to only once in 2005 (see figure 4.1 (**e**)). The first peak occurred in April-June and the second in September-October, with concentrations up to 4 mg m^{-3}. The 2005 peak was weaker, up to 3 mg m^{-3}, and occurred in April to July. The September-October peak is most likely an indication of a fall bloom, but there was not a strong fCO_2 drawdown that coincided with the chl-*a* peak. This indicate primary production from regenerated, and not new, nutrients (Olsen et al., 2008). West of the chl-*a* maximum in April-June, at latitudes between 5 and 15°W, fCO_2 was very low, with values of around 220-280 μatm (ΔfCO_2 down to -110 μatm). Such low values were not observed in 2005. The low

fCO_2 values were not associated with unusually high chl-*a* data. Cold water could give rise to the unusually low fCO_2, but this is not supported by figure 4.1 (**b**), which shows temperatures around 8-9°C.

The summer fCO_2 drawdown, figure 4.2 (**c**), in the IcB and IrB lasted for a more extended period in 2006 (April-November), compared to 2005 (May-September). This is most likely a consequence of the delayed errosion of the mixed layer depth as noted above. The strength of the fCO_2 drawdown was approximately the same as, or a bit weaker than in 2005, with values between 320 and 340 μatm in the IcB, and around 340 μatm in the IrB. The water was never, as far as our observations goes, supersaturated with respect to the atmospheric fCO_2. This is probably due to the lack of data from the winter months. The summer undersaturation were overall stronger than in 2005 in the whole area.

4.1.3 2007 *Nuka* data

The 2007 *Nuka* data are presented in figure 4.3, and have a good spatial and temporal resolution. A total of 62774 measurements were obtained in 2007 (see table 4.1). The shallow bottom depths evident in figure 4.3 (**a**) at around 20-25°W in February, June and October indicate that the ship had a port call in Reykjavik. This was the reason for the low fCO_2 and high chl-*a* in the same region in June.

In May the SST started to increase across the entire area (see figure 4.3 (**b**)), and by the end of May, the MLD had shoaled to depths < 50 m in the IcB and IrB as illustrated in figure 4.3 (**f**). In the North Sea the most shallow MLD was reached already in February, with MLD < 50 m. The warming and shoaling of the MLD happened around the same time as in 2005.

The winter SST in the NS was much higher than in 2005, with 5-10°C compared to 3-8°C in 2005. The spring bloom, indicated by high chl-*a* concentrations, started in March in eastern part, and evolved westward with time. In the eastern North Sea, the chl-*a* concentration was high, up to 5 mg m^{-3} (figure 4.3 (**e**)), and fCO_2 was low, between 260 and 320 μatm (figure 4.3 (**c**)), from March to October. This was a much longer, and more intense, period with high chl-*a*, low fCO_2 than in 2005, when chl-*a* only reached 3 mg m^{-3}.

Disregarding data from the port call at 20-25°W in June, figure 4.3 (**c**) reveals a summer fCO_2 between 320 and 340 μatm in the IcB (same as in 2005 and 2006), and fCO_2 between 300 and 320 μatm in the IrB (lower than in 2005 and 2006). Previous years summer fCO_2 was always higher in the Irminger Sea than in the Iceland Basin, but

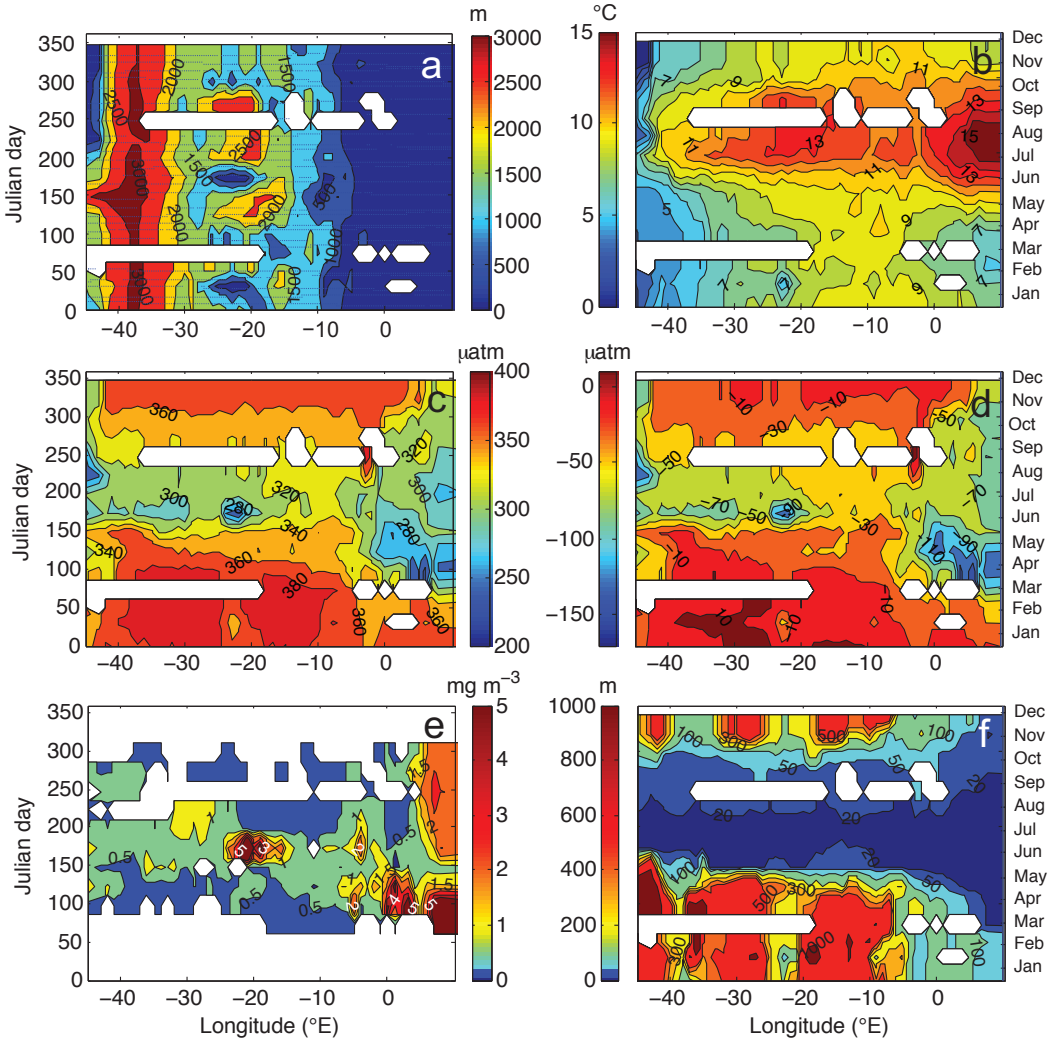

FIGURE 4.3: Hovmöller diagrams of (**a**) *Nuka* bathymetry ship tracks (blue lines), (**b**) SST, (**c**) fCO_2, (**d**) ΔfCO_2, (**e**) chl-*a*, and (**f**) MLD along the ship tracks of *Nuka* in 2007.

this year IrB had the lowest fCO_2. In 2005 the low summer fCO_2 in the IcB was associated with high chl-*a* concentrations. In 2007 however, there was no unusually high chl-*a* concentration connected to the low fCO_2 in either of the two basins (this is when disregarding the port call to Reykjavik in June).

The surface ocean fCO_2 undersaturation (figure 4.3 (**d**)) during summer was stronger than previous years in the IcB and IrB, with ΔfCO_2 from -50 to -70 μatm compared to around -10 to -50 in 2005 and 2006. This is most likely connected to a stronger biological activity, since no large differences in SST between the years is evident. The water was supersaturated in parts of the IrB in January and February. A supersaturation also occurred in 2005, but then over a much larger area, in both the Iceland Basin and the Irminger Sea.

4.1.4 2008 *Nuka* data

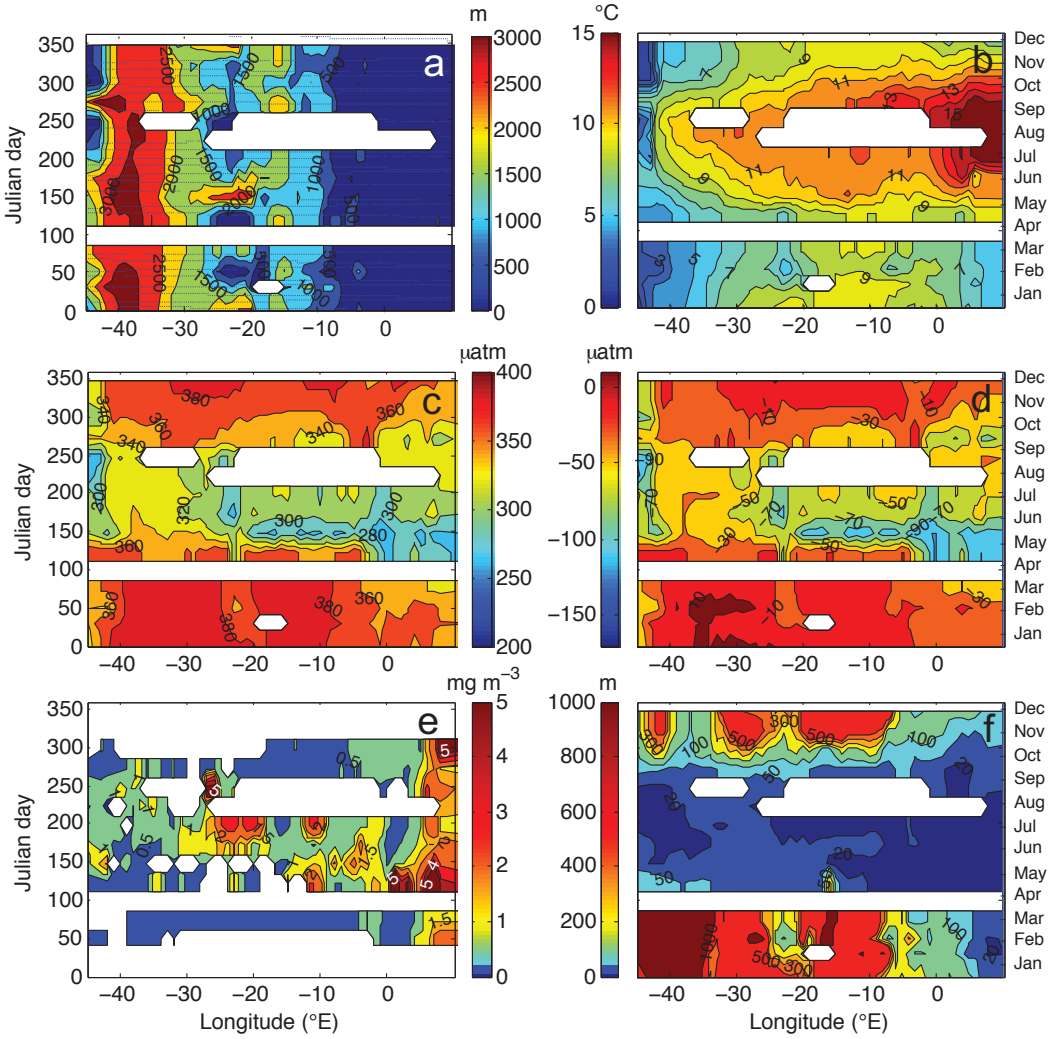

FIGURE 4.4: Hovmöller diagrams of (**a**) *Nuka* bathymetry ship tracks (blue lines), (**b**) SST, (**c**) fCO_2, (**d**) ΔfCO_2, (**e**) chl-*a*, and (**f**) MLD along the ship tracks of *Nuka* in 2008.

The 2008 *Nuka* data are presented in figure 4.4. No data were obtained in April, and due to instrument failure few measurements were available from August and September. A total of 58573 measurements were obtained in 2008 (see table 4.1). The reoccurring shallow depths (< 500m) in figure 4.4 (**a**) between 20 and 30°W indicate that the ship had several port calls in Reykjavik.

The lack of data from April makes it difficult to conclude exactly when the MLD shoaled, but figure 4.4 (**f**) shows that by May it had reached depths < 50 m, a few weeks earlier than the previous years. This also applies to the sea surface temperature, it started to increase in May, a few weeks earlier than previous years, which contributed to the early shoaling of the mixed layer depth (see figure 4.4 (**b**)).

In the NS two chl-*a* peaks are visible, with concentrations up to 5 mg m^{-3} as seen in figure 4.4 (**e**). The first chl-*a* peak occurred in April and May, starting in east and evolving westward with time. The second peak in October was limited to the eastern part of the basin. In association with the first peak, the spring bloom, fCO_2 was reduced from 340 to 280 μatm (see figure 4.4 (**c**)). No clear fCO_2 drawdown was associated with the second peak. This probably reflects production by regenerated and not new nutrients like in 2006. The strength of the chl-*a* peak, concentrations up to 5 mg m^{-3}, was similar to that in 2007. However, the fCO_2 was much lower in 2007 than in 2008, especially from June to September. This is most likely attributed to lower summer temperatures in 2007, as figure 4.3 (**b**) reveal that a smaller area of the North Sea exceeded 15°C in 2007 compared to 2008.

In the IcB the summer fCO_2 was low, between 280 and 320 μatm, which is the lowest summer fCO_2 of the years investigated so far. In particular low fCO_2 occurred in May and June, down to 280 μatm, which is a much earlier, and stronger, fCO_2 drawdown than previous years. The chl-*a* peak in July at about 20-25°W was most likely due to a port call in Reykjavik. The two chl-*a* peaks, up to 2 mg m^{-3} around 10-15°W, in May and July indicate that the phytoplankton bloom in the IcB was strong in 2008. The summer fCO_2 drawdown in the IrB was weak, with values around 340 μatm from May to September. No chl-*a* peak occurred either, with concentrations between 0.5-1 mg m^{-3} throughout summer. This was much the same situation as in 2005 and 2006 with summer fCO_2 between 320 and 340 μatm and chl-*a* concentrations under 1 mg m^{-3}. A pattern is starting to become clear: the summer fCO_2 drawdown is stronger in the IcB and NS than in the IrB. One exception so far, 2007 as described in section 4.1.3, stood out with a much stronger fCO_2 drawdown (down to 300 μatm) in the IrB than in the IcB. Like in 2007, the surface water was supersaturated by 10 μatm in the IrB in January and February, a smaller area of supersaturation than in 2005.

4.1.5 2009 *Nuka* data

Figure 4.5 presents the 2009 *Nuka* data. No data are available for October and November. A total of 50667 measurements were obtained in 2009 (see table 4.1).

As illustrated in figure 4.5 (**e**) two chl-*a* blooms occurred in the eastern NS in 2009. An intense spring bloom, associated with chl-*a* concentrations of up to 5 mg m^{-3} in February-May, and a weaker fall bloom in September, associated with chl-*a* concentrations of up to 1.5 mg m^{-3}. The first chl-*a* peak, associated with the spring bloom, started in February in east and evolved westward with time. This westward propagation of the spring bloom has been present in the NS all the years, and the MLD data indicates

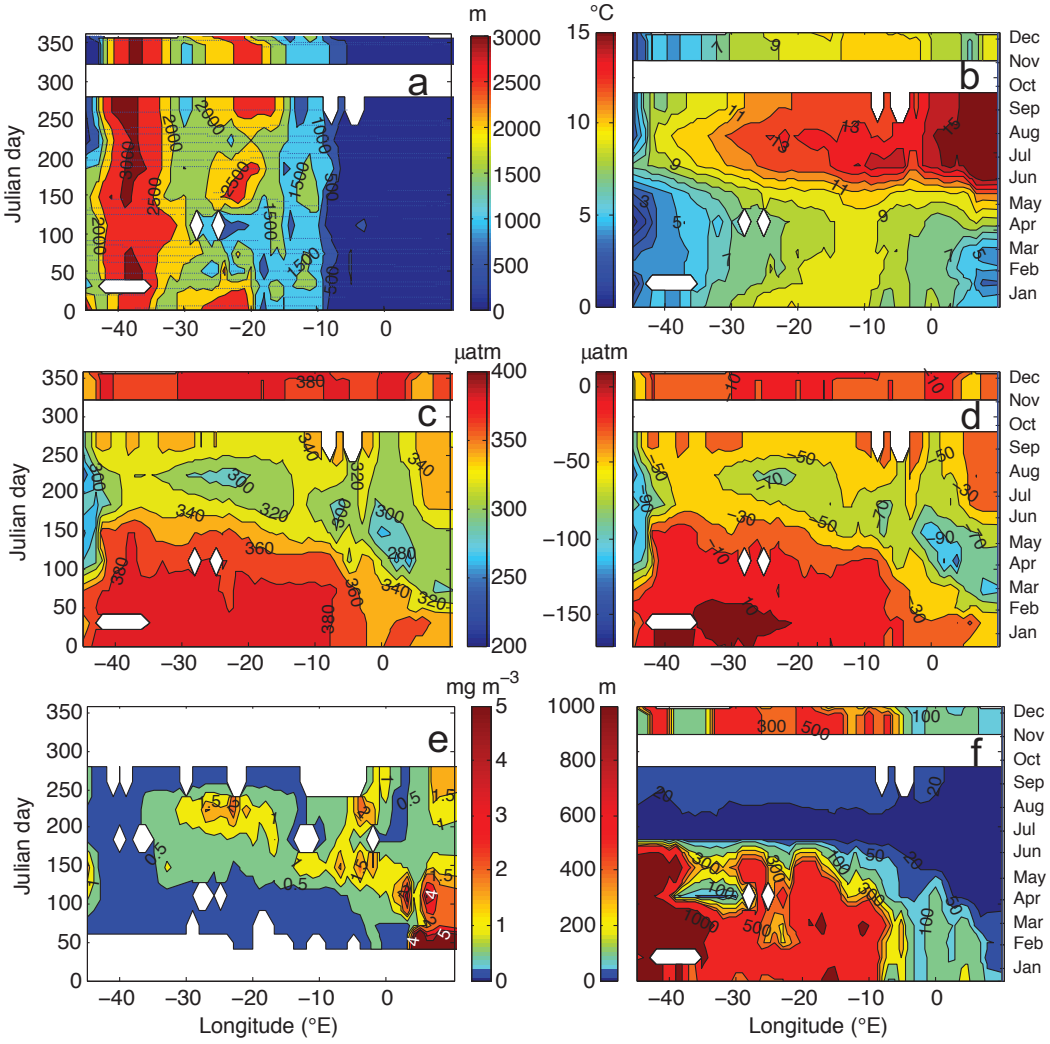

FIGURE 4.5: Hovmöller diagrams of (**a**) *Nuka* bathymetry ship tracks (blue lines), (**b**) SST, (**c**) fCO_2, (**d**) ΔfCO_2, (**e**) chl-*a*, and (**f**) MLD along the ship tracks of *Nuka* in 2009.

that this westward propagation follows the shoaling of the mixed layer depth. Figure 4.5 (**c**)) reveal that a fCO_2 drawdown was associated with the spring bloom, with values between 280 and 320 μatm. The fall bloom, however, was not associated with a fCO_2 drawdown. Like in 2006 and 2008 this was most likely due to regenerated production rather than new production.

The largest difference from previous years was the very late shoaling of the MLD in the IcB and IrB, it did not reach depths $<$ 50 m until late June (see figure 4.5 (**e**)), 1-2 months later than previous years. A late, but relatively abrupt warming of the water in June in this region is the reason (see figure 4.5 (**b**)). This resulted in a late bloom in the IcB and IrB indicated by high May and June fCO_2 values of around 340-360 μatm. A relatively strong fCO_2 drawdown followed the late shoaling of the MLD in the Iceland

Basin, with July to September fCO_2 values between 300 and 320 μatm, and a coinciding chl-*a* peak, up to 2 mg m^{-3}. After the late fCO_2 drawdown in the Irminger Sea, the June and July fCO_2 values were around 320-340 μatm. This is similar to previous years, except 2007 which had unusually low fCO_2. The chl-*a* concentrations were considerably lower than any previous years, with concentrations less than 0.5 mg m^{-3} compared to around 0.5-1 mg m^{-2} in the previous years. The water was supersaturated in IrB in January and February (figure 4.5 (**d**)), which is approximately the same as in 2007 and 2008 and a smaller area of supersaturation than in 2005.

4.1.6 2010 *Nuka* data

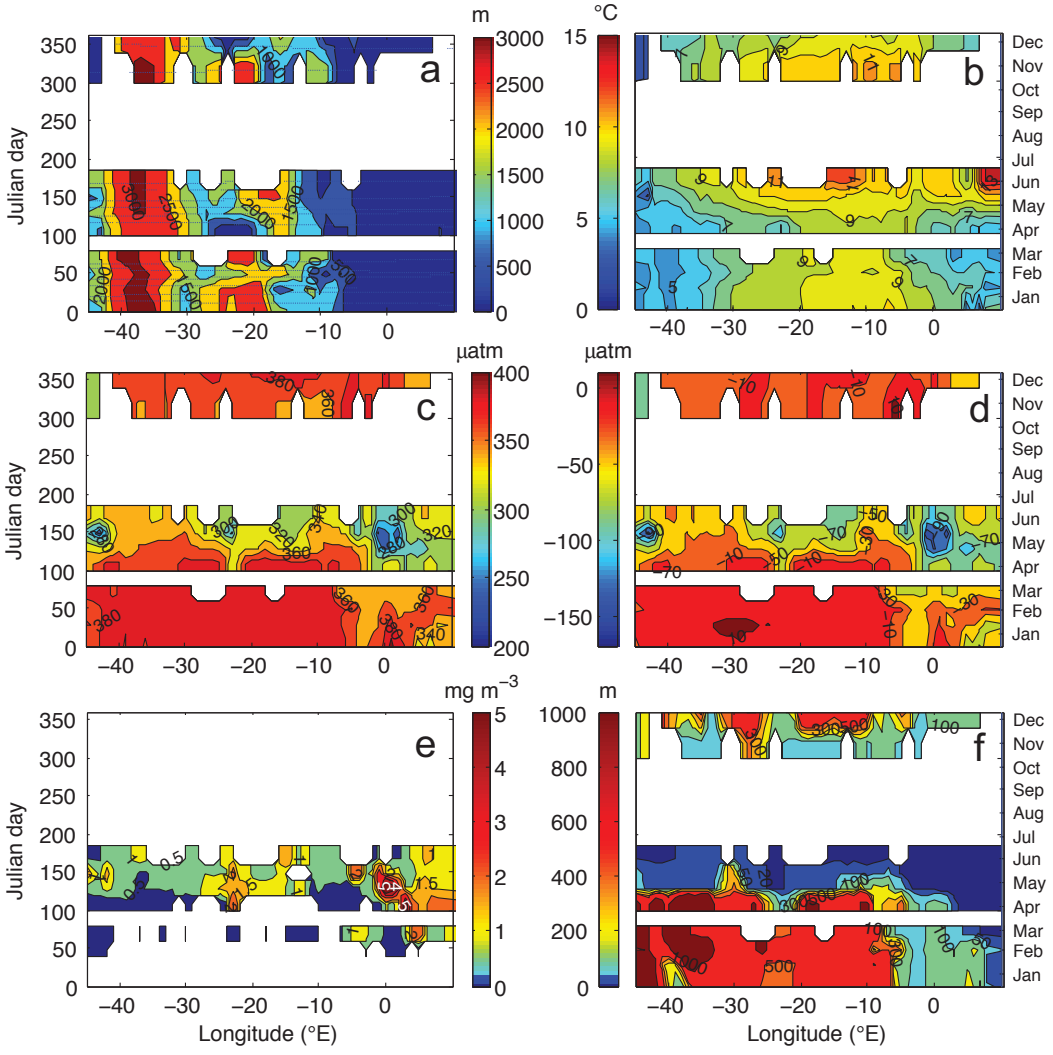

FIGURE 4.6: Hovmöller diagrams of (**a**) *Nuka* bathymetry ship tracks (blue lines), (**b**) SST, (**c**) fCO_2, (**d**) ΔfCO_2, (**e**) chl-*a*, and (**f**) MLD along the ship tracks of *Nuka* in 2010.

Figure 4.6 presents the 2010 *Nuka* data. A total of 28518 measurements were obtained in 2010, and no data were obtained from July through October (see table 4.1). This makes it difficult to interpret the data and compare 2010 with the previous years.

The chl-*a* data shows that the spring bloom in the NS took place in March, and propagated westward with time, with concentrations up to 5 mg m^{-3} in western part in June. Like in 2008, the MLD shoaled relatively early, and reached depths < 50 m in May in the Iceland Basin and the Irminger Sea, see figure 4.6 (**f**). This initiated the spring bloom, with a decrease in fCO_2 to 300-340 μatm (figure 4.6 (**c**)) and a chl-*a* increase to 0.5-1.5 mg m^{-3} (figure 4.6 (**e**)) in the IcB and IrB. This bloom was relatively strong compared to the previous years in both the IcB and IrB, which did not have such high chl-*a* concentrations so early. The highest chl-*a* concentration (>2 mg m^{-3}) at around 20-25°W in April was due to a port call to Reykjavik. The waters were supersaturated for a short period at around 30°W in late January to early February, a less distinct supersaturation than previous years.

4.1.7 2011 *Nuka* data

Figure 4.7 presents the 2011 *Nuka* data. The spatial and temporal representation is relatively good, but no data were obtained in January, and data from March and June are scarse. A total of 36893 measurements were obtained in 2011 (see table 4.1). The shallow bottom depths in the IcB in March, April, August and November in figure 4.7 (**a**) indicate that the ship was on its way to port calls in Iceland (port call in April 16, August 23 and November 24), or took different routes (sailed north of Iceland in March). Hence we disregard the chl-*a* peak in the IcB in August. Few chl-*a* observations, see figure 4.7 (**e**), were available in the IrB due to cloud cover.

Like in 2009, the MLD in the Iceland Basin and Irminger Sea shoaled late, and reached depths < 50 m in June, causing a late phytoplankton bloom. The reason for the late shoaling was, like in 2009, a late warming of the water column: the SST did not start to increase until June. This was reflected in high May fCO_2 values, around 360-380 μatm.

In the North Sea the spring bloom started in March in the eastern part, and evolved westward with time, indicated by the high chl-*a* concentrations, up to 5 mg m^{-3}, and very low fCO_2, less than 280 μatm. The chl-*a* data show that a fall bloom took place in eastern parts in August and September, with chl-*a* concentrations up to 2 mg m^{-3} and fCO_2 less than 320 μatm. The main difference compared to the previous years, disregarding the fCO_2 drawdown due to the fall bloom, was the relatively high fCO_2 values, around 340 μatm, in July and August. July and August fCO_2 values have been much lower in the previous years, with values down to 260-280 μatm. The SST was not

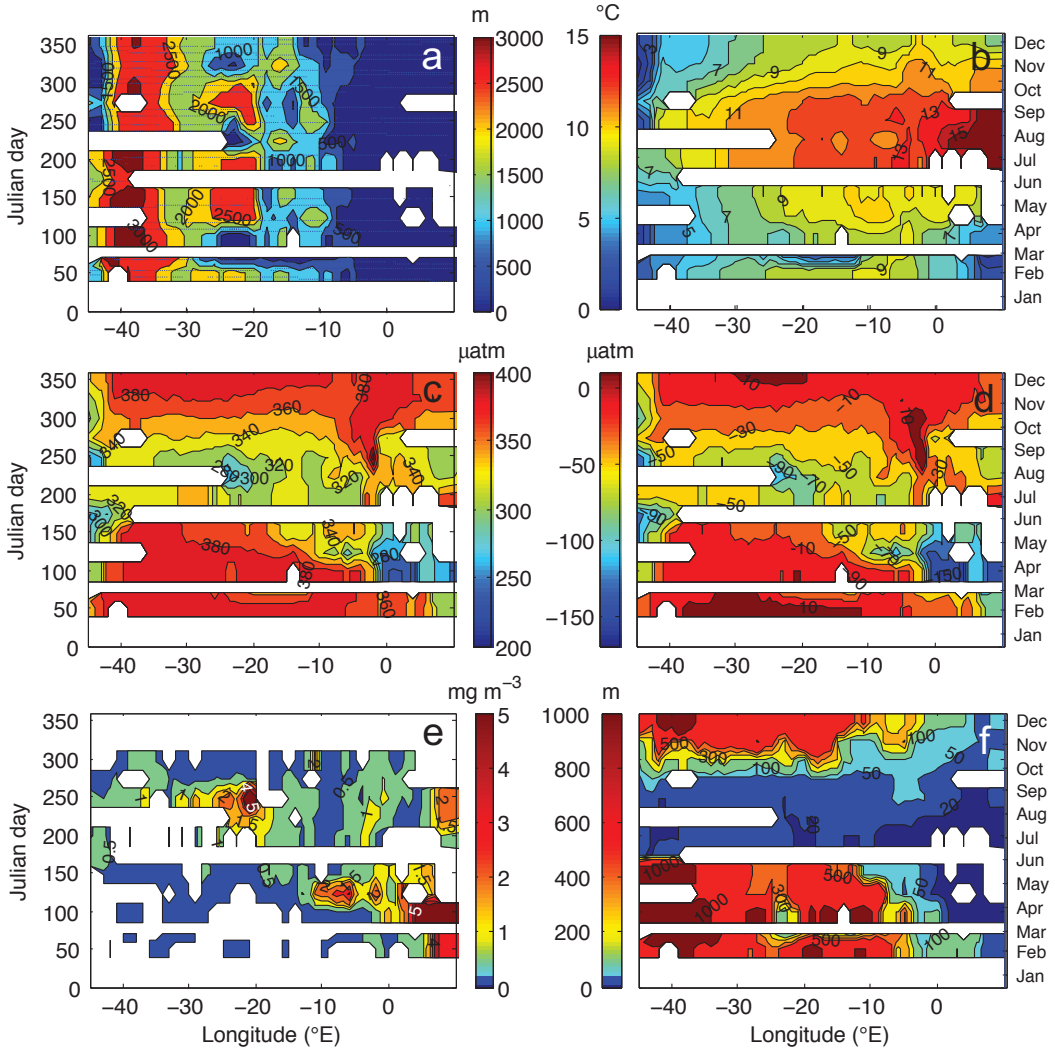

FIGURE 4.7: Hovmöller diagrams of (**a**) *Nuka* bathymetry ship tracks (blue lines), (**b**) SST, (**c**) fCO_2, (**d**) ΔfCO_2, (**e**) chl-*a*, and (**f**) MLD along the ship tracks of *Nuka* in 2011.

considerably higher than other years, so the high fCO_2 is most likely linked to reduced primary production due to cloud cover.

Excluding the port call to Reykjavik on August 23, the June to September fCO_2 in the IcB was between 320 and 340 μatm, and the chl-*a* concentrations reached 2 mg m^{-3}. A strong chl-*a* peak, with concentrations up to 5 mg m^{-3}, occurred in September between longitudes 20 and 25 °W. This did not coincide with a port call, and was not associated with unusually low fCO_2 values. Investigating this further, the chl-*a* concentrations measured at these longitudes were unrealistically high, with concentrations up to 15 mg m^{-3}, and the chl-*a* data are not considered reliable. Almost no chl-*a* data were available from the Irminger Sea during summer. The summer fCO_2 drawdown was delayed due

to a late spring bloom, and from June to September the values were around 340 μatm, a normal summertime fCO_2 value in the IrB.

4.1.8 2012 *Nuka* data

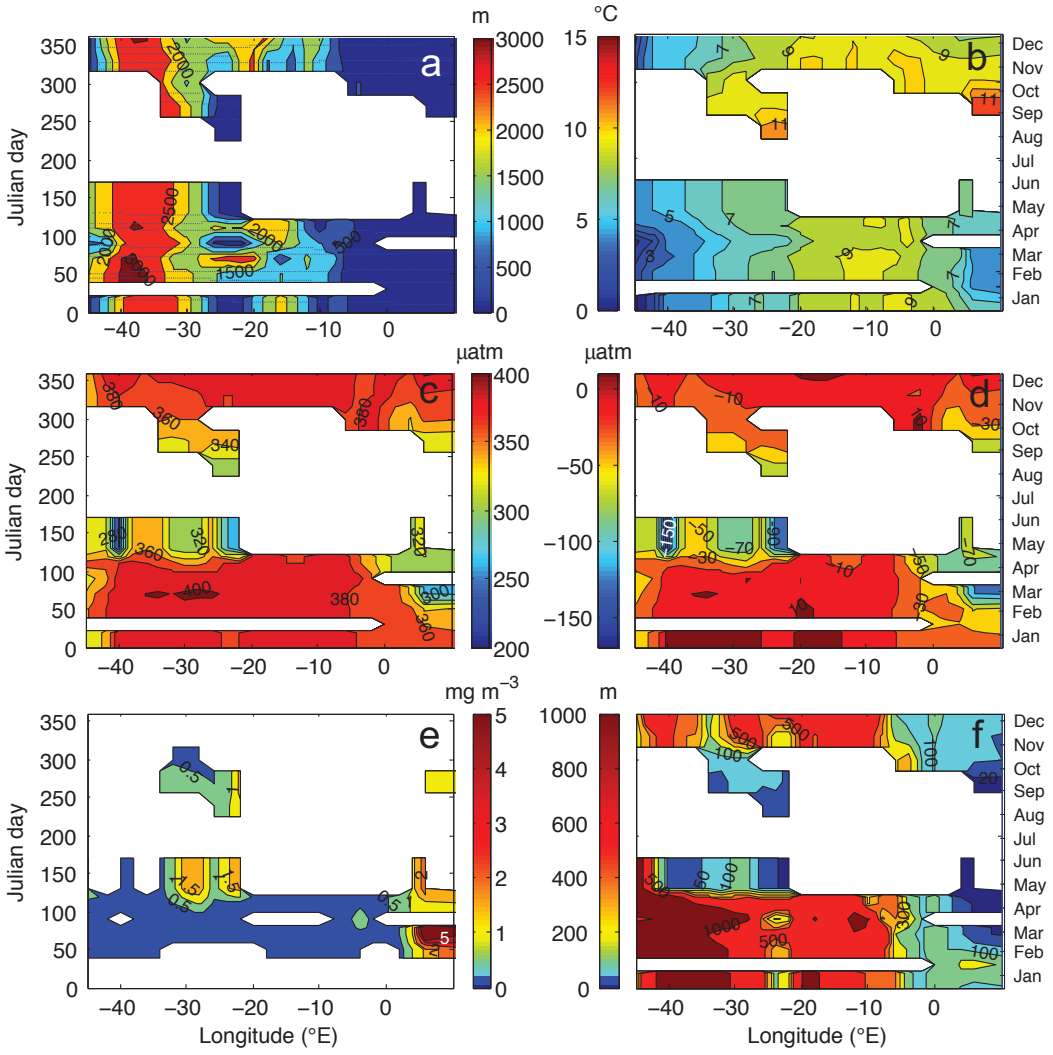

FIGURE 4.8: Hovmöller diagrams of (**a**) *Nuka* bathymetry ship tracks (blue lines), (**b**) SST, (**c**) fCO_2, (**d**) ΔfCO_2, (**e**) chl-*a*, and (**f**) MLD along the ship tracks of *Nuka* in 2012.

Figure 4.8 presents the 2012 *Nuka* data. No data are available for June, July and August, and data from May, September and October are scarce. It is therefore difficult to compare the seasonal cycle to the previous years. A total of 30962 measurements were obtained in 2010. Additionally, the reoccurring shallow bathymetry in the IcB indicate several port calls, which further complicate the process of comparing it with other years. The ship had port calls January 14-15, February 11, March 24, May 6, September 9, November 11 and December 2.

The fCO_2 data in figure 4.8 (**c**) show that 2012 was the first year with $fCO_2 > 400$ μatm. These values occurred around 25-35°W in March. This is linked to the increasing uptake of CO_2 due to anthropogenic CO_2. A chl-*a* peak occurred in the eastern NS in February to March, with concentrations up to 5 mg m^{-3} in figure 4.8 (**e**), and associated low fCO_2 values, under 300 μatm as seen in figure 4.8 (**c**).

The shallow MLD, high chl-*a* and low fCO_2 values in the Iceland Basin in May was due to the port call on May 6th. In the Irminger Sea the MLD shoaled relatively early, with depth < 50 m, in May, and the fCO_2 was reduced to 340 μatm. The low fCO_2, less than 280 μatm, and strong undersaturation, -150 μatm, around 40°W in May were most likely water from the East Greenland current.

4.1.9 2013 *Nuka* data

Figure 4.9 presents the 2013 *Nuka* data. Few measurements from May and July makes it difficult to see the full sesonal cycle and compare with the other years. A total of 40368 measurements were obtained in 2013 (see table 4.1).

Two chl-*a* peaks can be identified in the NS, the first in March and April, and the second in October, indicating a fall bloom (see figure 4.9 (**e**)). Figure 4.9 (**c**) shows that a strong fCO_2 drawdown to around 300 μatm coincided with the spring bloom but not with the fall bloom. This was seen in 2006, 2008 and 2009 too, where no strong fCO_2 drawdown was associated with the fall bloom. This was attributed to occurrence of regenerated rather than new production.

In the Iceland Basin and Irminger Sea the MLD reached depths < 50 m in June (see figure 4.9 (**d**)). The fCO_2 data show relatively high fCO_2 values in June, around 340 μatm in the IcB and around 360-380 μatm in the IrB, indicating a late onset of the spring bloom. Figure 4.9 (**e**) reveal a lot of gaps in the chl-*a* data during summer, and the reason is most likely reduced satellite coverage due to clouds. Cloud cover during spring, together with a late warming of the water and shoaling of the MLD, was most likely the reason for the delayed spring bloom indicated by the high June fCO_2 values. The summer fCO_2 drawdown was not strong, with values between 340 and 360 μatm in the IcB and IrB from July to September. Supersaturation occurred at 20°W in January, and at 30°W in April. A supersaturation in April is unusual, and it was the first time this happened. Again, this is most likely connected to the late onset of the spring bloom.

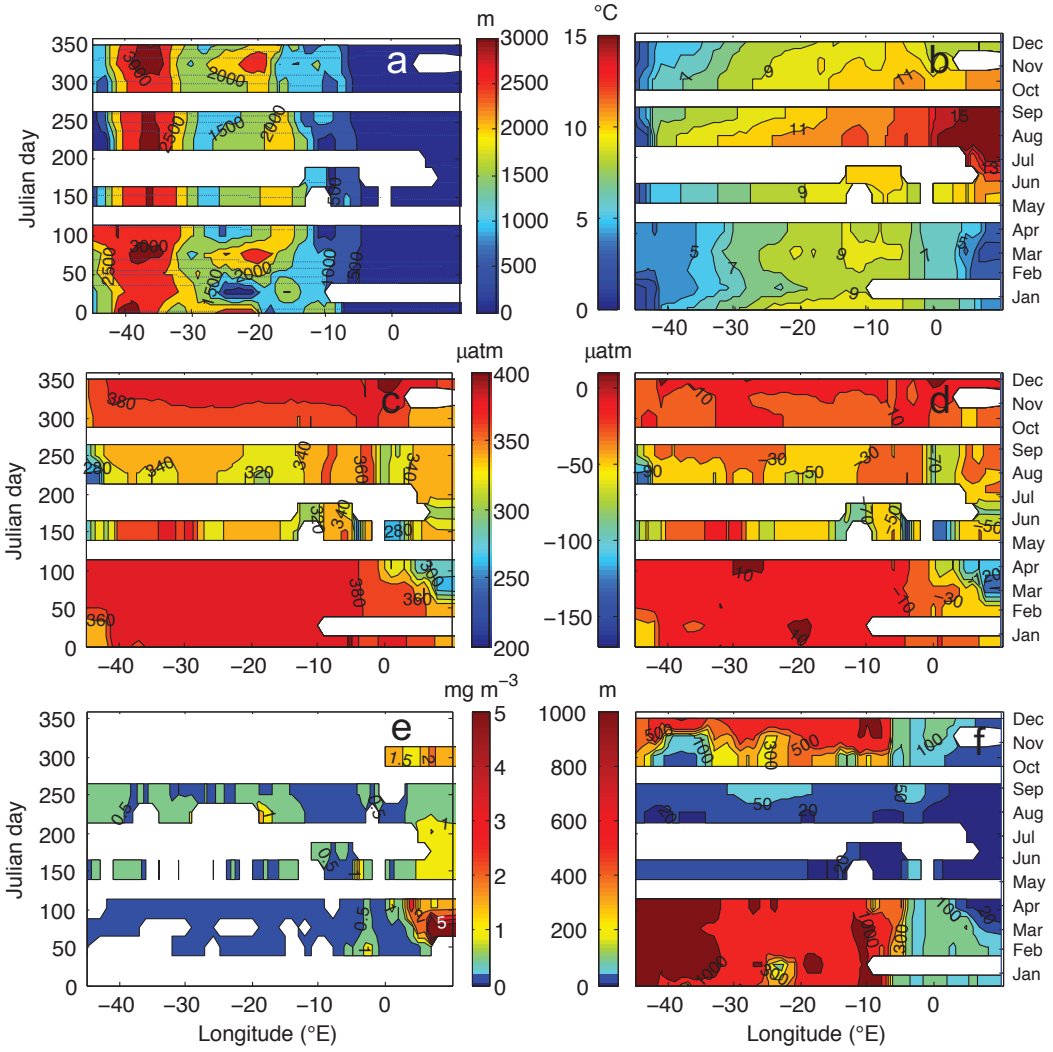

FIGURE 4.9: Hovmöller diagrams of (**a**) *Nuka* bathymetry ship tracks (blue lines), (**b**) SST, (**c**) fCO_2, (**d**) ΔfCO_2, (**e**) chl-*a*, and (**f**) MLD along the ship tracks of *Nuka* in 2013.

4.1.10 Summary

It is clear that the seasonal cycle in the North Sea follow a different pattern than in the Iceland Basin and the Irminger Sea. Firstly, the onset of the spring bloom happens up to 4 months earlier than in the two other basins. The spring bloom starts in the eastern part of the basin, and shows a tendency to propagate westward with time, following the shoaling of the MLD. Secondly, the strength of the bloom is much stronger, with the highest chl-*a* concentrations, over 5 mg m^{-3}, and lowest fCO_2 values, under 280 μatm, during the strongest blooms.

Focusing on the IcB and IrB, the years with the lowest summer fCO_2 were 2007, 2008 and 2009. In these years, fCO_2 fell to values between 300 and 320 μatm, while in the

other years, typical fCO_2 values during summer were 320 μatm or higher. In 2008 and 2009 the low summer fCO_2 were mainly restricted to the IcB, and as expected it corresponded to higher than usual chl-a concentrations in the IcB. In 2007 the low fCO_2 values were restricted to the IrB. 2007 was an exception, in the others years the summertime fCO_2 drawdown was generally stronger in the IcB than in the IrB. In 2007 there was no clear connection between low fCO_2 and unusually high chl-a in the IrB. This probably reflects that a 1:1 relationships can not be expected between fCO_2 and chl-a.

In 2008 and 2010 the shallow mixed layer in the IcB and IrB was formed early, reaching depths < 50 m in May, compared to June the other years. The chl-a data from 2008 and 2010 in figure 4.4 and 4.6 (**e**) show high May chl-a concentrations in the IcB, indicating that the early shoaling of the MLD set the stage for an early spring bloom in the Iceland Basin in these years. The early shoaling of the mixed layer depth did not affect the onset of spring bloom in the Irminger Sea, where no early spring bloom was evident in 2008 and 2010.

4.2 Interannual variations in selected oceanographic regions

The aim of this thesis is to identify the year to year variations in summertime fCO_2 and their drivers. The first objective is to establish which years exhibit unusual fCO_2 values, and then connect these anomalies to oceanic drivers and climate forcing. This section evaluates the interannual summertime fCO_2 and fCO_2^{ytn} variations in two of the oceanographic regions covered by *Nuka Arctica*: the Iceland Basin and the Irminger Sea as defined in figure 3.4. See section 3.9 for calculations of fCO_2 and fCO_2^{ytn}. Both fCO_2 and fCO_2^{ytn} will be presented in this section in order to demonstrate the effect the year and temperature normalisation has on the observed fCO_2 values. To show the characteristics of the seasonal cycle, the winter months are included in the figures of monthly mean data, but it is the summer months that are the main focus of the analysis. Variations in summertime fCO_2^{ytn} are driven by primary production, which is caused by shallow mixing and detected by chl-*a*. Chl-*a* and mixed layer depth data collocated in time and space with the *Nuka* fCO_2 data were therefore used to explain the observed variations in fCO_2^{ytn}. Regression analyses between the parameters have been carried out to detect any significant relationships.

4.2.1 The Irminger Sea

Interannual variations of fCO_2

Figure 4.10 shows the monthly mean observed fCO_2 in the Irminger Sea, measured aboard *Nuka* from 2005 to 2013. The winter values (November-March) are between 380 to 400 μatm, which is in accordance with the winter values in figures 4.1-4.9. The drawdown of fCO_2 starts in May when the spring bloom starts, and minimum fCO_2 values are reached in June-August. By August the summer stratification starts to collapse and CO_2 rich water is mixed up, resulting in increased surface fCO_2. If the light availability is sufficient a fall bloom can be initiated when mixing starts due to entrainment of nutrients into the well lit surface layer. Hence, this is a feature that is most likely to happen if the MLD deepens early (Martinez et al., 2011). By November the fCO_2 reaches winter values. Most of the years follow this cycle, but some years stand out with special features that deviates from the normal seasonal cycle. These years will be identified in this section. The focus of the following presentation of the *Nuka* fCO_2 data will be on the timing of spring/summer fCO_2 drawdown, the magnitude of the drawdown, and occurrences of fall blooms.

The fCO_2 data presented in figure 4.10 show unusually low fCO_2 values in May 2006 and 2012, at approximately 340 and 325 μatm respectively. The low May fCO_2 values

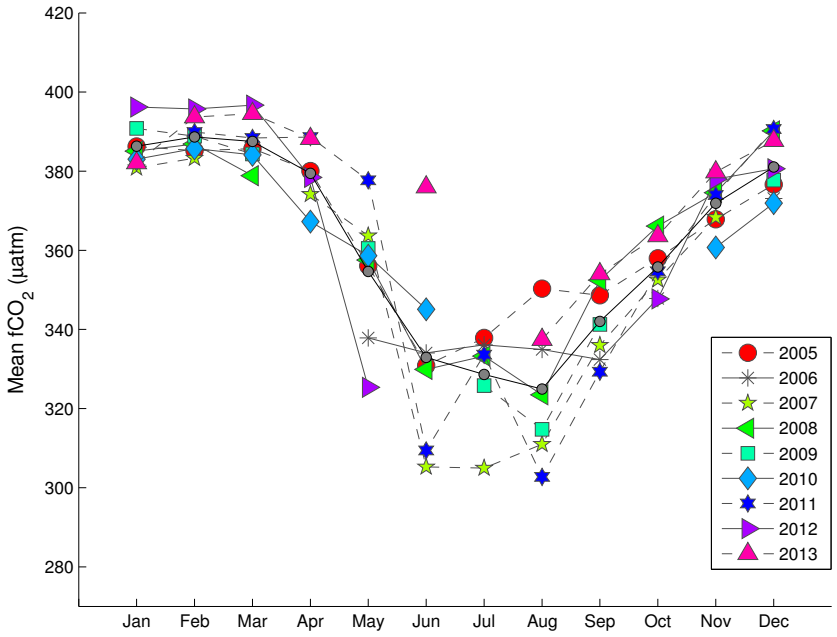

FIGURE 4.10: Monthly mean fCO_2 data as observed from MV *Nuka Arctica* in the IrB from 2005 to 2013. The grey circles are long term monthly means based on the same data.

indicate an early onset of the spring bloom. A late spring bloom most likely occurred in 2011 and 2013 indicated by unusually high spring and early summer fCO_2 values: 380 μatm in May 2011 and 380 μatm in June 2013. Figure 4.10 (and figure 4.3 (**c**)) shows that the 2007 June to August fCO_2 was very low, between 305 and 315 μatm. Also, in 2011, after a late bloom the fCO_2 values decreased by 70 μatm, to approximately 310 μatm, from May to June. This indicate that even tough the spring bloom was late, it was relatively strong when first initiated. No data were available for May and July 2013, but high August fCO_2 values, around 340 μatm, indicates that the summer fCO_2 drawdown was weak in 2013. In 2005 and 2006 there was a weak fCO_2 drawdown from August to September, indicating a fall bloom.

Interannual variations of fCO_2^{ytn}

When adjusting monthly mean fCO_2 to a reference year (described in section 3.9) all observations prior to 2009 will increase, all observations after 2009 will decrease and 2009 will remain unchanged, see figure 4.11a. The temperature normalisation (described in section 3.9) will increase fCO_2 in years with low temperatures and it will decrease fCO_2 in years with high temperatures, see figure 4.11b. Figure 4.12 shows the net effect of the year an temperature normalisation, denoted ΔfCO_2^n (fCO_2^{ytn} - fCO_2). For large positive or negative ΔfCO_2^n temperature contribute the most. Large positive/negative

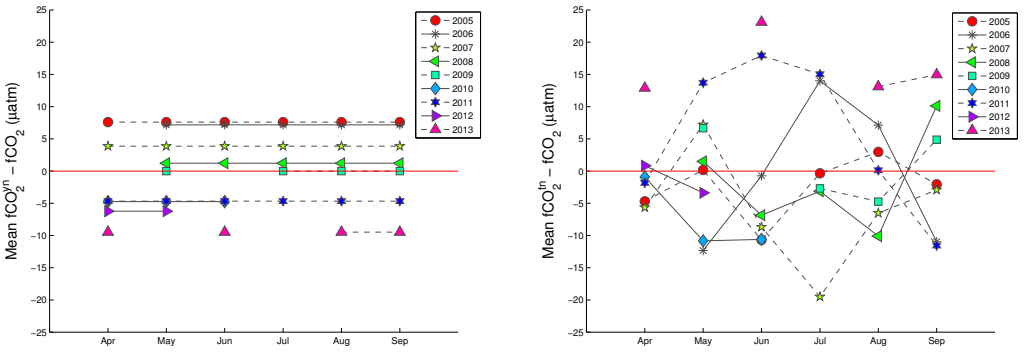

(A) Effect of fCO_2 adjusted to a reference year (2009).

(B) Effect of fCO_2 normalised to monthly mean temperatures.

FIGURE 4.11: Effect of the year (A) and temperature (B) normalisation on fCO_2 in the IrB.

values, indicate that unusually cold/warm waters in the respective year hid biological high/low fCO_2 values. In July 2006 fCO_2^{ytn} increased by almost 25 μatm indicating that very low July temperatures in the Irminger Sea caused low fCO_2 values. In May and June 2010 and July 2007 fCO_2^{ytn} decreased by approximately 15 μatm, indicating that those months were dominated by relatively warm water, hiding the full drawdown effect by biological activity.

fCO_2^{ytn} is presented in figure 4.13. Chl-a data are presented in figure 4.14 and are used to define the strength of the primary production. An increase in chl-a which coincides with a fCO_2^{ytn} decrease strongly implies that the fCO_2^{ytn} drawdown is a response to primary production. Figure 4.13 shows low fCO_2^{ytn} values in May 2006 and 2012, approximately 330 μatm and 315 μatm. Figure 4.14 reveals that the low fCO_2^{ytn} coincided with high chl-a concentrations in both years, confirming that an early spring bloom was responsible for the early fCO_2^{ytn} drawdown. Figure 4.13 also reveals relatively low May fCO_2^{ytn} values in 2010, around 345 μatm compared to a mean around 360 μatm. The negative ΔfCO_2^n in figure 4.12 indicates that warm temperatures masked the biological drawdown. The chl-a data show relatively high chl-a concentrations in May 2010, implying that an early spring bloom did occur in 2010. High fCO_2^{ytn} values ($\sim$ 390 μatm) occurred in May 2011 and June 2013, strengthening the indications of a late spring bloom in these years. Figure 4.12 shows a positive ΔfCO_2^n of around 10 μatm in May 2007 resulting in a fCO_2^{ytn} value around 375 μatm. The chl-a data show unusually low May chl-a concentrations in 2007 and 2011 and in June chl-a 2013, which imply that the high spring fCO_2^{ytn} values in these three years were a result of a delayed spring bloom.

Removing the effect of temperature and expected trend with time resulted in abnormally low fCO_2^{ytn} values in June and July 2007, 300 μatm and 290 μatm respectively (see figure

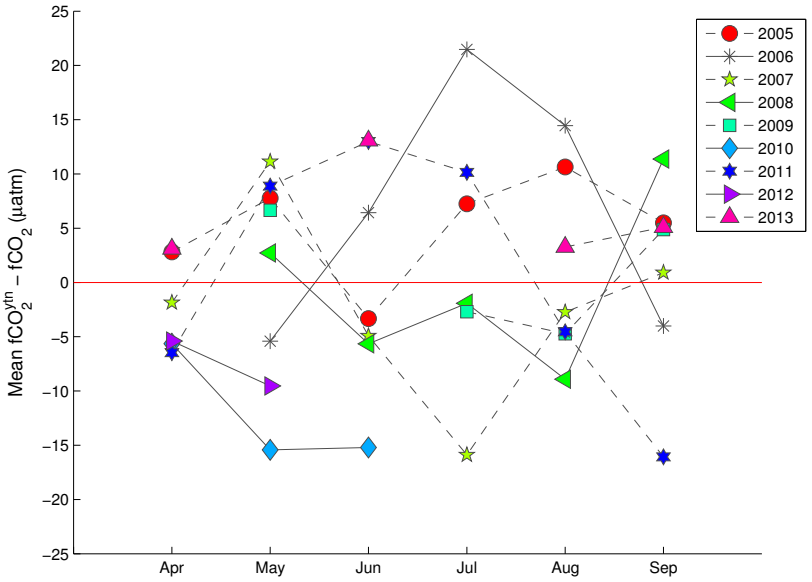

FIGURE 4.12: The combined effect of year and temperature normalisation on fCO_2 in the IrB.

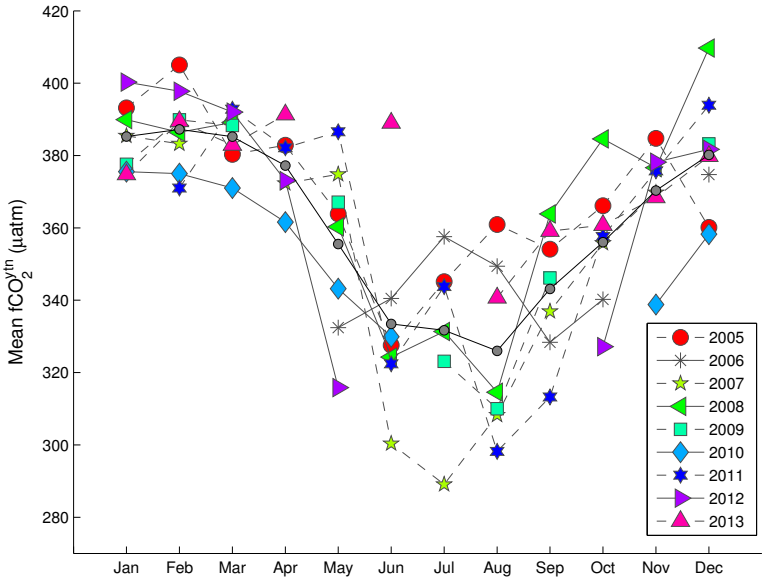

FIGURE 4.13: Monthly mean fCO_2^{ytn} data as observed from MV *Nuka Arctica* in the IrB from 2005 to 2013. The grey circles are long term monthly means based on the same data.

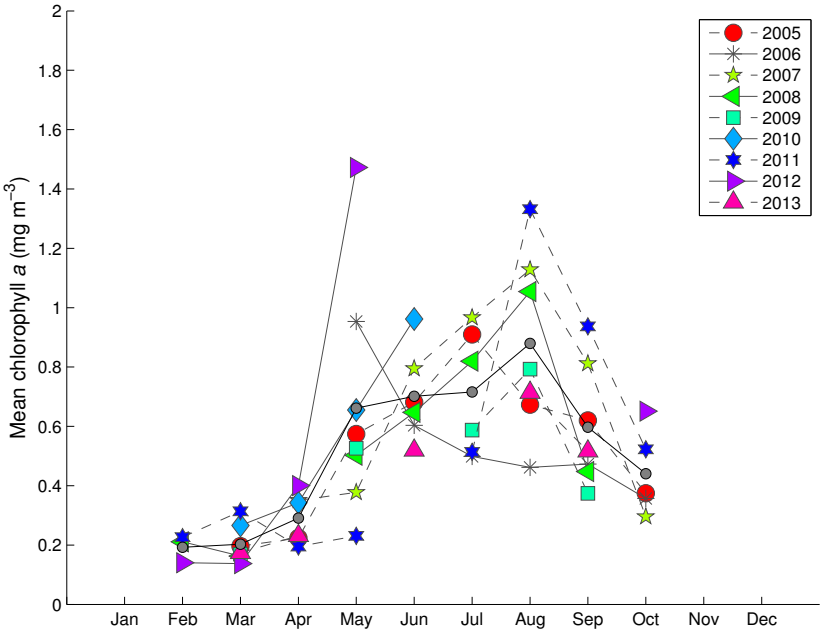

FIGURE 4.14: Monthly mean chl-a concentration collocated with *Nuka* data in the IrB from 2005 to 2013. The grey circles are long term monthly means based on the same data.

4.13). This indicates that the unusually low summer fCO_2 values seen in figure 4.10 were not a result of unusually low temperatures but rather despite high temperatures, and due to strong biological activity in the summer of 2007. This is reflected in the chl-a concentration which gradually increases through the summer with a peak chl-a concentration in August of $\sim$ 1.1 mg m^{-3}. Figure 4.12 shows a ΔfCO_2^n increase of approximately 12 μatm in June 2011 resulting in a fCO_2^{ytn} value around the mean, approximately 325 μatm, figure 4.13. This indicate that the unusually low June fCO_2 value this year, evident in figure 4.10, was driven by low temperatures. Figure 4.12 shows that fCO_2 in 2006 increased when correcting for temperature and fCO_2 trend, resulting in high fCO_2^{ytn} values throughout the summer of 2006. This indicates that unusually low temperatures caused the low fCO_2 values. The high June to August fCO_2^{ytn} values are explained by weak biological activity and/or unusually mixing events in the summer of 2006. The corresponding chl-a concentration was unusually low in 2006, with values around 0.5-0.6 mg m^{-3} from June to September, compared to a mean around 0.7-0.9 mg m^{-3}.

fCO_2^{ytn} decreases from August to September in 2005 and 2006, indicating a fall bloom. Martinez et al. (2011) defined a fall bloom as a chl-a peak between September and January. Following this the fCO_2 drawdown may indicate a fall bloom if it is connected to an increase in chl-a. Figure 4.14 shows a decrease in chl-a concentration from August

to September in 2005, refuting the possibility of a fall bloom. In 2006 there was a slight chl-*a* increase, suggesting that a weak fall bloom occurred in 2006. After relatively high fCO_2^{ytn} values in July 2011 the August and September fCO_2^{ytn} values were exceptionally low, see figure 4.13. Such low values indicate that a fall bloom occurred. The chl-*a* concentration rise from $\sim$ 0.5 mg m^{-3} to as much as $\sim$ 1.4 mg m^{-3} from July to August. The chl-*a* concentration in September of $\sim$ 1 mg m^{-3} is the highest September concentration observed in the time series. There is a good correspondence between fCO_2^{ytn} and chl-*a* data, which indicate that an intense, and relatively long lasting bloom occurred in the fall of 2011.

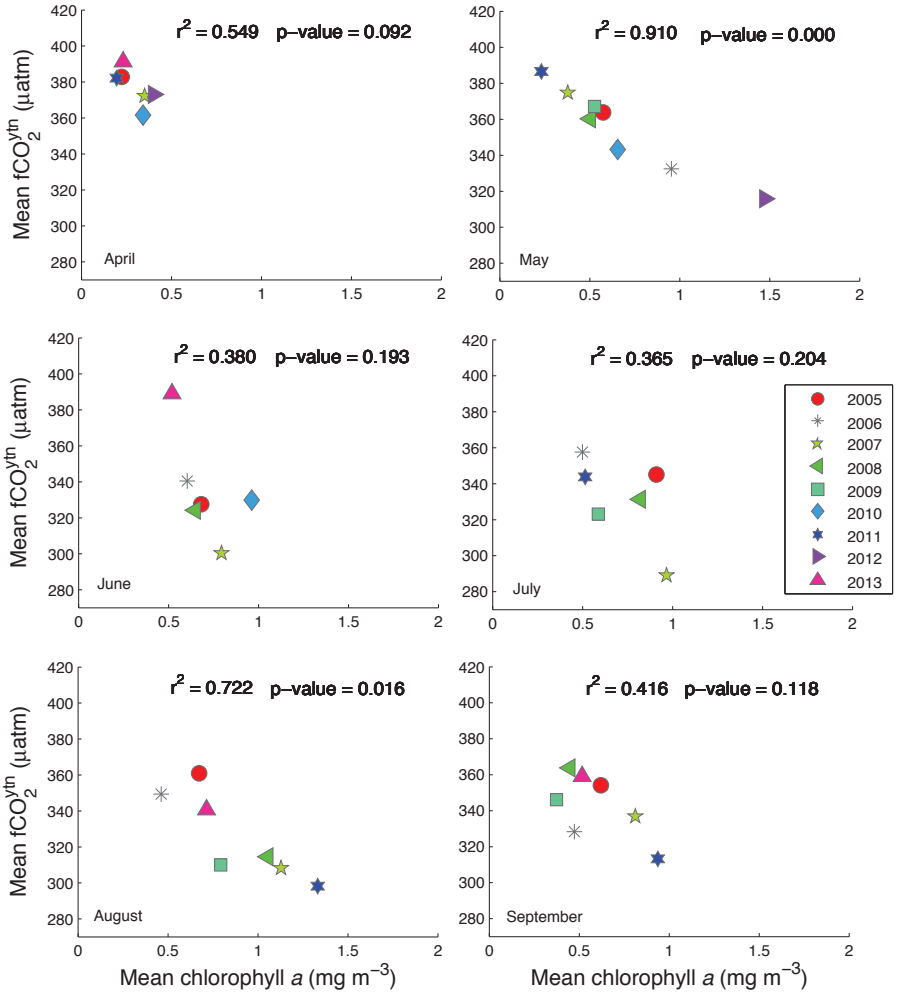

FIGURE 4.15: Monthly mean (April to September) fCO_2^{ytn} plotted against monthly mean chl-*a* collocated with the *Nuka* data in the IrB from 2005 to 2013.

fCO_2^{ytn} vs. chl-*a*

Figure 4.15 shows the monthly mean (April to September) fCO_2^{ytn} from *MV Nuka*

Arctica plotted against the monthly mean chl-*a* collocated with the *Nuka* data. Also included in the figure are the coefficient of determination, r^2, and the p-value. The regression is performed in order to see when and how dependent fCO_2^{ytn} is to changes in chl-*a*. The correlation is negative for all months, i.e when chl-*a* increases, fCO_2^{ytn} decreases. The relationship is strongest in May (r^2=0.919, p=0) and August (r^2=0.722, p=0.016). In June, July and September the correlation is not statistically significant at a significance level of 90% (p>0.1). The strong correlation in May is expected, the fCO_2^{ytn}-chl-*a* relationship is strongest during blooms when there is a reduction in fCO_2^{ytn} due to primary production (Olsen et al., 2008). 2007, 2008 and 2011 reached their peak chl-*a* concentration in August with corresponding low fCO_2 values. 2005, 2006 and 2013 had the lowest chl-*a* values in August. These are the two groups that form the base of this relationship. For the high fCO_2^{ytn}, low chl-*a* group, a combination of upwelling of DIC rich water and reduced primary production most likely dominates. For the low fCO_2^{ytn}, high chl-*a* group primary production continues, increasing chl-*a* and reducing fCO_2^{ytn}. Hence, the relationship in August possibly reflects the interannual variations in the length of the main productive season. From the results presented in this figure, it is clear that the timing of the fCO_2^{ytn} drawdown is controlled by the chl-*a*, whereas the magnitude is not. The timing of the fCO_2^{ytn} increase is also possibly controlled by the chl-*a* in the IrB, impacted by the perseverance of the phytoplankton bloom.

fCO_2^{ytn} vs. mixed layer depth

Figure 4.16 shows the monthly mean (April to September) fCO_2^{ytn} plotted against the monthly mean MLD collocated with the *Nuka* data. Weaker relationships are expected between fCO_2^{ytn} and MLD than between fCO_2^{ytn} and chl-*a*, as the MLD affects the primary production (chl-*a*), which in turn directly affect fCO_2^{ytn}. This relationship is still interesting to explore as it gives an indication of the water column forcing on the fCO_2^{ytn}. The only statistical significant correlation (at a significance level of 90%) between MLD and fCO_2^{ytn} occur in May and July, with r^2=0.453, p=0.067 in May and r^2=0.922, p=0.002 in July. Figure 4.16 shows large interannual variations in May MLD, and in June-August the MLD was around 8-40 m. 2006 and 2008 had MLDs more shallow than 100 m in May, which fits well with the observed early spring bloom onset in 2006. An early spring bloom did not occur in 2008 even though the MLD was around 50 m, which should be shallow enough to initiate a spring bloom. This shows that a shallow May mixed layer depth does not inevitably result in an early spring bloom. Deep May MLD on the other hand, implicate a late drawdown. This is related to Sverdrup's critical depth, Cr_d (Sverdrup, 1953). The mixed layer depth need to be shallower than the critical depth in order to initiate a net phytoplankton growth and increase chl-*a*. But a MLD shallower than the Cr_d is not always sufficient and does not necessarily

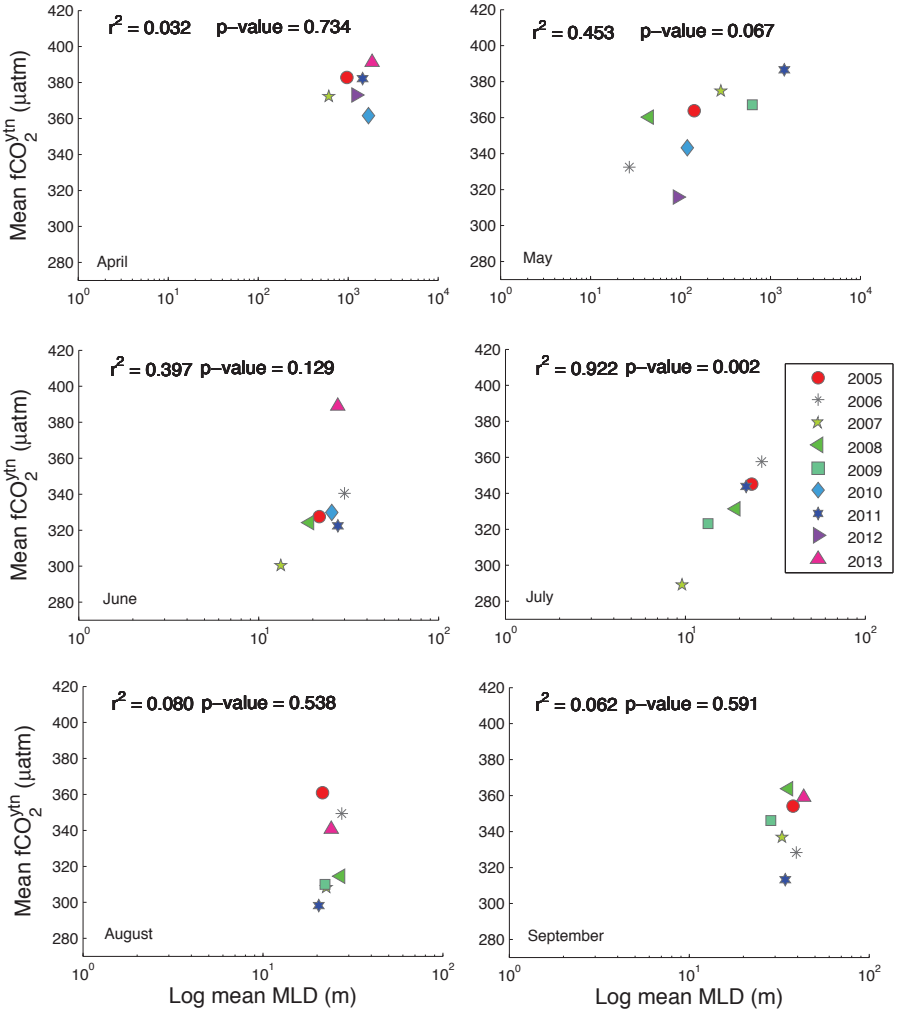

FIGURE 4.16: Monthly mean (April to September) fCO_2^{ytn} plotted against monthly mean MLD collocated with the *Nuka* data in the IrB from 2005 to 2013. Note the different x-axis definitions in the two upper plots.

mean that the phytoplankton bloom starts immediately (Henson et al., 2006). This is reflected in the data presented here, a fCO_2^{ytn} drawdown and spring bloom does not necessarily follow a formation of a shallow MLD.

The MLD explains around half the fCO_2^{ytn} variation in May (r^2=0.453) which indicate that the timing of the fCO_2^{ytn} drawdown is in part governed by the MLD. The magnitude of the bloom, with r^2=0.922 in July, is likely to be governed by the MLD. This is linked to the water column forcing of fCO_2^{ytn}. Deep MLD gives high fCO_2^{ytn} which most likely reflects that high DIC water leaks to the surface when the MLD is deep, which again is linked to a weak stratification.

4.2.2 The Iceland Basin

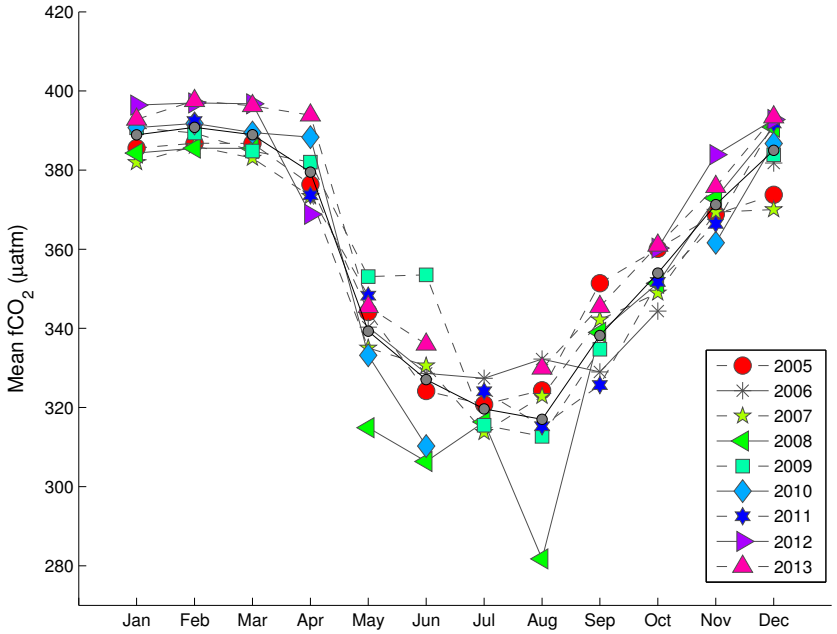

FIGURE 4.17: Monthly mean observed fCO_2 data as observed from MV *Nuka Arctica* in the IcB from 2005 to 2013. The grey circles are long term monthly means based on the same data.

Interannual variations of fCO_2

Figure 4.17 shows the monthly mean observed fCO_2 in the Iceland Basin, measured aboard *Nuka* from 2005 to 2013. The seasonal cycle is the same as in the Irminger Sea and will not be further discussed here. In section 4.1 it was pointed out that the MLD in 2008 and 2010 shoaled earlier than other years and initiated an early spring bloom. The monthly mean fCO_2 data in figure 4.17 shows low fCO_2 values, around 320 μatm in May 2008, further confirming that an early spring bloom occurred in 2008. Figure 4.17 does not reveal unusually low fCO_2 values in May 2010, despite the early shoaling observed in figure 4.6. On the other hand, 2009 was mentioned as a year with an unusually late shoaling of the MLD, up to two months later than other years. This is evident in figure 4.17, the fCO_2 in May and June 2009 was around 350 μatm. This indicate a late onset of the spring bloom this year. 2008 had exceptionally low fCO_2 values in June (310 μatm) and August (280 μatm) after an early bloom. In July fCO_2 was closer to the mean, around 320 μatm. This is also in accordance with figure 4.4 where 2008 stood out as the year with lowest fCO_2 in the IcB. In June 2010, fCO_2 was unusually low, but unfortunately no data were available for the rest of the summer. A fCO_2 drawdown occurred from August to September 2006, which indicate a fall bloom. All the other years featured a relatively strong fCO_2 increase from August to September.

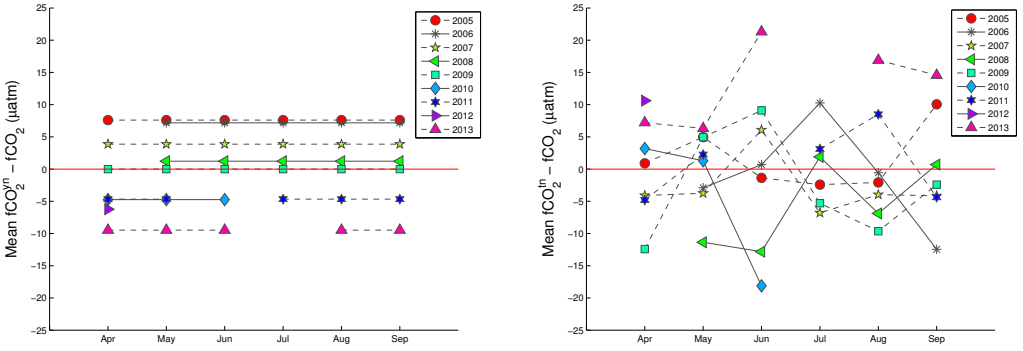

(A) Effect of fCO_2 adjusted to a reference year (2009).

(B) Effect of fCO_2 normalised to monthly mean temperatures.

FIGURE 4.18: Effect of the year (A) and temperature (B) normalisation on fCO_2 in the IcB.

Interannual variations of fCO_2^{ytn}

Like in section 4.2.1 I include figures 4.18a, 4.18b and 4.19 to show the effect of the normalisation on fCO_2. Figure 4.20 presents the fCO_2^{ytn} data, and shows May 2008 fCO_2^{ytn} values around 305 μatm. Figure 4.19 reveals that the fCO_2 decreased by 10 μatm after normalisation in May 2008, where the largest effect was due to temperature, see figures 4.18a and 4.18b. This indicate that fCO_2 in May 2008 was low despite relatively high temperatures. Figure 4.21 reveal that the chl-a concentration was very high, $\sim$ 1.8 mg m^{-3}, which indicate that an early spring bloom and a strong biological fCO_2 drawdown took place in 2008. High fCO_2^{ytn} values in May 2005 and 2009 indicate late spring blooms these years. The chl-a data, however, does not show particularly low May chl-a concentrations, with values around the mean, of $\sim$ 0.7 mg m^{-3}.

The June and August 2008 fCO_2^{ytn} values were low, around 300 μatm and 280 μatm respectively. In July fCO_2^{ytn} was around the mean, with values $\sim$ 320 μatm. Unfortunately no chl-a data were available from August, but the June and July chl-a concentrations were stable at around 0.9 mg m^{-3}. The chl-a concentrations in June and July do not reflect the large fCO_2^{ytn} differences in June and July. Possible reasons are errors in the fCO_2^{ytn} measurements, or calcification by a Coccolithophores bloom which uses alkalinity and increase fCO_2^{ytn}. This will be further discussed in chapter 5. The low June 2010 fCO_2^{ytn} values in figure 4.20 and the high chl-a concentrations in figure 4.21 indicate a strong biological fCO_2^{ytn} drawdown. Unfortunately, no *Nuka* data were available for the rest of the summer. Figure 4.20 shows high June 2009 fCO_2^{ytn} values, $\sim$ 365 μatm, and low July and August fCO_2^{ytn}, around 320 and 310 μatm, indicating a late, but relatively strong bloom. The chl-a concentration, figure 4.21, in June and July was around 1 mg m^{-3}, although July had a much lower fCO_2^{ytn} value. By August both the fCO_2^{ytn} and the chl-a data show a decrease, hence chl-a does not reflect the

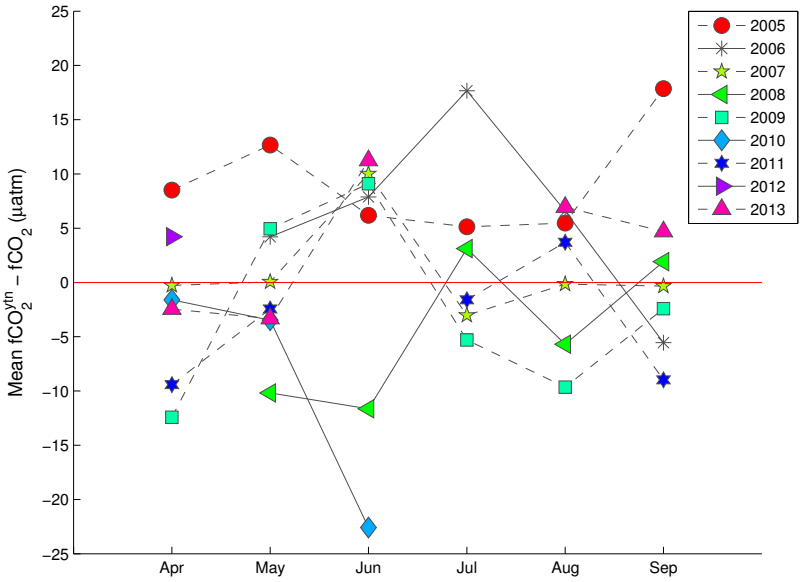

FIGURE 4.19: The combined effect of year and temperature normalisation on fCO_2 in the IcB.

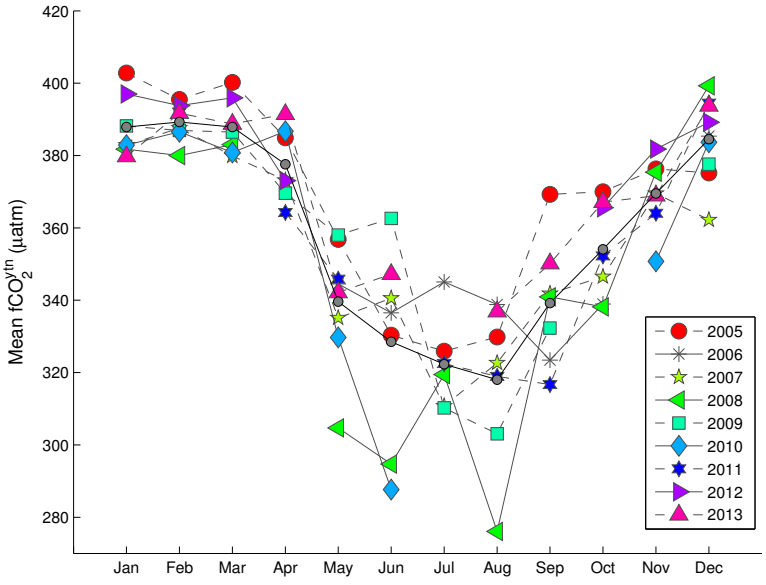

FIGURE 4.20: Monthly mean fCO_2^{ytn} as observed from MV *Nuka Arctica* in the IcB from 2005 to 2013. The grey circles are long term monthly means based on the same data.

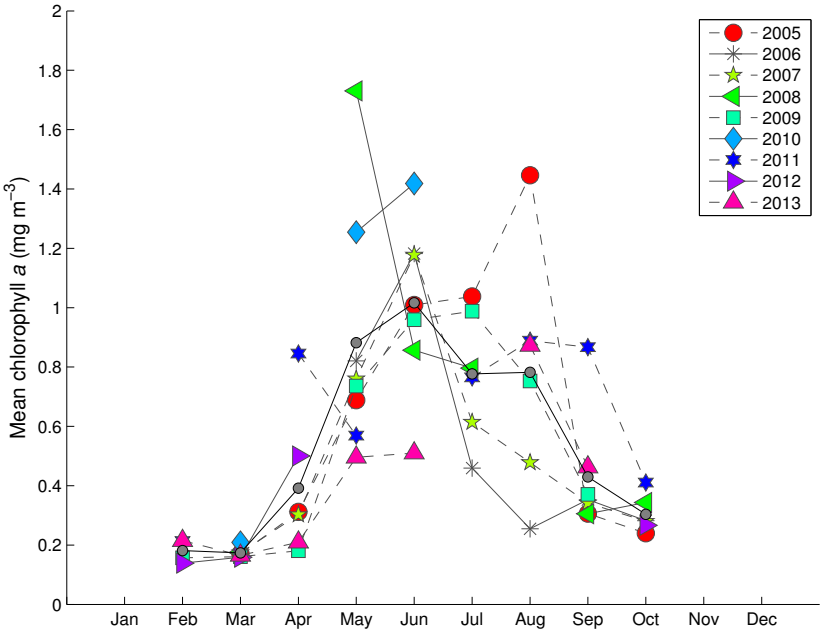

FIGURE 4.21: Monthly mean chl-*a* concentration collocated with the *Nuka* data in the IcB from 2005 to 2013. The grey circles are long term monthly means based on the same data.

fCO_2^{ytn} very well. In 2005 the June to August fCO_2^{ytn} values were around the mean, $\sim$ 330 μatm. The chl-*a* data reveal a chl-*a* increase from 1 mg m^{-3} to 1.5 mg m^{-3} from July to August. Incidents where the chl-*a* concentration increase but the fCO_2^{ytn} is unaffected indicate primary production from regenerated rather than new production. This will be further discussed in chapter 5.

fCO_2^{ytn} data from 2006 and 2011 indicate that a fall bloom took place, with a fCO_2^{ytn} drawdown from August to September. Figure 4.21 shows a small increase in chl-*a* concentration from August to September in 2006, from 0.3 mg m^{-3} to 0.4 mg m^{-3}. This indicate that a weak fall bloom occurred in the Iceland Basin in September 2006. This is probably the small chl-*a* peak evident in figure 4.2 (**e**), at around 30-32°W. In 2011 fCO_2^{ytn} decreased gradually through the summer, and reached a minimum in September with 320 μatm, figure 4.20. The chl-*a* data show relatively high chl-*a* concentrations in August and September, around 0.9 mg m^{-3} in figure 4.21. This is similar to the results from the Irminger Sea, where 2011 had the lowest August and September fCO_2^{ytn} values and the highest chl-*a* concentrations. This indicate that a relatively strong, and long lasting fall bloom occurred in both basins in 2011.

fCO_2^{ytn} vs. chl-*a*

Figure 4.22 shows the monthly mean (April to September) fCO_2^{ytn} from MV *Nuka*

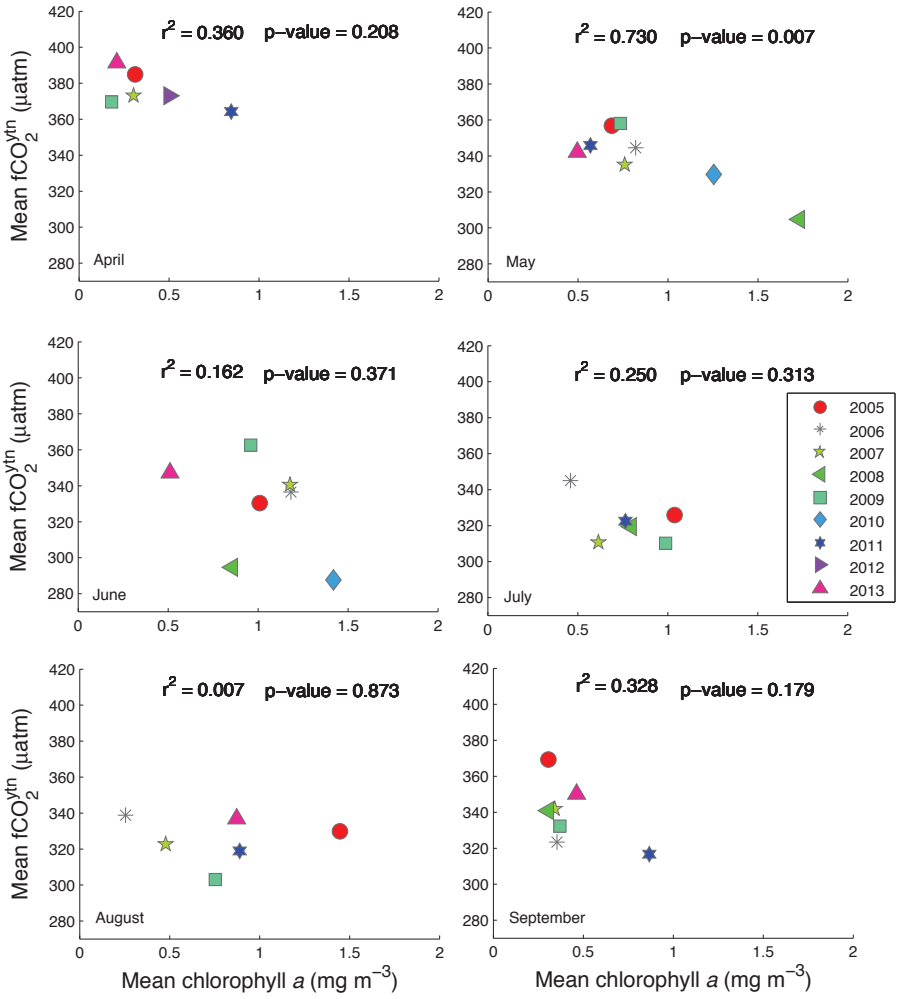

FIGURE 4.22: Monthly mean (April to September) fCO_2^{ytn} plotted against the monthly mean chl-*a* collocated with the *Nuka* data in the IcB ifrom 2005 to 2013.

Arctica plotted against the monthly mean chl-*a* collocated with the *Nuka* data. Also included in the figure are the coefficient of determination, r^2, and the p-value. May is the only month with a significant relationship between fCO_2^{ytn} and chl-*a* with r^2=0.730 and p-value=0.007. The other months have p-values > 0.1 (and $r^2 < 0.4$), which is above the chosen significance level. As mentioned in section 4.2.1, a relationship in May is expected because of the fCO_2^{ytn} reduction by primary production. This shows that the timing of the fCO_2^{ytn} drawdown is controlled by the chl-*a*.

fCO_2^{ytn} vs. mixed layer depth

Figure 4.23 shows the monthly mean (April to September) fCO_2^{ytn} plotted against the monthly mean MLD collocated with the *Nuka* data. The strongest, and only statistical significant ($p < 0.1$), relationships occur in April and September, with $r^2 = 0.507$ and r^2

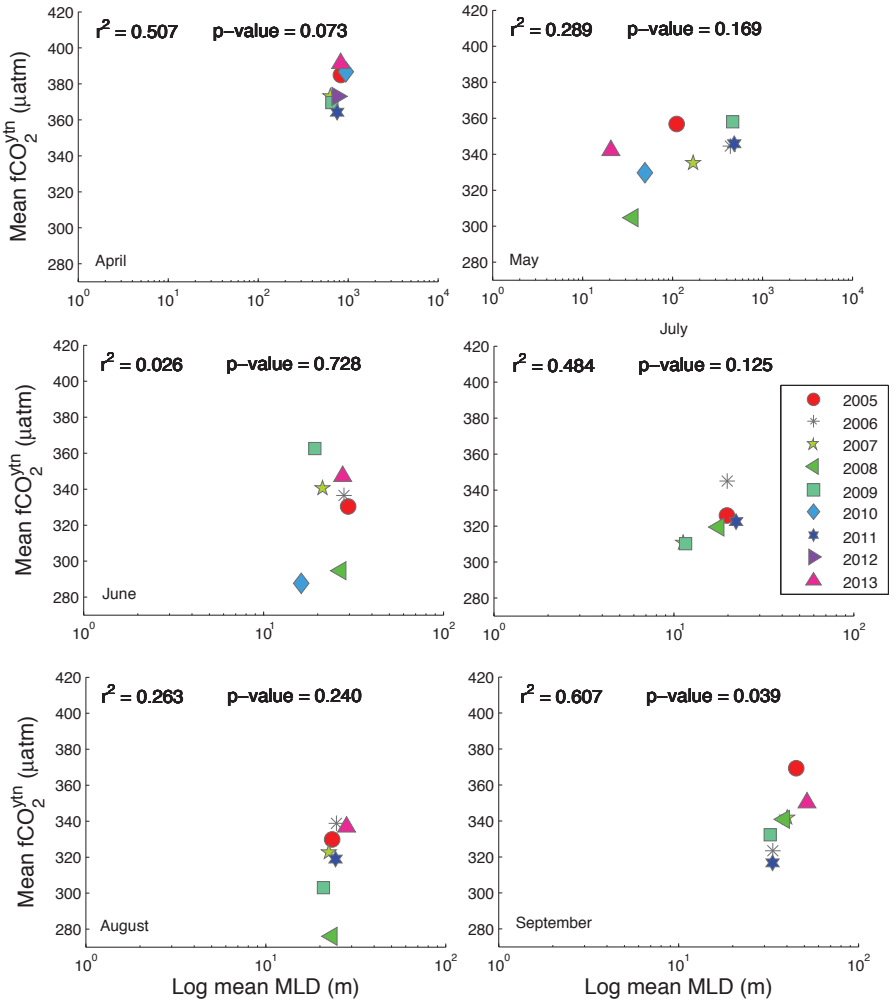

FIGURE 4.23: Monthly mean (April to September) fCO_2^{ytn} plotted against the monthly mean MLD collocated with the *Nuka* data in the IcB ifrom 2005 to 2013.

= 0.607 respectively. In April, the mean MLDs was never shallower than 600 m, and the tendency is for the fCO_2^{ytn} to increase with increasing mixed layer depth. This indicate that a deeper mixed layer depth in April brings more DIC rich water to the surface. However, this is not connected to the onset of the spring bloom, the fCO_2^{ytn} is still high. The correlation in September reflects the water column forcing on the fCO_2^{ytn}. A deep MLD, and most likely weak stratification, enables DIC rich water to reach the surface, whereas shallow a MLD, i.e stronger stratification, inhibit mixing and this prevents DIC rich water from reaching the surface, and together with primary production keeps fCO_2^{ytn} low. This shows that the timing of the fCO_2^{ytn} increase is partly controlled by the mixed layer depth. The correlation between fCO_2^{ytn} and MLD in July, with r^2 = 0.484 and p = 0.125 is not statistically significant. Nevertheless, the tendency is that deeper MLD implies higher fCO_2^{ytn} values as found in figure 4.16, where the correlation

in July was statistical significant.

4.2.3 Summary

Comparing figures 4.13 and 4.20 makes it clear that the summertime fCO_2^{ytn} variations are larger in the Irminger Sea than in the Iceland Basin, and the fCO_2^{ytn} is on average slightly higher in the Irminger Sea. The timing of the fCO_2^{ytn} drawdown is controlled by the onset of the spring bloom, indicated by the strong relationships between fCO_2^{ytn} and chl-*a* in May in both basins ($r^2 = 0.910$ in IrB and $r^2 = 0.730$ in IcB). In July there is a correlation between MLD and fCO_2^{ytn} in the IrB, which indicate that the magnitude of the summer fCO_2^{ytn} drawdown in the IrB is partly determined by the mixed layer depth. Even though there is no statistical significant relationship between fCO_2^{ytn} and MLD in July in the Iceland Basin ($p = 0.125$), a r^2 around 0.5 suggests that a relationship exists in the Iceland Basin as well. By comparing fCO_2^{ytn} and collocated chl-*a* in both basins, it is evident that there is a good correlation between summertime fCO_2^{ytn} and chl-*a* on a seasonal basis This is most likely not reflected in the regression plots since the interannual variability of the fCO_2^{ytn} drawdown is not directly linked to the magnitude of the chl-*a* concentration. Further, the timing and magnitude of fCO_2 drawdown showed no similarities between the basins, except in 2006 when both basins had high fCO_2^{ytn} and low chl-*a* concentrations. This suggest that the oceanic drivers in the two basins are governed by different processes and environmental impacts from year to year.

Chapter 5

Discussion

In chapter 4 I analysed the interannual variations in the observed fCO_2 and the calculated fCO_2^{ytn} from *MV Nuka Arctica* and compared it to collocated chl-*a* and MLD data. I identified the years where temperature was the reason for unusually fCO_2 values, and the years where biology and mixing gave rise to unusually fCO_2 values. There was a good agreement between low/high *Nuka* fCO_2^{ytn} and high/low chl-*a* concentrations and mixed layer depths. However, there are uncertainties of whether the *Nuka* data are representative for the entire Irminger Sea and Iceland Basin. In section 5.1 I discard the *Nuka* observations that I consider unrealistic and not representative of the entire basins based on amount of measurements and coverage of the basins. When the non-representative data are removed, the fCO_2^{ytn} data from the years and months that are considered to be representative for the whole region remain. These will be discussed in section 5.2, where climate forcing of oceanic drivers and fCO_2^{ytn} will be evaluated.

5.1 Representativity of the *Nuka* data

The *Nuka* data have, as mentioned earlier, a good temporal but a bad spatial representation. The only areas of the selected regions represented are the lines that the ship traversed (figure 3.1). Therefore, it is not certain that the data collected aboard MV *Nuka Arctica* are fully representative for the two regions in question, the Irminger Sea and Iceland Basin as defined in figure 3.4. I discard the observations that have a bad spatial and/or temporal representation based on amount of measurements and coverage of the basins. Tables 5.1 and 5.2 show the total amounts of monthly measurements from April to September in the Irminger Sea and Iceland Basin respectively. From the Irminger Sea, months with less than 200 measurements (red in table 5.1) are discarded. From the Iceland Basin, which is defined over a larger area and have more

observations, months with less than 300 measurements (red in table 5.2) are discarded. Figures of monthly cruise tracks (not included) from the IrB and IcB show that months with few measurements, not surprisingly, also have a bad spatial representation. The months which were discarded due to few measurements and bad spatial representation are displayed in table 5.3.

	2005	2006	2007	2008	2009	2010	2011	2012	2013
April	831	0	1071	0	0	163	590	767	750
May	1153	159	789	425	812	1227	248	184	0
June	893	560	936	1181	0	428	60	0	377
July	1065	876	1003	986	1111	0	200	0	0
August	997	750	429	395	982	0	156	0	413
September	530	679	388	441	407	0	473	0	757

TABLE 5.1: Monthly numbers of measurements from the Irminger Sea. Months with less than 200 measurements are marked red.

	2005	2006	2007	2008	2009	2010	2011	2012	2013
April	1028	0	1190	0	503	178	624	694	472
May	1461	236	1071	1024	1381	1551	702	0	307
June	1919	807	915	1062	77	224	0	0	283
July	1621	1670	1576	1174	1459	0	739	0	0
August	1811	1048	1101	62	1818	0	330	0	572
September	1204	1253	694	342	592	0	1042	0	632

TABLE 5.2: Monthly numbers of measurements from the Iceland Basin. Months with less than 300 measurements are marked red.

Irminger Sea

Month	Year
April	2010
May	2006
	2012
June	2011
August	2011

Iceland Basin

Month	Year
April	2010
May	2006
June	2010
	2013
	2009
August	2008

TABLE 5.3: Discarded observations from the Irminger Sea and the Iceland Basin.

5.2 Relationship between fCO_2 and environmental parameters

In section 4.2 the timing of fCO_2^{ytn} drawdown, magnitude of fCO_2^{ytn} drawdown and occurrences of fall blooms were evaluated and compared to the collocated monthly mean chl-*a* and MLD data. Good agreements between these parameters were found for the *Nuka* data. It was revealed that the timing of the fCO_2^{ytn} drawdown is controlled by the chl-*a*. Some unclear relationships between the fCO_2^{ytn} and MLD were presented, but there were indications that the magnitude of the drawdown is to some degree controlled by the mixed layer depth. SST also contribute to the interannual fCO_2 variations, but for fCO_2^{ytn} the effect of temperature was corrected for (section 3.9). This section will focus on the environmental parameters and how they affect the primary production (chl-*a*) and MLD, which in turn determine the fCO_2^{ytn}. Only the year and temperature normalised fCO_2, fCO_2^{ytn}, will be used. This is because the aim is to investigate to what extent environmental parameters affect the biology and mixing: the drivers behind summertime fCO_2^{ytn}.

Monthly mean chl-*a* concentrations were estimated from the eight day, 9 km resolution satellite chl-*a* data from the entire Irminger Sea and the entire Iceland Basin. The monthly mean chl-*a* concentrations from the Irminger Sea and the Iceland Basin are presented in figure 5.1 and 5.10 and will be referred to as chl-a^{IrB} and chl-a^{IcB} respectively. The environmental parameters used are monthly mean sea surface temperatures (figure 5.2 and 5.11), air temperatures (figure 5.3 and 5.12) and wind speeds (figure 5.4 and 5.13) averaged over the entire Irminger Sea and Iceland Basin. The monthly mean MLD data presented in this section are the monthly mean, 12.5 km resolution data from the entire Irminger Sea and the entire Iceland Basin, presented in figures 5.5 (January to December MLD) and 5.6 (June to September MLD) and figures 5.14 (January to December MLD) and 5.15 (June to September MLD) respectively. Since the data presented in this thesis are monthly means, it is important to keep in mind that variations on time scales less than a month will not be detected.

A comparison between fCO_2^{ytn}, collocated chl-*a* and chl-$a^{IrB/IcB}$ will also be carried out in this section. This is to further evaluate if the *Nuka* measurements are representative. Large differences between collocated chl-*a* and chl-$a^{IrB/IcB}$ indicate that the *Nuka* fCO_2^{ytn} data are biased towards higher of lower values. In cases where the fCO_2^{ytn} data were discarded or are missing, chl-a^{IrB} and chl-a^{IcB} data will be used as a proxy for the fCO_2^{ytn}. For example in 2010, where no summer fCO_2^{ytn} data was available, but chl-*a* data show unusually high concentrations in the Irminger Sea. This is worth discussing even though no observational data were available from the *Nuka* data. The following

discussion will evolve around the years and months that displayed unusual fCO_2^{ytn} values in figure 4.13 and 4.20 and were identified in section 4.2. This chapter ends with an summary of the main features and climate forcing of the years evaluated, presented in table 5.4 for the Irminger Sea and in table 5.5 for the Iceland Basin.

5.2.1 The Irminger Sea

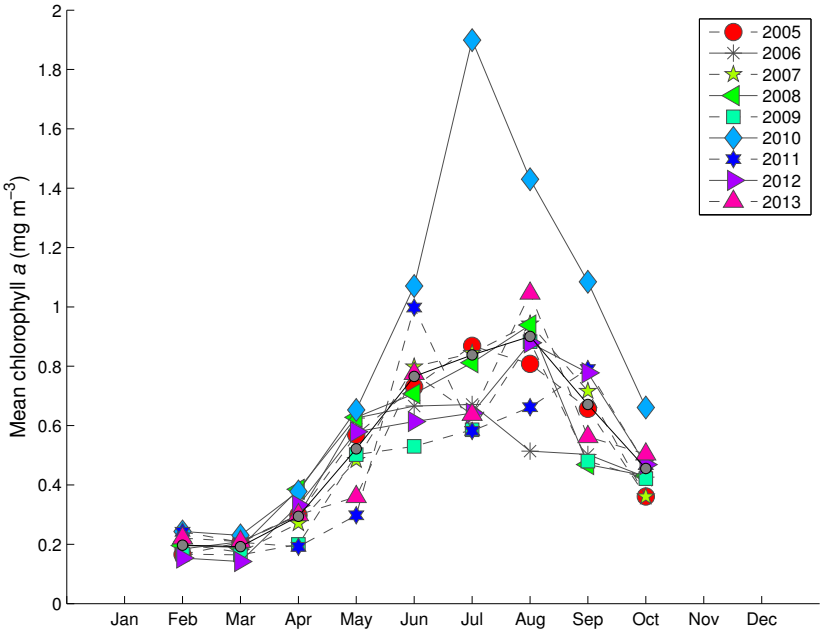

FIGURE 5.1: Monthly mean satellite chl-a concentrations in the IrB. The grey circles are long term monthly means based on the same data.

Timing of fCO_2^{ytn} drawdown

For clarity, I will specify that chl-a^{IrB} refers to the monthly mean chl-a concentrations over the entire region estimated from the satellite data, while chl-a refers to the monthly mean estimated from the chl-a collocated with the *Nuka* data. The fCO_2^{ytn} data in figure 4.13 revealed that early fCO_2^{ytn} drawdowns took place in 2006, 2010 and 2012. The collocated chl-a data in figure 4.14 showed that these years also had the highest May chl-a concentrations. Figure 5.1 presents the chl-a^{IrB} data, and reveal large differences from the collocated chl-a concentrations in May 2006 and 2012 (differences of $\sim$ 0.4 mg m^{-3} and $\sim$ 1 mg m^{-3} respectively). This indicate that the high chl-a, low fCO_2^{ytn} values most likely occurred due to a local bloom, and are not representative for the whole area, and the decision to discard the data was correct, see table 5.3. The chl-a data from 2010 compare well with the chl-a^{IrB} data, which shows more or less the same May

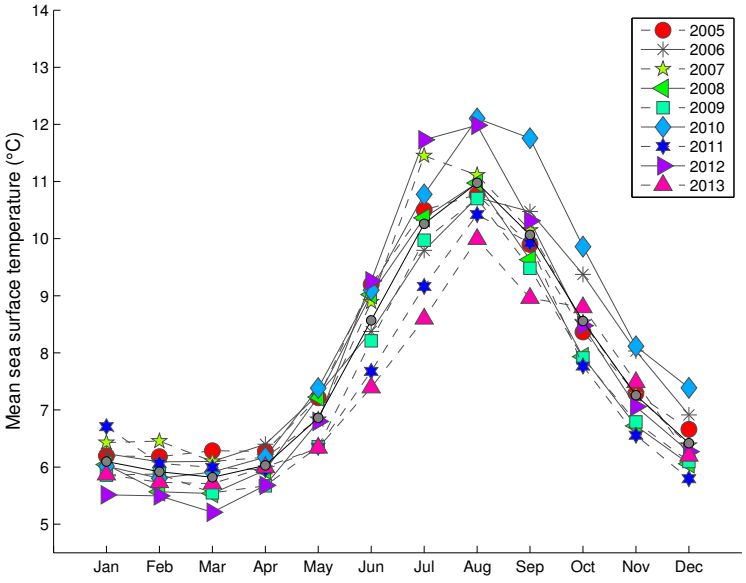

FIGURE 5.2: Monthly mean sea surface temperatures in the IrB. The grey circles are long term monthly means based on the same data.

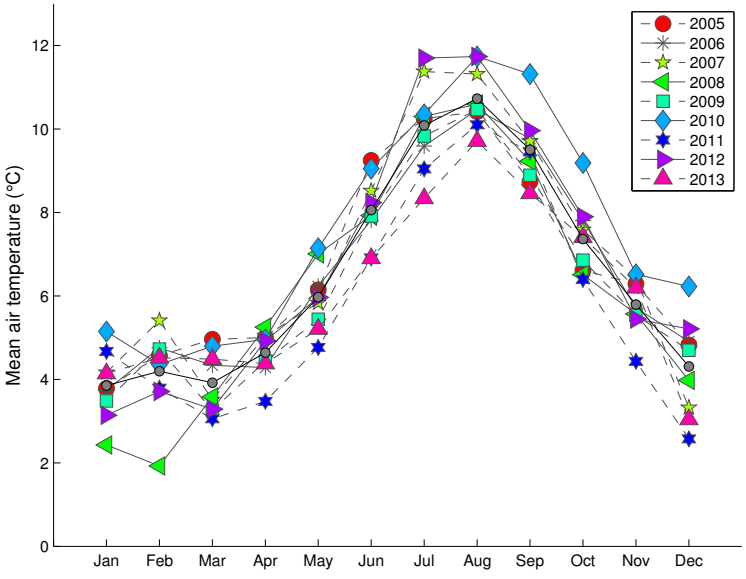

FIGURE 5.3: Monthly mean air temperatures at 2 m in the IrB. The grey circles are long term monthly means based on the same data.

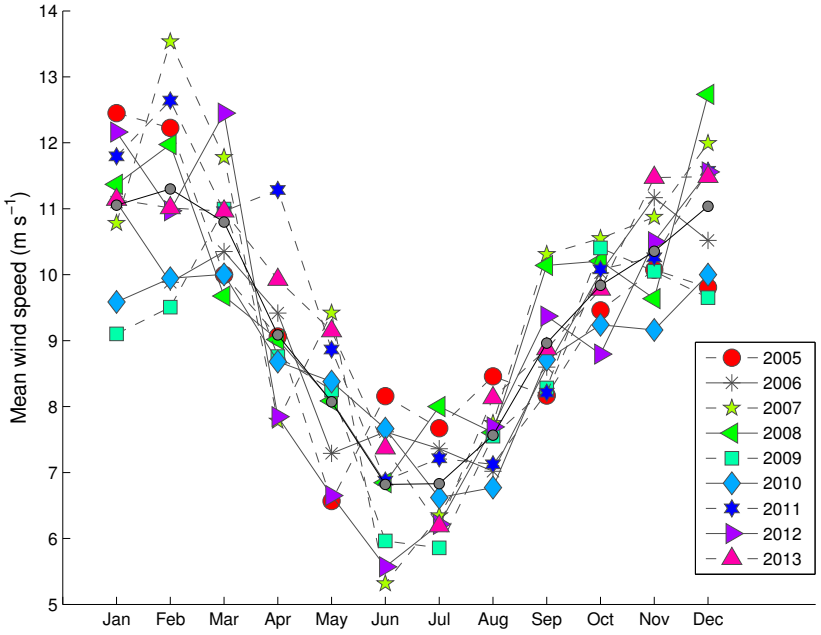

FIGURE 5.4: Monthly mean wind speeds at 10 m in the IrB. The grey circles are long term monthly means based on the same data.

chl-a concentration of $\sim$ 0.6 mg m^{-3}. Late fCO_2^{ytn} drawdown occurred in 2007, 2011 and 2013, and figure 4.14 shows that the high fCO_2^{ytn} values correspond to low chl-a concentrations. In 2011 the chl-a and chl-a^{IrB} data show good correspondence, with concentrations around 0.2 mg m^{-3}. The chl-a data in May 2007 and June 2013 have 0.1 mg m^{-3} and 0.3 mg m^{-3} lower chl-a concentrations than chl-a^{IrB}. This suggest that the May 2007 fCO_2^{ytn} data are representative for the whole area, but that the June 2013 fCO_2^{ytn} value is shifted towards a higher fCO_2^{ytn} value than what is expected based on the chl-a^{IrB} data. The representativity of the *Nuka* fCO_2^{ytn} data in May 2007, 2010 and 2011 has now been confirmed. The June 2013 fCO_2 data are considered not representative. Nevertheless, low chl-a^{IrB} concentrations in May 2013 indicate that a late bloom did occur in 2013. The environmental impact on the fCO_2^{ytn} drawdown in 2007, 2010, 2011 and 2013 will be determined, using the monthly mean sea surface temperature (figure 5.2), air temperature (figure 5.3), wind speed (figure 5.4), and mixed layer depth, figures 5.5 (January to December MLD) and 5.6 (June to September MLD).

2010 had the highest May SST and air temperature of all years, 7.5°C and 7°C respectively, and a wind speed around the mean, 8.5 m s^{-1}. This probably worked to stratify the water column, with temperature as the strongest contributor, and led to an early shoaling of the MLD, which reached 60 m in May (see figure 5.5) and the spring bloom was initiated. Figure 5.5 shows that also 2005 and 2008 had May mixed layer depths under 60 m, but no early fCO_2^{ytn} drawdown was evident in these years (see figure 4.13).

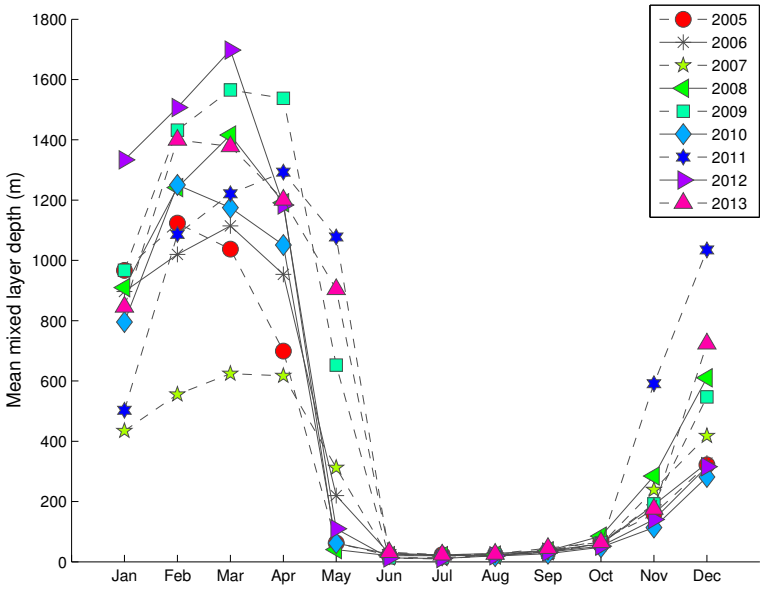

FIGURE 5.5: Monthly mean mixed layer depths in the IrB.

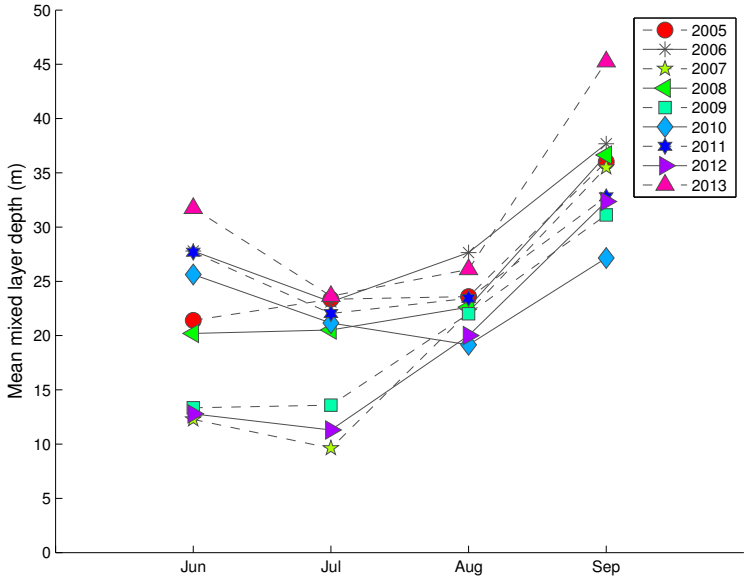

FIGURE 5.6: Monthly mean mixed layer depths from June to September in the IrB.

The chl-a^{IrB} data, however, show chl-a concentration similar to 2010, around 0.6 mg m^{-3}. 2005 and 2008 had amongst the highest SST and air temperatures, 2005 had the weakest wind speeds of all years, around 6.5 m s^{-1}, and 2008 had wind speeds similar to 2010. A possible explanation to the high fCO_2^{ytn} and high chl-a in 2005 and 2008 is that the primary production had not been going on long enough to significantly impact the fCO_2^{ytn}. In 2008 the mean wind was relatively strong but the MLD was shallow,

like in 2010, which indicate that high temperatures gave rise to a strong stratification which was not significantly affected by the mixing effect caused by strong winds.

Late fCO_2^{ytn} drawdown occurred in 2007, 2011 and 2013, evident in figure 4.13. Common for 2011 and 2013 was low SST, $\sim 6°C$, and air temperatures $\sim 5°C$. Common by all the three years was strong winds in May, around 9 m s^{-1}. Low temperatures and strong winds inhibit stratification of the water column, and the MLD did not shoal until June resulting in a delayed spring bloom and late fCO_2^{ytn} drawdown. The MLD in May 2007, 2011 and 2013 was 300 m, 1100 m and 900 m respectively (see figure 5.5).

High temperatures and low winds in May result in a shallow mixed layer depth. This was reflected in high chl-*a* concentrations, indicating that primary production had started, but did not necessarily result in low fCO_2^{ytn} values, as in 2005 and 2008. This was attributed to primary production in its initial phase, it had not been going on long enough to significantly draw down the fCO_2^{ytn}. A deep mixed layer depth in May was reflected in high wind speeds and low temperatures which result in high fCO_2^{ytn}, and since chl-*a* is low, primary production has not started. High SST and relatively strong mean winds was evident in May 2008 and 2010, but the MLD was shallow and primary production was initiated. This indicate that the stratification caused by high SST was not affected by the the mixing effect of the winds, and that temperature is the main driver behind the timing of the drawdown as it has the strongest impact on the MLD and hence the primary production.

Magnitude of fCO_2^{ytn} drawdown

In section 4.2.1 it was revealed that 2006 was dominated by high summertime fCO_2^{ytn} values, see figure 4.13. This was reflected in low chl-*a* concentrations (see figure 4.14), which is in good agreement with the chl-a^{IrB} concentrations in figure 5.1 of around 0.5-0.6 mg m^{-3}. The fCO_2^{ytn} data in figure 4.13 revealed a strong summertime fCO_2^{ytn} drawdown in 2007. This was reflected in high chl-*a* concentrations throughout the summer of 2007. The chl-*a* and chl-a^{IrB} data show similar chl-*a* concentrations between 0.8 mg m^{-3} and 1 mg m^{-3} from June to August. This confirm that the unusually high, and low, fCO_2^{ytn} values that occurred in the Irminger Sea in 2006 and 2007 respectively, are representative. Next, environmental parameters will be used to unearth the processes behind these unusual fCO_2^{ytn} values.

In 2006 the summer SST and air temperatures were around the mean, or slightly lower than the mean, figure 5.2 and 5.3 show temperatures just under 10°C in July. The wind was relatively strong throughout the summer, with mean wind speeds around 7-7.5 m s^{-1} from May to August, see figure 5.4. Low SST and air temperatures, and relatively strong summer winds, are conditions that lead to deep MLD. From figure 5.6 it is evident

that the MLD was relatively deep, around 25-30 m in June, July and August. The density profiles from 2006 shown in figure 5.7 indicate that the stratification was weak compared to the density profiles in 2007 (see figure 5.8). Weak stratification enables DIC rich waters to be mixed up to the surface during summer and contribute to the high fCO_2^{ytn}. When DIC rich waters are able to penetrate the weak thermocline, so are nutrients. A constant supply of nutrients would result in good conditions for primary production. But the chl-a is low throughout the summer, with maximum values around 0.65 mg m^{-3} in June and July (see figure 5.1). This probably reflects the two opposing effects a weak stratification has on the primary production. It supplies the surface with nutrients, but on the other hand, phytoplankton in the surface are subject to an unstable water column, and they fluctuate between the well lit surface layer and the subsurface where they can not photosynthesise.

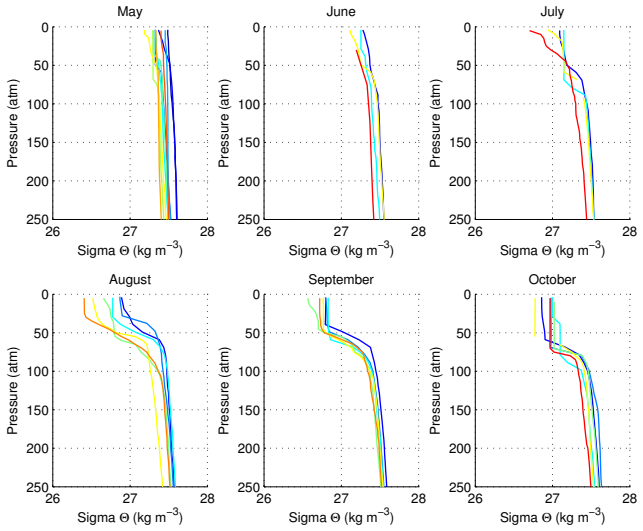

FIGURE 5.7: Density profiles from the Irminger Sea from May to October 2006.

The summer sea surface and air temperatures in 2007 was amongst the highest of all years. Figure 5.2 and 5.3 show maximum summer SST and air temperatures in July, around 11.5°C. This was $\sim$ 1.5°C higher than the July 2006 temperature. fCO_2 was low despite high temperatures, and the unusually low fCO_2^{ytn} was a result of strong biological activity. Figure 5.4 shows strong winter wind speeds in 2007, up to 13.5 m s^{-1}, especially in February and March. Strong mean wind also in May, around 9.5 m s^{-1}, before weaker wind speeds dominated in June, with a mean wind speed around 5 m s^{-1}. The mean wind speed in June 2007 was $\sim$ 3 m s^{-1} lower than in June 2006. The windy winter and spring season which phase over to a calm summer period could be one of the the reasons for the late, but strong spring bloom. Martinez et al. (2011) suggested that strong winter winds may be related to a strong spring bloom because it induces deeper MLD which leads to an enhanced nutrient uplift. However, the winter MLD in 2007 was very shallow compared to the other years, between 400-600 m as seen in

figure 5.5. This indicate that strong winter winds had minor effect on the winter mixed layer depth, and suggest that the strongest contributor to induce deep mixing is the sea surface temperature. Figure 5.2 shows that the SST in December 2006 and January and February 2007 was amongst the highest of all years, which most likely prevented deep mixing and gave rise to the shallow winter MLD. This contradict the suggestion that enhanced nutrient uplift due to strong winter winds was the reason for the strong fCO_2^{ytn} drawdown, and also imply that the nutrient supply during winter does not affect the magnitude of the summertime fCO_2^{ytn} drawdown in the Irminger Sea. The chl-a concentrations increase steadily during summer, as evident in figure 5.1, and reach a maximum concentration in August, with approximately 0.95 mg m^{-3}, indicating that nutrients and light were abundant and photosynthesis took place all summer. The high temperatures, both in air and sea surface, and low wind speeds in June are processes that contribute to a shallow summer MLD. Figure 5.6 reveal that the summer MLD was very shallow, with a mean depth of 12 m and 10 m in June and July, respectively. This indicates a strong water column stratification in 2007. Figure 5.8 shows density profiles from the Irminger Sea from May to October and confirms that the stratification in July and August was strong. A strong stratification prevents DIC from the deep to reach the surface, and is, together with ongoing primary production, likely the reason for the low fCO_2^{ytn} throughout the summer of 2007. Strong stratification and continued chl-a increase through the summer are, however, observations that intuitively should not occur at the same time. Strong stratification prevents DIC rich water to enter the surface, but it also prevents nutrients to reach the surface. This would eventually decrease the chl-a when the surface water is nutrient depleted. There are two possible explanation to this, i) nutrients were abundant all summer and not a limiting factor for primary production, and ii) the amount of zooplankton was low, and grazing did not exceed photosynthesis. This will not be confirmed, as I do not have nutrients or plankton data.

The correlation between fCO_2^{ytn} (see figure 4.13) and chl-a^{IrB} data (see figure 5.1) was good in both 2006 and 2007, hence chl-a is a good indicator of the magnitude of the fCO_2^{ytn} drawdown. Both the summertime winds and temperatures are factors determining the magnitude of the summertime fCO_2^{ytn} drawdown due to their impact on the mixed layer depth. The summer winds in 2007 was weak and the SST was high, keeping the MLD shallow and the stratification strong. In 2006 the summertime winds was relatively strong and SST $\sim$ 1.5°C lower than in 2007, contributing to a relatively deep MLD and an unstable stratification. Also, winds was suggested to have little effect on wintertime MLD, and the wintertime MLD in 2006 was much deeper than in 2007. This indicates that the nutrient supply to the surface water during winter do not affect the strength of the summertime fCO_2^{ytn} drawdown and that nutrients are not the limiting factor of primary production in the Irminger Sea.

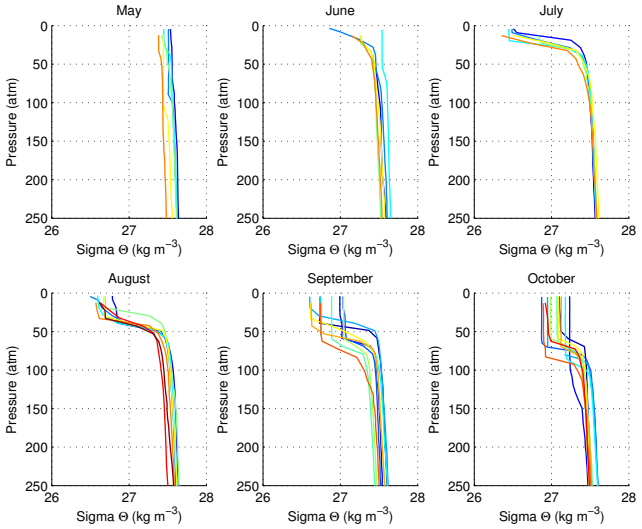

FIGURE 5.8: Density profiles from the Irminger Sea from May to October 2007.

No *Nuka* fCO_2 data were available from the summer of 2010 due to instrument failure, but the spring and summer chl-*a* concentration in the Irminger Sea was exceptional high, as evident in figure 5.1. The observed chl-*a* concentration in July was almost 2 mg m^{-3}, more than twice the mean chl-*a* concentration, and the chl-*a* concentration was generally high from May to October. Henson et al. (2013) studied the unusual bloom in 2010 and investigated the effect of two unusual events that occurred in 2010: the NAO was in an unusually strong negative phase in the winter of 2009/2010, and the volcano Eyafjallajökull erupted, depositing tephra (iron) into the subpolar North Atlantic. Henson et al. (2013) concluded that the iron from the volcano eruption had only minor effects on the phytoplankton bloom, and the main reason was most likely the anomalously hydrographic conditions caused by the negative North Atlantic Oscillation (NAO). During negative phases of the NAO, the Icelandic low pressure strengthens, and the Azores high pressure weakens, resulting in a southward shift of the storm tracks and weaker westerlies. This gave rise to anomalous surface conditions, and an enhanced freshwater flux into the Irminger Sea originating from the Labrador Current may have been a result of this. A fresh density anomaly were found in the upper 50-80 m, and together with relatively high temperatures, this was reflected in shallow mixed layer depths throughout summer and autumn. Also, the area may have been introduced to increased nutrient supply due to the unusual hydrographic conditions, but this alone could not have been responsible for the strong primary production. However, the relatively high SST and the shallow mixed layer persisting through the summer and autumn were suggested to have increased the rates of nitrogen recycling compared to others years (Henson et al., 2013). This would be reflected in high chl-*a* concentrations, but not necessarily in extremely low fCO_2^{ytn} values since regenerated nutrients were used. Unfortunately no fCO_2 measurements were made aboard the *Nuka Arctica* during the summer of 2010.

Fall bloom

In section 4.2.1 I concluded that a weak fall bloom occurred in 2006 due to a slight chl-a increase in the chl-a data from August to September, figure 4.14. Comparison between chl-a and chl-a^{IrB}, figure 5.1, show a disagreement. The whole area averaged chl-a data does not increase from August to September. This indicates that the fall bloom detected in the *Nuka* observations was a result of spatial variations, and not representative for the whole area. fCO_2^{ytn} data from June and August 2011 were discarded due to few measurements and poor spatial representation, see table 5.3. No chl-a data were available for June 2011, and bad agreements between the chl-a and chl-a^{IrB} concentrations in August 2011 support the decision to discard these values since they are not representative for the area as a whole. The chl-a and chl-a^{IrB} data agree for September 2011, with concentrations around 0.8 mg m^{-3}. Since both the June and August 2011 fCO_2^{ytn} values were discarded, the following discussion will be based on the chl-a^{IrB} data, figure 5.1. These data show that the chl-a peaked two times in 2011, the first, and strongest peak occurred in June, with chl-$a \sim 1$ mg m^{-3}. The second peak occurred in September with a concentration of ~ 0.8 mg m^{-3}, which support the suggestion from section 4.2.1 that a fall bloom occurred in 2011.

Lévy et al. (2005) suggested that north of 49°N light limitations inhibit a full consumption of the available nutrients. This can provide an explanation to the the gradual increase in the long term monthly mean chl-a concentrations from May to August in figure 5.1. Nutrients are abundant all summer, like in 2007, unless other forces interfere with the nutrient supply and/or the primary production, like in 2006. The chl-a decrease from June to July in 2011 could possibly be a response to light limitation. Data of the chl-a coverage give indications of the light conditions. Clouds reduce the satellite coverage, reflected in reduced chl-a observations in cloudy months. Figure 5.9 shows the satellite coverage in the Irminger Sea given in percentage of chl-a observations available from each month. Indications are strong that July 2011 was cloudy, with a coverage between 50-60%. The satellite coverage was low also in July 2013, between 40-50%, which also coincide with low chl-a concentrations, see figure 5.1. This can be reflected in low chl-a concentrations in two ways, i) few measurements were available and the mean chl-a concentration was biased towards low values, or ii) reduced primary production as a response to light limitation. The fall bloom indicated by a chl-a increase and a fCO_2^{ytn} reduction form July to August was possibly a response to the initiation of primary production after a period of weaker production due to light limitations. Bear in mind that poor satellite coverage does not necessarily mean that the light availability is reduced to an extent so that it reduces primary production. High clouds will reduce the satellite coverage, but it will have minimal effect on the primary production. The

indications given by the chl-a data coverage must therefore not be given considerably emphasis. Irradiance data would be useful in order to confirm these suggestions.

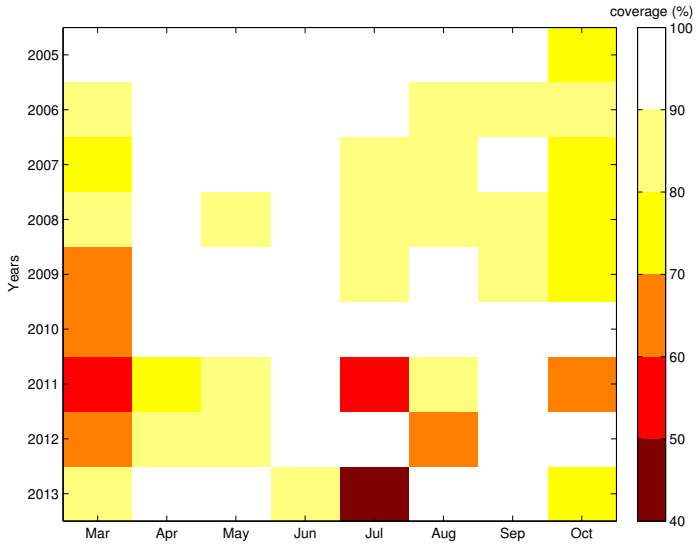

FIGURE 5.9: Satellite coverage in the Irminger Sea based on amounts of chl-a observations available each month, given in percentage.

Connection between timing of bloom and magnitude of bloom

Henson et al. (2006) suggested that a late bloom gave a reduced magnitude of the bloom in the Irminger Sea. Two possible explanation to this was given. First, the phytoplankton has missed its "window of opportunity" and the period of light and mixing conditions good enough to result in phytoplankton growth is shorter. Second, the zooplankton has had time to reproduce, and is able to keep the phytoplankton concentration down when bloom starts. The data I have do not give a clear connection between a late bloom and a weak bloom. In the Irminger Sea late blooms occurred in 2007, 2011 and 2013. 2007 had the strongest fCO_2^{ytn} drawdown of all years, and relatively high chl-a concentration. The chl-a data from 2011 shows that a strong spring bloom occurred in June, with chl-$a \sim 1$ mg m^{-3}, followed by a relatively strong fall bloom in September, see figure 5.1. In 2013 the chl-a data indicate that a weak spring bloom occurred in June with chl-a concentrations around 0.8 mg m^{-3} and a stronger fall bloom occurred in August, with values around 1 mg m^{-3}. Based on my data, indications are strong that a late spring bloom result in a normal, or even stronger, summer fCO_2^{ytn} drawdown and primary production than unusual. The largest uncertainty in my data is that I only use monthly means, and I do not present accurate data of when the bloom started. In this case onset differences of a couple of weeks could be decisive.

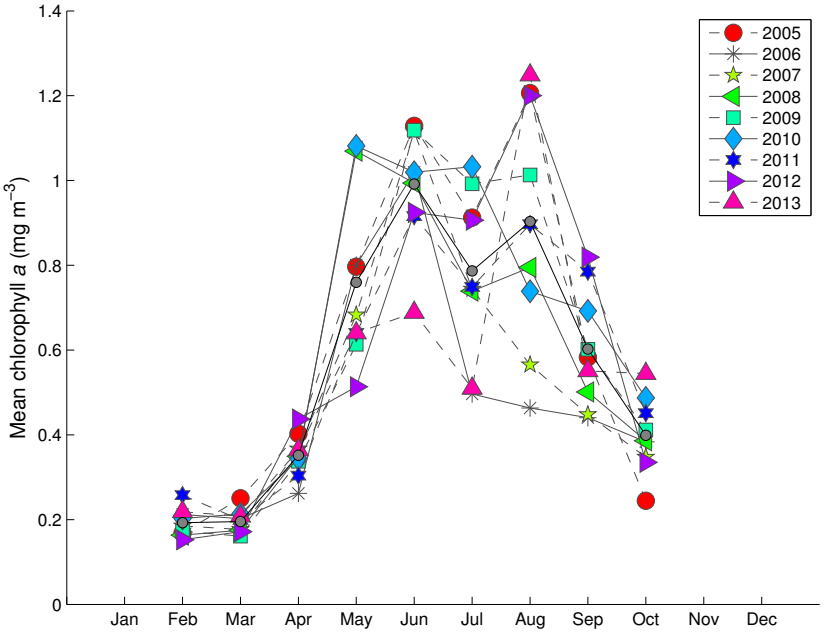

FIGURE 5.10: Monthly mean satellite chl-a concentrations in the IcB. The grey circles are long term monthly means based on the same data. Note: different y-axis definition than in figure 5.1

5.2.2 The Iceland Basin

Timing of fCO_2^{ytn} drawdown

The fCO_2^{ytn} data in figure 4.20 (section 4.2.2) showed that early fCO_2^{ytn} drawdowns occurred in 2008 and 2010. The chl-a data, figure 4.14, revealed that these years also had the highest chl-a concentrations. Figure 5.10 shows the monthly mean chl-a concentration over the entire Iceland Basin, referred to as chl-a^{IcB}. For clarity, I will specify that chl-a^{IcB} refers to the monthly mean chl-a concentrations over the entire region estimated from the satellite data, while chl-a refers to the monthly mean estimated from the collocated chl-a data. The May 2008 chl-a^{IcB} concentration is ~ 0.7 mg m^{-3} lower than the chl-a concentration. This indicate that the fCO_2^{ytn} is not representative for the entire area that month. Nevertheless, high chl-a^{IcB} concentration in May 2008, around 1.1 mg m^{-3}, show that an early spring bloom did occur, just not as strong as indicated in figure 4.20. Almost similar chl-a and chl-a^{IcB} concentrations are evident in May 2010, around 1.1-1.2 mg m^{-3}. Figure 4.20 shows that late fCO_2^{ytn} drawdowns occurred in 2005 and 2009, but the corresponding chl-a concentration was not particularly low. The chl-a^{IcB} data show relatively high chl-a concentration in May 2005 and relatively low chl-a concentration in May 2009. Even though some differences occur between the chl-a^{IcB} and chl-a data, no additional data will be discarded. The representativity of the *Nuka*

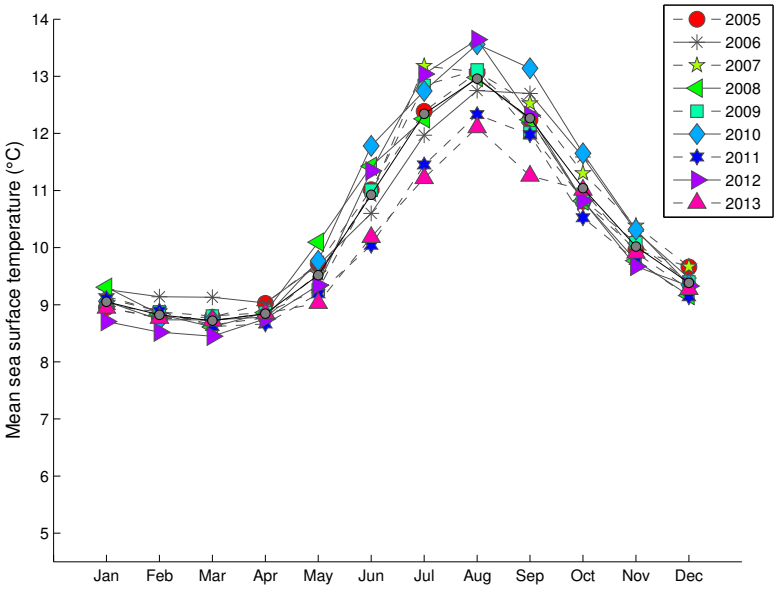

FIGURE 5.11: Monthly mean sea surface temperatures in the IcB. The grey circles are long term monthly means based on the same data.

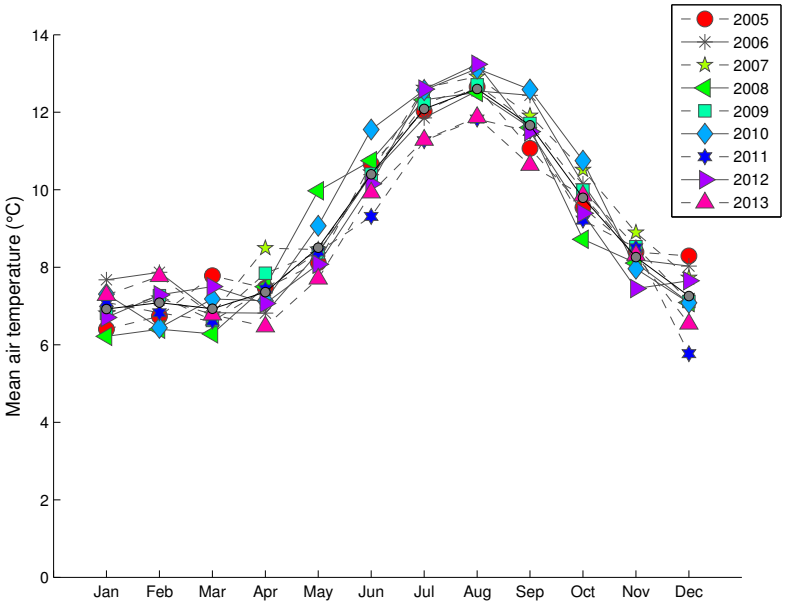

FIGURE 5.12: Monthly mean air temperatures at 2 m in the IcB. The grey circles are long term monthly means based on the same data.

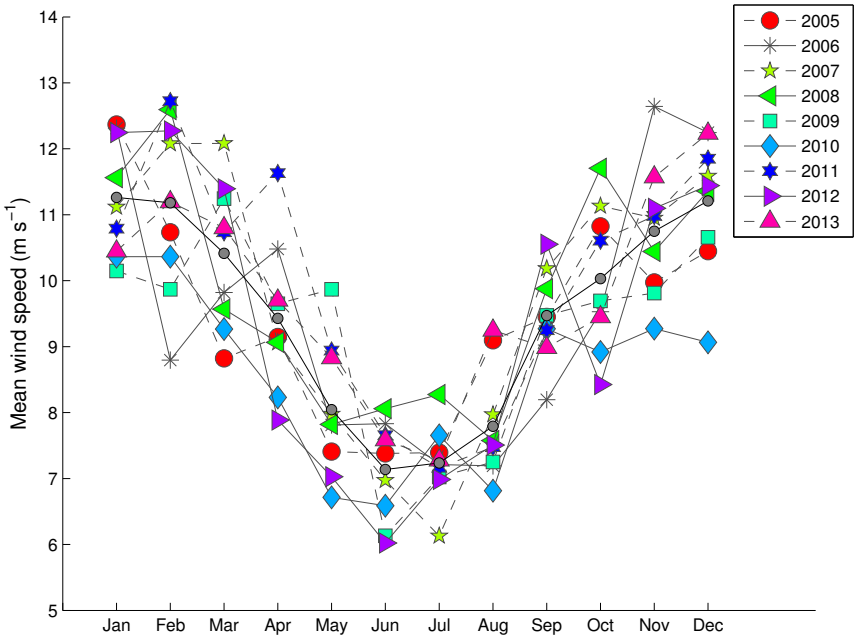

FIGURE 5.13: Monthly mean wind speeds at 10 m in the IcB. The grey circles are long term monthly means based on the same data.

data in 2005, 2008, 2009 and 2010 has now been confirmed, and next, environmental impact on the timing of the fCO_2^{ytn} drawdown will be determined.

The same processes that caused an early fCO_2^{ytn} drawdown in the IrB, as described in section 5.2.1, were present in the respective years in the IcB. 2008 and 2010 had the two highest May SSTs, around 10°C and 9.5°C (see figure 5.11), and air temperatures, around 9.5°C and 9°C (see figure 5.12) respectively. Figure 5.13 reveal that the lowest May wind speed occurred in 2010, with a mean wind speed around 6.5 m s^{-1}. Higher mean wind speed is evident in 2008, around 8 m s^{-1}. Figure 5.14 shows that 2008 and 2010 had the shallowest MLD of all years in May, around 25-50 m. The MLD in 2008 was shallow even though the winds was relatively strong, and as indicated by the high May chl-*a* concentration in figure 5.10, the phytoplankton bloom was initiated. This indicate that the high sea surface temperatures, around 10°C, gave rise to a strong stratification that counteracted the mixing effect caused by the winds. Figure 5.14 show that the MLD in May 2012 was deep, around 300 m, despite a very weak mean wind. The SST was low, approximately 1°C lower than in 2008, which support the suggestion that temperature exerts the strongest effect on the MLD and stratification. In 2010 the shallow MLD was most likely a result of the high temperatures combined with low wind speed, which combined with enough light, was the reason for the early spring bloom and fCO_2^{ytn} drawdown.

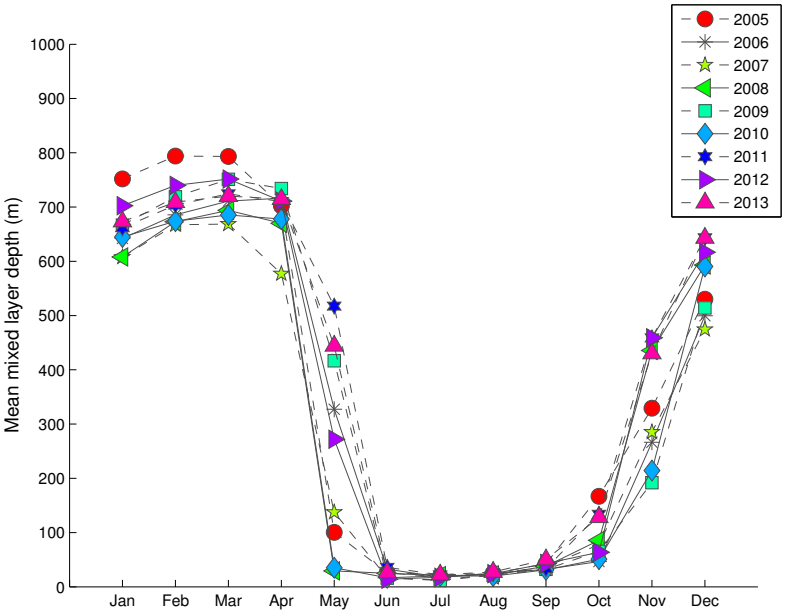

FIGURE 5.14: Monthly mean mixed layer depths in the IcB.

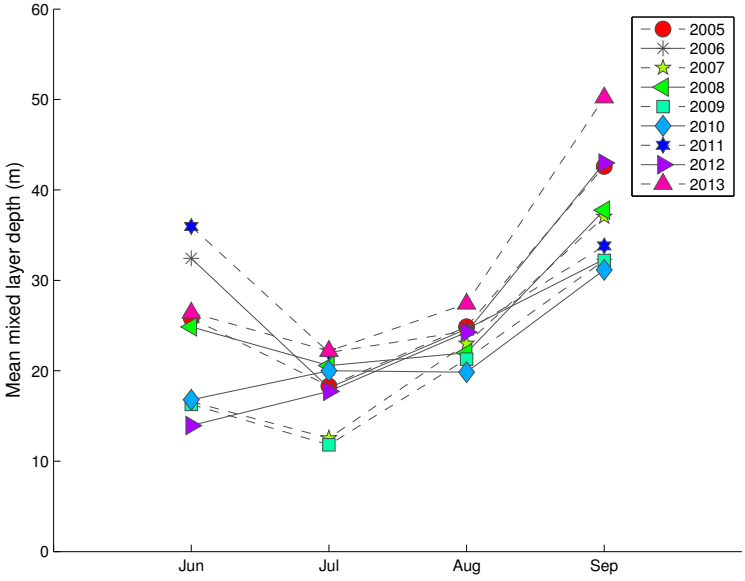

FIGURE 5.15: Monthly mean mixed layer depths from June to September in the IcB.

Late fCO_2^{ytn} drawdowns occurred in 2005 and 2009. Figure 5.10 shows relatively high chl-a concentrations in May 2005, and low chl-a concentrations in May 2009. In 2005 both fCO_2^{ytn} and chl-a^{IcB} was high. This feature can be a result of two processes, or a combination of the two: i) primary production is in its initial state, it has increased the chl-a concentration, but not lasted long enough to cause a significant reduction in fCO_2^{ytn}, and ii) figure 5.13 shows stronger May winds in 2005 compared to 2010, and a

MLD $\sim$ 100 m is evident in figure 5.14, which is relatively deep in regards to Sverdrup's critical depth (Sverdrup, 1953). Strong spring winds can either prevent or initiate spring bloom dependent on the balance between the depth-averaged irradiance and the nutrient supply (Henson et al., 2006). In 2005 the effect of the increased nutrient supply most likely exceeded the reduction in depth-averaged irradiance due to mixing and turbulence. This resulted in a net phytoplankton growth and increased chl-a concentrations, but no decrease in fCO_2^{ytn} since DIC rich water was brought up. In May 2009 the mixed layer depth was deep, around 425 m. This was most likely a result of the strong winds in May 2009 (mean wind speed $\sim$ 10 m s^{-1}), and together with low chl-a concentration this indicate that the primary production had not started yet.

Weak May winds and high temperatures caused a shallow MLD in 2010, resulting in an early spring bloom and fCO_2^{ytn} drawdown. A shallow MLD and early spring bloom did also occur in 2008 even though the mean wind in May was relatively strong compared to 2010. The temperatures were high, which indicate that the SST had a strong effect on the stratification and counteracted the mixing effect caused by the winds. Deep mixed layer depth in May is associated with high wind speeds and low temperatures. As a response to the deep May MLD, primary production was delayed as reflected in high fCO_2^{ytn} and low chl-a concentrations in 2009. In 2005 different mechanisms was suggested to give rise to the occurrence of high chl-a and high fCO_2^{ytn}, and no definite conclusion to the feature is provided. As in the Irminger Sea, the interplay between wind strengths and temperatures, but with temperature as the strongest contributor, is the main driver behind the variations observed in the timing of the fCO_2^{ytn} drawdown, as impacted by the MLD.

Magnitude of the fCO_2^{ytn} drawdown

The collocated chl-a data (see figure 4.21) and chl-a^{IcB} data (see figure 5.10) present similar chl-a concentrations in 2005, 2006. fCO_2^{ytn} data from 2008, see figure 4.20, show unusually low values in June and August, and values around the mean in July. The collocated chl-a data did not reflect the fCO_2^{ytn} very good. No chl-a data were available from August. The chl-a^{IcB} data show chl-a concentrations around 1 mg m^{-3} in June and a decrease to $\sim$ 0.75 mg m^{-3} in July. This reflects the fCO_2^{ytn} better. The chl-a^{IcB} concentration in August was relatively high, around 0.8 mg m^{-3}, and do not correspond to the unusually low fCO_2^{ytn} value in August. This support the decision to discard the August 2008 fCO_2^{ytn} value as not being representative (see table 5.3). In 2009 the unusually high June fCO_2^{ytn} value did not correspond to unusually low chl-a values. The chl-a^{IcB} data show that the chl-a concentration in June was relatively high, around 1.1 mg m^{-3}. This indicate that the high fCO_2^{ytn} value in June 2009 is not representative for the entire region, and the decision to discard it was correct. In July 2009, the chl-a

and chl-a^{IcB} show similar concentrations around 1 mg m^{-3}. The chl-a^{IcB} data show a small chl-a increase from July to August 2009, while the collocated chl-a data showed a decrease from July to August.This indicate that the fCO_2^{ytn} value in August 2009 may be slightly underestimated compared to the entire region. However, the amount of measurements from August 2009 was plentiful (see table 5.2), and the chl-a^{IcB} data did reflect the low fCO_2^{ytn} relatively good, so it is regarded as representative. Now that the representativity of the *Nuka* fCO_2^{ytn} data in 2005, 2006, 2008 and 2009 has been confirmed, the following discussion will connect the unusual features to climate forcing. In months where *Nuka* data has been discarded, chl-a^{IcB} data will be used as a proxy.

In 2005 the fCO_2^{ytn} was around 330 μatm in June and August. Figure 5.10 shows that the chl-a concentration increased from ∼0.9 to ∼ 1.25 from July to August. The chl-a increased, but fCO_2^{ytn} did not change, see figures 4.20 and 5.10. This possibly reflects primary production from regenerated and not new nutrients (Olsen et al., 2008). This was also mentioned in sections 4.1.2, 4.1.4 and 4.1.5. When plankton photosynthesise they use carbon and nutrients in a constant stoichiometric ratio, following equation 2.12. For each phosphate used, 106 carbon is used. When the organic matter is remineralized in the water column, the carbon and phosphate return to the water column in the same stoichiometric ratio, as regenerated nutrients. When the regenerated inorganic matter is brought to the surface, it can be used again by plankton in the same constant ratio, hence this will increase the chl-a concentration of the water, but not affect the fCO_2^{ytn}. In 2005 relatively strong winds occurred in August, indicated by a mean wind speed around 9 m s^{-1} in figure 5.13, which most likely weakened the stratification and enabled regenerated nutrients to be brought to the surface. This initiated a phytoplankton bloom from regenerated nutrients, indicated by a strong chl-a increase from August to September but not a change in fCO_2^{ytn}.

2006 had high summertime fCO_2^{ytn} values, around 340 μatm from June to August (see figure 4.20). High summertime fCO_2^{ytn} was also evident in the Irminger Sea (see figure 4.13), which suggest that the process leading to high fCO_2^{ytn} there, is also the dominant process in the Iceland Basin. Figure 5.11 show sea surface temperatures from June to August approximately 0.5°C lower than the mean. The June to August mean winds were also around the mean, between 7 and 8 m s^{-1} (see figure 5.13). Unfortunately I do not have density profiles from June and July 2006 as no Argo data were available in my data set from this region in those months. But the relatively low sea surface temperatures and the deep MLD in June 2006 indicates that the stratification was relatively weak in the Iceland Basin in 2006 as it was in the Irminger Sea (see figure 5.15). If this suggestion yields for the Iceland Basin as well, a weak stratification was most likely the reason for the high fCO_2^{ytn} since it enables DIC rich water to penetrate the thermocline and reach the surface layer, resulting in high fCO_2^{ytn} values. The chl-a concentration

in May and June were relatively high, figure 5.10 shows concentrations around 0.75 mg m^{-3} and 1 mg m^{-3} respectively. The concentration decreased to around 0.5 mg m^{-3} from July to September, which indicate that the primary production was weak. The relatively high chl-*a* concentrations in May and June were possibly results of intermittent stratification and shallowing of the MLD, resulting in primary production even though the mean MLD data show deep mixed layers. The weak primary production reflected in low chl-*a* concentrations from July to September is also most likely a result of a weak stratification. A weak stratification supply the surface with nutrients, but it also make the phytoplankton fluctuate between the well lit surface water and the subsurface water where photosynthesis is not possible.

After the early spring bloom and fCO_2^{ytn} drawdown in 2008 the primary production continued in June, reflected in the low fCO_2^{ytn} (see figure 4.20) and high chl-*a* concentrations (see figure 5.10). High SST, around 11.5°C, air temperatures around 11°C and a relatively shallow MLD around 25 m indicates that the conditions were good for primary production (see figures 5.11, 5.12 and 5.15). Figure 5.13 reveal relatively strong June wind speeds with a mean around 8 m s^{-3}. However, the stratification caused by high sea surface temperature was most likely too strong for the winds to have any significant impact. In July the fCO_2^{ytn} suddenly increased to values around the mean, $\sim$ 330 μatm, an 30 μatm increase from June to July. This could be a result of nutrient depletion and a strong stratification inhibiting new nutrients to reach the surface. This would result in a chl-*a* decrease, but a reduced primary production should not cause such an immediate and strong fCO_2^{ytn} increase as seen in figure 4.20. The reason for the sudden, and strong, fCO_2^{ytn} increase could be attributed to a strong coccolithophore bloom. Coccolithophores bloom can cause the fCO_2^{ytn} to increase due to their utilization of alkalinity (fCO_2^{ytn} increase) if it exceeds their utilization of DIC (fCO_2^{ytn} decrease). This would increase the fCO_2^{ytn}, i.e calcification exceeds photosynthesis. Several studies have investigated this relationship and found that coccolithophore blooms increase the fCO_2^{ytn} (Brown and Yoder (1994), Holligan et al. (1993), Fernandez et al. (1993)). However, recent studies have found that the net increase in fCO_2^{ytn} due to calcification is much lower than the decrease in fCO_2^{ytn} due to photosynthesis (Suykens et al. (2010), Signorini et al. (2012)).

After a late spring bloom in 2009 the fCO_2^{ytn} values decreased rapidly and in July and August fCO_2^{ytn} were between 300 μatm and 310 μatm as seen in figure 4.20. The June fCO_2^{ytn} observations were discarded due to few available measurements (see table 5.3. However, the high chl-*a* concentration in June seen in figure 5.10 indicate that a relatively strong primary production was initiated in June. The monthly mean SST were around 13°C and the air temperatures around 12°C in July and August. Unique for this year was the strong mean wind speed in May, around 10 m s^{-1}, figure 5.13.

This indicate that May was affected by storms, or incidents of really strong winds. The strong winds inhibited a stratification of the water column, and the MLD in May was deep, around 450 m, preventing a initiation of the spring bloom. By June the winds had weakened drastically, with a mean wind speed around 6 m s^{-1}. Weak winds together with relatively high summer temperatures gave rise to a shallow MLD, between 10 m and 20 m in June to August as seen in figure 5.14 and 5.15). This led to good conditions for primary production, and the phytoplankton bloom and fCO_2^{ytn} drawdown could start, albeit a bit delayed.

In 2006 high winds in June, and winds around the mean in July and August, and relatively low SST in these months resulted in a deep MLD, especially in June, and most likely a weak stratification. This was most likely the reason for the weak primary production, indicated by low chl-a and high summertime fCO_2^{ytn}. Weak summertime winds and high temperatures caused a shallow MLD, which resulted in low fCO_2^{ytn} and high chl-a concentrations. When the winds was strong, but the temperature was high, the stratification caused by high temperatures was suggested to be strong enough to resist mixing by the winds. This suggest that the interplay between wind and temperature and how they affect the MLD are the governing factors in controlling the magnitude of the fCO_2^{ytn} drawdown.

Fall bloom

In chapter 4 fall blooms was detected in 2006 and 2011, indicated by a decrease in fCO_2^{ytn} (figure 4.20) and an increase in chl-a (figure 4.21). Figure 5.10, however, shows chl-a^{IcB} concentrations around 0.5 mg m^{-3} from July to October, and no chl-a increase in the fall of 2006. This indicate that a very local fall bloom occurred in 2006, or it occurred due changes in cruise tracks from August to September. In 2011 the chl-a (figure 4.21) and the chl-a^{IcB} (figure 5.10) show similar chl-a concentrations in August and September. Figure 5.10 shows that two chl-a peaks occurred in 2011, one in June around 0.9 mg m^{-3} and a second in August around 0.8 mg m^{-3}. This support the suggestion that a fall bloom occurred in 2011, in addition to a spring bloom in June. No fCO_2 measurements were available from June 2011, hence the June chl-a peak was not detected from the *Nuka* data. Figure 5.16 shows the satellite coverage in the Irminger Sea, given in percentage of chl-a observations available each month. The situation is similar to the Irminger Sea, with reduced coverage in July 2011 and 2013. Figure 5.16 show a 70-80% coverage in July 2011 and 40-50% in July 2013, which suggest that the light availability in the Iceland Basin was reduced in these months. This could be the the reason for the low chl-a concentrations observed in July, either due to light limitations and its impact on the primary production, or that the chl-a concentration was biased towards lower values because of reduced observations. If the former did

occur, the chl-a peaks observed are due to re-initiation of primary production after a period of poor production due to light limitations, as was suggested in the Irminger Sea (see section 5.2.1). However, indications given by the chl-a data coverage should not be given considerably emphasis, as high clouds will reduce the satellite coverage but have minimal effect on the primary production. 2013 has not been given much emphasize earlier, but the high chl-a concentration in September, around 1.3 mg m^{-3}, is worth noticing (see figure 5.10). This peak coincided with high fCO_2^{ytn} values, around 340 μatm, and strong mean wind speeds around 9.5 m s^{-1} occurred in August and September (see figures 4.20 and 5.13). The strong winds probably resulted in a weakened stratification, and regenerated nutrients was brought to the surface and initiated a fall bloom. As mentioned in section 5.2.1, regenerated production results in increased chl-a concentrations, but no change in fCO_2, which is evident in the fall of 2013.

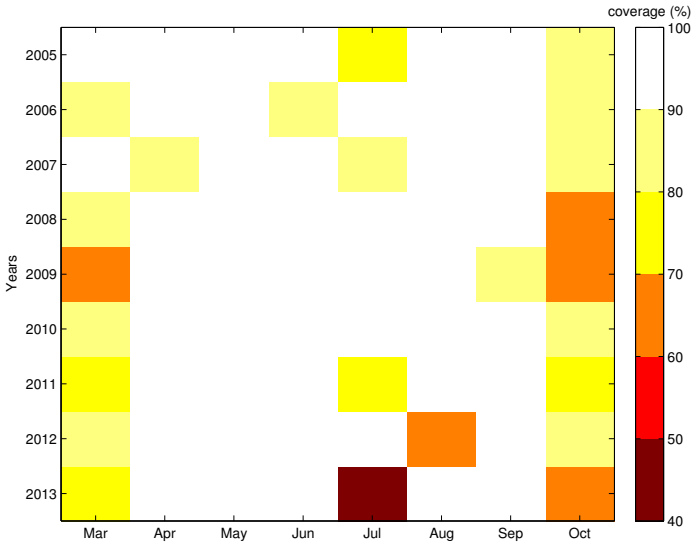

FIGURE 5.16: Satellite coverage in the Irminger Sea based on amounts of chl-a observations available each month, given in percentage.

5.3 Summary

The main features of the interannual fCO_2^{ytn} variations were identified in chapter 4, and possible explanations to these variations with roots in climate forcing were discussed in chapter 5. Table 5.4 and 5.5 provide a short summary of the main findings from the Irminger Sea and the Iceland Basin.

Year	**Feature**	**Climate forcing**
2005	Relatively late fCO_2^{ytn} drawdown	Weak winds and high SST cause a shallow MLD. Primary production in its initial state and has not had time to significantly reduce fCO_2^{ytn}.
2006	Weak fCO_2^{ytn} drawdown	Strong winds and low SST cause a deep MLD and weak stratification. Weak primary production.
2007	- Late fCO_2^{ytn} drawdown - Strong fCO_2^{ytn} drawdown	- Strong winds and low SST cause a deep MLD. Primary production not initiated. - Weak winds and high SST cause a shallow MLD. Strong primary production.
2008	Relatively late fCO_2^{ytn} drawdown	High SST cause a shallow MLD. Primary production in its initial state and has not had time to significantly reduce fCO_2^{ytn}.
2010	- Early fCO_2^{ytn} drawdown - Strong primary production, no fCO_2^{ytn} data available	- High SST cause a shallow MLD. Primary production initiated. - Unusual hydrographic conditions as a result of a strong negative NAO phase.
2011	- Late fCO_2^{ytn} drawdown - Fall bloom	- Strong winds and low SST cause a deep MLD. Primary production not initiated. - Possibly due to re-initiation of primary production after light limitations in July (not documented).
2013	Late fCO_2^{ytn} drawdown	Strong winds and low SST cause a deep MLD. Primary production not initiated.

TABLE 5.4: Main features and climate forcing in the Irminger Sea.

Year	**Feature**	**Climate forcing**
2005	Late fCO_2^{ytn} drawdown	Winds and relatively high SST cause a MLD $\sim$ 100 m. Primary production in its initial state and has not had time to draw down fCO_2^{ytn}.
2006	Weak fCO_2^{ytn} drawdown	Strong winds and low SST cause a deep MLD and most likely a weak stratification (not documented). Weak primary production.
2008	- Early fCO_2^{ytn} drawdown - Sudden fCO_2^{ytn} increase	- High SST cause a shallow MLD. Primary production initiated. - Possibly due to a coccolithophores bloom (not documented).
2009	- Late fCO_2^{ytn} drawdown - Strong fCO_2^{ytn} drawdown	- Strong winds and low SST cause a deep MLD. Primary production not initiated. - Weak winds and high SST cause a shallow MLD. Relatively strong primary production.
2010	Early fCO_2^{ytn} drawdown	Weak winds and high SST cause a shallow MLD. Primary production initiated.
2011	Fall bloom	Possibly due to re-initiation of primary production after light limitations in July (not documented).

TABLE 5.5: Main features and climate forcing in the Iceland Basin.

Chapter 6

Concluding remarks

The aim of this thesis was to determine interannual variations in summertime fCO_2 drawdown based on the oceanic drivers and to identify climate forcing. Based on a 9-year long time series from MV *Nuka Arctica* together with chl-*a*, mixed layer depth and environmental parameters I have determined the fCO_2^{ytn} variability and its roots in climate forcing.

Temperature, with wind playing a lesser role, is the governing environmental parameter affecting the timing of the fCO_2^{ytn} drawdown in both basins. Strong winds and low temperatures in May contribute to a deep MLD, which prevents the onset of primary production and fCO_2^{ytn} drawdown. Weak winds in May together with high temperatures result in a shallow MLD which initiate primary production and a fCO_2^{ytn} drawdown. High temperatures in the spring were suggested to give rise to a strong stratification, strong enough to withstand the mixing effects caused by strong winds. This was indicated by occurrences of shallow MLD in years with strong winds but high SST, and deep MLD in years with weak winds and low SST.

A shallow MLD and a seasonal thermocline is established in May/June and remain relatively stable to August/September. In these months, the interplay between winds and temperatures govern the magnitude of the fCO_2^{ytn} drawdown in both basins. In the summer strong winds and low SST reduce the magnitude of fCO_2^{ytn} drawdown by weakening the stratification of the thermocline indicated by a deeper MLD. This enables DIC rich water to reach the surface, and reduces primary production since phytoplankton fluctuate between the well lit surface layer and the subsurface. Low summertime winds and high SST result in a shallow MLD, a strong stratification and low fCO_2^{ytn}. There are strong indications that light, rather than nutrients, is the limiting factor of primary production in the Irminger Sea. This is evident from the gradual increase in the long

term monthly mean chl-*a* concentrations throughout the summer, which suggest that primary production occur all summer.

Future work

At present, the MV *Nuka Arctica* is the northernmost VOS ship, which makes fCO_2 surveying in this area vulnerable to potential instrument failure. Failure with the equipment aboard was the reason why few, if any, fCO_2 measurements were available in the the summer of 2010, 2012 and 2013. This show the importance of having fCO_2 instruments set up on several VOS ship traversing approximately the same line, which would increase the number of measurements and improve the representativity of the fCO_2 data. This is achievable, as the Royal Arctic Line (RAL) operates more boats in addition to *Nuka Arctica*. The water column forcing along with primary production determine the fCO_2^{ytn} variations, and it would be useful to have more data on the stratification and mixed layers. Argo data would provide this and help to fully determine the impacts of wind and temperature on the summertime stratification and mixed layer depth. This is something I would have explored further if time allowed it. Weak summertime fCO_2^{ytn} drawdown has been associated with a weak stratification, which enables DIC rich water to penetrate the thermocline and reach the surface. Surface nutrient concentrations and DIC/Alk data would confirm/disprove these assumptions, and help to better quantify the effect of the water column forcing of fCO_2^{ytn}. In situ measurements of nutrients can be provided by an autosampler installed on VOS ships, by sensors or by physical retrieval of water samples by the crew aboard the ship.

Bibliography

Bakker, D., Hankin, S., Olsen, A., Pfeil, B., Smith, K., Alin, S., Cosca, C., Hales, B., Harasawa, S., Kozyr, A., et al., 2014. An update to the Surface Ocean CO_2 Atlas (SOCAT version 2). Earth.

Brown, C. W., Yoder, J. A., 1994. Coccolithophorid blooms in the global ocean. Journal Of Geophysical Research-All Series- 99, 7467–7467.

Brown, E., Colling, A., Park, D., Phillips, J., Rothery, D., Wright, J., 2001. Chapter 4 - The north atlantic gyre: Observations and theories, second edition Edition. Butterworth-Heinemann, Oxford.

Dickson, A. G., Sabine, C. L., Christian, J. R., et al., 2007. Guide to best practices for ocean CO_2 measurements.

Dlugokencky, E., Lang, P., Masarie, K., Crotwell, A., Crotwell, M., 2015. Atmospheric Carbon Dioxide Dry Air Mole Fractions from the NOAA ESRL Carbon Cycle Cooperative Global Air Sampling Network, 1968-2014.
URL ftp://aftp.cmdl.noaa.gov/data/trace_gases/co2/flask/surface/

Emerson, S., Hedges, J., 2008. Chemical Oceanography and the Marine Carbon Cycle. Cambridge University Press.

Fernandez, E., Boyd, P., Holligan, P., Harbour, D., Jul 1993. Production Of Organic And Inorganic Carbon Within A Large-Scale Coccolithophore Bloom In The Northeast Atlantic-Ocean. Marine Ecology Progress Series 97 (3), 271–285.

Henson, S. A., Painter, S. C., Penny Holliday, N., Stinchcombe, M. C., Giering, S. L., 2013. Unusual subpolar North Atlantic phytoplankton bloom in 2010: volcanic fertilization or North Atlantic Oscillation? Journal of Geophysical Research: Oceans 118 (10), 4771–4780.

Henson, S. A., Robinson, I., Allen, J. T., Waniek, J. J., 2006. Effect of meteorological conditions on interannual variability in timing and magnitude of the spring bloom in the Irminger Basin, North Atlantic. Deep Sea Research Part I: Oceanographic Research Papers 53 (10), 1601–1615.

Holliday, N., Waniek, J., Davidson, R., Wilson, D., Brown, L., Sanders, R., Pollard, R., Allen, J., 2006. Large-scale physical controls on phytoplankton growth in the Irminger Sea Part I: Hydrographic zones, mixing and stratification. Journal of Marine Systems 59 (3), 201–218.

Holligan, P. M., Fernandez, E., Aiken, J., Balch, W. M., Boyd, P., Burkill, P. H., Finch, M., Groom, S. B., Malin, G., Muller, K., Purdie, D. A., Robinson, C., Trees, C. C., Turner, S. M., Vanderwal, P., Dec 1993. A Biogeochemical Study Of The Coccolithophore, Emiliania-Huxleyi, In The North-Atlantic. Global Biogeochemical Cycles 7 (4), 879–900.

Kalnay, E., Kanamitsu, M., Kistler, R., Collins, W., Deaven, D., Gandin, L., Iredell, M., Saha, S., White, G., Woollen, J., et al., 1996. The NCEP/NCAR 40-year reanalysis project. Bulletin of the American meteorological Society 77 (3), 437–471.

Le Quéré, C., Raupach, M. R., Canadell, J. G., Marland, G., Bopp, L., Ciais, P., Conway, T. J., Doney, S. C., Feely, R. A., Foster, P., et al., 2009. Trends in the sources and sinks of carbon dioxide. Nature Geoscience 2 (12), 831–836.

Lévy, M., Lehahn, Y., André, J.-M., Mémery, L., Loisel, H., Heifetz, E., 2005. Production regimes in the northeast Atlantic: A study based on Sea-viewing Wide Field-of-view Sensor (SeaWiFS) chlorophyll and ocean general circulation model mixed layer depth. Journal of Geophysical Research: Oceans (1978–2012) 110 (C7).

Martinez, E., Antoine, D., D'Ortenzio, F., Montegut, C. d. B., Nov 19 2011. Phytoplankton spring and fall blooms in the North Atlantic in the 1980s and 2000s. Journal Of Geophysical Research-Oceans 116.

Metzl, N., Corbière, A., Reverdin, G., Lenton, A., Takahashi, T., Olsen, A., Johannessen, T., Pierrot, D., Wanninkhof, R., Ólafsdóttir, S. R., et al., 2010. Recent acceleration of the sea surface fCO_2 growth rate in the North Atlantic subpolar gyre (1993–2008) revealed by winter observations. Global Biogeochemical Cycles 24 (4).

Olsen, A., Brown, K. R., Chierici, M., Johannessen, T., Neill, C., Apr. 2008. Sea-surface CO_2 fugacity in the subpolar North Atlantic. Biogeosciences 5 (2), 535–547.
URL https://hal.archives-ouvertes.fr/hal-00297683

Pfeil, B., Olsen, A., Bakker, D. C., Hankin, S., Koyuk, H., Kozyr, A., Malczyk, J., Manke, A., Metzl, N., Sabine, C., et al., 2012. A uniform, quality controlled Surface Ocean CO_2 Atlas (SOCAT). Earth System Science Data Discussions 5 (2), 735–780.

Pierrot, D., Neill, C., Sullivan, K., Castle, R., Wanninkhof, R., Lüger, H., Johannessen, T., Olsen, A., Feely, R. A., Cosca, C. E., 2009. Recommendations for autonomous

underway pCO_2 measuring systems and data-reduction routines. Deep Sea Research Part II: Topical Studies in Oceanography 56 (8–10), 512 – 522, surface Ocean CO_2 Variability and Vulnerabilities.
URL http://www.sciencedirect.com/science/article/pii/S0967064508004268

Reynolds, R. W., Rayner, N. A., Smith, T. M., Stokes, D. C., Wang, W., 2002. An improved in situ and satellite SST analysis for climate. Journal of climate 15 (13), 1609–1625.

Sakov, P., Counillon, F., Bertino, L., Lisæter, K., Oke, P., Korablev, A., 2012. TOPAZ4: an ocean-sea ice data assimilation system for the North Atlantic and Arctic. Ocean Science 8 (4), 633.

Sarmiento, J. L., Gruber, N., 2006. Ocean Biogeochemical Dynamics. Princeton University Press.

Signorini, S., Häkkinen, S., Gudmundsson, K., Olsen, A., Omar, A., Olafsson, J., Reverdin, G., Henson, S., McClain, C., Worthen, D., 2012. The role of phytoplankton dynamics in the seasonal and interannual variability of carbon in the subpolar North Atlantic–a modeling study. Geoscientific Model Development 5 (3), 683–707.

Suykens, K., Delille, B., Chou, L., De Bodt, C., Harlay, J., Borges, A. V., 2010. Dissolved inorganic carbon dynamics and air-sea carbon dioxide fluxes during coccolithophore blooms in the northwest European continental margin (northern Bay of Biscay). Global biogeochemical cycles 24 (3).

Sverdrup, H., 1953. On conditions for the vernal blooming of phytoplankton. Journal du Conseil 18 (3), 287–295.

Takahashi, T., Olafsson, J., Goddard, J. G., Chipman, D. W., Sutherland, S., 1993. Seasonal variation of CO_2 and nutrients in the high-latitude surface oceans: A comparative study. Global Biogeochemical Cycles 7 (4), 843–878.

Takahashi, T., Sutherland, S. C., Sweeney, C., Poisson, A., Metzl, N., Tilbrook, B., Bates, N., Wanninkhof, R., Feely, R. A., Sabine, C., Olafsson, J., Nojiri, Y., 2002. Global sea–air CO_2 flux based on climatological surface ocean pCO_2, and seasonal biological and temperature effects. Deep Sea Research Part II: Topical Studies in Oceanography 49 (9–10), 1601 – 1622, the Southern Ocean I: Climatic Changes in the Cycle of Carbon in the Southern Ocean.
URL http://www.sciencedirect.com/science/article/pii/S0967064502000036

Takahashi, T., Sutherland, S. C., Wanninkhof, R., Sweeney, C., Feely, R. A., Chipman, D. W., Hales, B., Friederich, G., Chavez, F., Sabine, C., Watson, A., Bakker, D. C.,

Schuster, U., Metzl, N., Yoshikawa-Inoue, H., Ishii, M., Midorikawa, T., Nojiri, Y., Körtzinger, A., Steinhoff, T., Hoppema, M., Olafsson, J., Arnarson, T. S., Tilbrook, B., Johannessen, T., Olsen, A., Bellerby, R., Wong, C., Delille, B., Bates, N., de Baar, H. J., 2009. Climatological mean and decadal change in surface ocean pCO_2, and net sea–air CO_2 flux over the global oceans. Deep Sea Research Part II: Topical Studies in Oceanography 56 (8–10), 554 – 577, surface Ocean {CO2} Variability and Vulnerabilities.
URL http://www.sciencedirect.com/science/article/pii/S0967064508004311

Thomson, R. E., Emery, W. J., 2014. Chapter 3 - Statistical Methods and Error Handling, third edition Edition. Elsevier, Boston.

Tjiputra, J., Olsen, A., Assmann, K., Pfeil, B., Heinze, C., 2012. A model study of the seasonal and long-term north atlantic surface pco2 variability. Biogeosciences 9 (3), 907–923.

Tjiputra, J. F., Olsen, A., Bopp, L., Lenton, A., Pfeil, B., Roy, T., Segschneider, J., Totterdell, I., Heinze, C., 2014. Long-term surface pCO_2 trends from observations and models. Tellus B 66.

Vage, K., Pickart, R. S., Thierry, V., Reverdin, G., Lee, C. M., Petrie, B., Agnew, T. A., Wong, A., Ribergaard, M. H., 01 2009. Surprising return of deep convection to the subpolar North Atlantic Ocean in winter 2007-2008. Nature Geosci 2 (1), 67–72.
URL http://dx.doi.org/10.1038/ngeo382

Wanninkhof, R., 1992. Relationship between wind speed and gas exchange over the ocean. Journal of Geophysical Research: Oceans 97, 7373–7382.

Watson, A. J., Schuster, U., Bakker, D. C. E., Bates, N. R., Corbiere, A., Gonzalez-Davila, M., Friedrich, T., Hauck, J., Heinze, C., Johannessen, T., Kortzinger, A., Metzl, N., Olafsson, J., Olsen, A., Oschlies, A., Padin, X. A., Pfeil, B., Santana-Casiano, J. M., Steinhoff, T., Telszewski, M., Rios, A. F., Wallace, D. W. R., Wanninkhof, R., 2009. Tracking the Variable North Atlantic Sink for Atmospheric CO_2. Science 326, 1391–1393.

Weiss, R., 1974. Carbon dioxide in water and seawater: the solubility of a non-ideal gas. Marine Chemistry 2 (3), 203 – 215.
URL http://www.sciencedirect.com/science/article/pii/0304420374900152

Weiss, R., Price, B., 1980. Nitrous oxide solubility in water and seawater. Marine Chemistry 8 (4), 347 – 359.
URL http://www.sciencedirect.com/science/article/pii/0304420380900249

Zeebe, R. E., Wolf-Gladrow, D., 2001. CO_2 in seawater: equilibrium, kinetics, isotopes. Vol. 65. Elsevier.